Effects of *In Situ* Bioremediation Strategies on the Biodegradation and Bioavailability of Polycyclic Aromatic Hydrocarbons in Weathered Manufactured Gas Plant Soil

Stephen David Richardson

A dissertation submitted to the faculty of the University of North Carolina at Chapel Hill in partial fulfillment of the requirements for the degree of Doctor of Philosophy in the Department of Environmental Sciences and Engineering, Gillings School of Global Public Health

Chapel Hill
2010

Approved by:

Michael D. Aitken, Advisor

Gaylen R. Brubaker

Richard M. Kamens

Barbara J. MacGregor

Cass T. Miller

Frederic K. Pfaender

Abstract

Stephen David Richardson: Effects of *In Situ* Bioremediation Strategies on the Biodegradation and Bioavailability of Polycyclic Aromatic Hydrocarbons in Weathered Manufactured Gas Plant Soil

(Under the direction of Michael D. Aitken)

Poor waste management practices at former manufactured gas plant (MGP) sites have left behind a legacy of soil, groundwater, and surface water contamination. MGP waste residues contain a number of hazardous compounds, including polycyclic aromatic hydrocarbons (PAHs), which require effective remediation strategies to mitigate environmental and health impacts. *In situ* bioremediation is a lower cost alternative for sites where conventional remediation strategies (*e.g.*, excavation and landfill disposal) are either cost-prohibitive or infeasible; biological strategies are sometimes combined with more aggressive treatments such as chemical oxidation, to reduce treatment times. To realize the potential for *in situ* bioremediation at MGP sites, a series of continuous-flow columns packed with contaminated MGP soil were operated for over two years, representing treatment by persulfate oxidation, treatment by biostimulation, and a control. Changes in PAH distribution and bioavailability, soil- and aqueous-phase PAH concentrations, and the quantity and activity of the indigenous microbial community and known PAH-degrading bacteria were monitored over time.

Persulfate oxidation did adversely impact the overall microbial community and specific PAH-degrading bacteria; however, recovery of PAH degraders occurred well after the general microbial community. These findings suggest that the use of total bacterial quantity as a surrogate for the recovery of contaminant degraders may be inappropriate for evaluating the compatibility of chemical treatment with subsequent bioremediation.

Biostimulation resulted in significant PAH removal (up to 80%). Spatial and temporal variations in soil PAH concentration and PAH-degrader abundance were strongly correlated to dissolved oxygen advancement, suggesting that oxygen was the limiting factor in PAH removal.

Bacterial transport was also implicated as a factor in the establishment of PAH-degrading bacteria ahead of the oxygen front.

Density-separation of the MGP soil revealed that a majority of PAH mass was associated with carbonaceous particles. Desorption of PAHs from this soil fraction was substantially reduced after biostimulation, although a small portion remained bioavailable. Fast-desorbing fractions in the original MGP soil, quantified by a two-site desorption model, were found to be poor predictors of PAH bioavailability under long-term biostimulation. Overall, this research highlights the importance of physical and biological assessment tools for the evaluation and implementation of *in situ* bioremediation at MGP sites.

To my father, Edward, and my wife, Aimee: my two favorite engineers.

Acknowledgements

This document, my dissertation, is a culmination of years of hard work, dedication, and sacrifice that would not have been possible without the support and guidance of a special group of individuals. Their advice and encouragement have helped me navigate the many ups and downs of this journey. To my academic advisor, Dr. Michael Aitken: thank you for giving me the freedom to pursue my research interests and for asking the right questions. To my committee members: thank you for encouraging me to see my work from a variety of perspectives. To members of my research group and other research colleagues: thank you for the many helpful discussions and advice and for teaching me skills I never thought I would learn. To Melany: thank you for showing me that the Ph.D. was not just something “to do” but to experience. To my parents, Edward and Patricia, and my sister, Beth: thank you for your unconditional love and for believing in me without hesitation.

And to my wife, Aimee: You are my cornerstone. Thank you for making this little dream come true.

Thank you.

Table of Contents

List of Tables

List of Figures

1 Introduction

Between the early 1800s and mid-1900s, up to 5,000 manufactured gas plants (MGPs) operated nationwide to produce and distribute gas to households, businesses, and industry. During gas production, solid and liquid waste byproducts were generated, including coal tar, coke, creosote, lampblack, and spent purifier waste. These residues contain a number of known and suspected carcinogens and other hazardous compounds, including polycyclic aromatic hydrocarbons (PAHs), benzene, ammonia, metals, cyanide, and phenols (1, 2). Poor waste management practices throughout the manufactured gas industry have led to present-day contamination of underlying soil, groundwater, and surface water bodies (2).

PAHs are the contaminants of greatest concern at former MGP sites due to their abundance, persistence, and toxicity (3). Sixteen PAHs are regulated by the U.S. Environmental Protection Agency (USEPA) in aquatic and terrestrial ecosystems (4), with seven of these PAHs classified as 'probable human carcinogens' (5). PAHs are strongly hydrophobic and poorly water-soluble (with the exception of naphthalene), resulting in long-term sequestration in various organic domains of the soil matrix and reduced mass transfer into passing groundwater (6).

Remediation of former MGP sites can be expensive and challenging due to the complex nature of waste residues, site location (*e.g.,* near waterways, adjacent properties), and site conditions (*e.g.,* small footprint, existing infrastructure). Total cleanup costs for former MGPs and related coal tar sites across the United States are estimated to range from $26 to $128 billion (1). *In situ* bioremediation is an effective, lower cost alternative for sites where conventional *ex situ* remediation strategies such as excavation and landfill disposal are either cost-prohibitive or infeasible (*e.g.,* significant depth of contamination). Extensive biodegradation of PAHs has been well-documented in

field-contaminated soils, although the rate of PAH biodegradation tends to decrease with increasing molecular weight (or ring number) of the PAH molecule (7).

PAH biodegradation studies on field-contaminated soils are frequently conducted in slurried, continuously mixed batch incubations, microcosms, or bioreactors to maximize contact between indigenous microbial communities, contaminants, co-substrates, electron acceptors, nutrients, and other amendments. Consequently, non-equilibrium effects of diffusion, bioavailability, and sorption hysteresis observed under field conditions are not considered, which can affect experimental endpoints (*e.g.,* biodegradation rates, biokinetic parameters) (8, 9). To better understand biodegradation activities under *in situ* conditions, continuous-flow columns are often employed. Although column systems are not directly representative of field conditions, they can yield additional data (*e.g.*, transport and spatial distribution of PAHs and bacteria), that when used in conjunction with batch results, can provide a more complete picture of physicochemical and biological processes in contaminated soils (10, 11).

Four continuous-flow columns containing contaminated soil from a former MGP site were operated for over two years to examine the long-term effects of biological and coupled chemical-biological remediation strategies on the concentration, distribution, availability, and biodegradation of PAHs in weathered MGP soil. Two columns represented potential treatment conditions: chemical oxidation (persulfate) and *in situ* biostimulation (oxygen-saturated and nutrient-amended groundwater), and a third column served as a control (air-saturated, unamended groundwater). A variety of physicochemical analyses and molecular techniques were employed to monitor changes in PAH distribution and bioavailability, soil- and aqueous-phase PAH concentrations, and the abundance and activity of the indigenous microbial community and known PAH-degrading bacteria in response to the imposed conditions.

1.1 Specific Aims and Rationale

The specific aims of my research are outlined below:

1. Determine the effects of persulfate oxidation on soil PAH concentration and the abundance and activity of the indigenous microbial community and specific phenanthrene-degrading bacteria in weathered MGP soil.

Coupling *in situ* chemical oxidation (ISCO) strategies, such as persulfate oxidation, with biological processes may serve as an attractive remediation strategy for the removal of PAHs from former MGP sites. The goal in a combined remediation approach would be to remove the bulk of the contaminant mass by physicochemical means (*e.g,* ISCO), while maintaining biological processes for secondary treatment of residual contamination (12, 13). The non-specific nature of persulfate and other chemical oxidants, however, can adversely affect soil microbial communities, potentially reducing concentrations of relevant organisms and limiting post-oxidation biological treatment. Understanding the effects of persulfate on PAH-degrading communities and their survival post-oxidation is important for the success of such a treatment strategy. Most studies investigating the effects of chemical oxidants on biological processes have found complete recovery or enhancement of the total microbial community post-oxidation (14-21). However, the impacts on specific bacterial species, in this case PAH degraders, have not been examined. Aim 1 considers the hypothesis that persulfate oxidation will select for varying microbial communities and could negatively impact PAH-degrading bacteria (specifically phenanthrene degraders), their rates of recovery, and PAH biodegradation post-oxidation.

2. Examine the long-term effects of in situ biostimulation on a) soil PAH concentration and b) the indigenous microbial community and specific PAH degraders in weathered MGP soil.

Former MGP sites are frequently nutrient- and oxygen-limited and available carbon is often sequestered in various organic domains in the soil (22), leading to reduced biodegradation potential. Addition of nutrients and oxygen (*e.g.,* biosparging) are common strategies for stimulation of indigenous microbial communities (23-26), although little is known about the effect of biostimulation on specific PAH degraders over time. Tracking the abundance and activity of specific degrading

bacteria during bioremediation activities may be a valuable tool for assessing and/or verifying biological activity. Aim 2 tests the hypotheses that biostimulation will improve PAH biodegradation under long-term *in situ* conditions and that populations of known PAH-degrading bacterial groups will increase over time.

3. Determine the impact of in situ biostimulation on the PAH distribution and bioavailability among various compartments of weathered MGP soil.

Sorbed PAHs are not uniformly distributed among the various compartments or domains of soil and, as such, have varying degrees of availability to indigenous microbial communities (27-29). Soil organic matter (SOM) and other carbonaceous materials are important reservoirs for sorption of PAHs (22) and tend to exhibit lower PAH availability (30, 31). The effects of bioremediation strategies such as *in situ* biostimulation on PAH distribution and bioavailability has not been extensively examined, particularly in continuous-flow systems. Aim 3 considers the hypothesis that *in situ* biostimulation will improve PAH removal in, not only the "heavier", more bioavailable material (*e.g.,* sand, silt, clay), but also the more recalcitrant, less bioavailable, "lighter" material (e.g., carbonaceous matter) as compared to the control condition. The effect of PAH distribution among soil domains on overall PAH bioavailability has important implications for assessing risk and improving decision-making for the management and treatment of PAHs at former MGP sites.

1.2 Dissertation Organization

This dissertation is a compilation of three manuscripts, each dedicated to one of the specific aims previously outlined. The first manuscript (Chapter 3) has been submitted to a peer-reviewed journal, while the second and third manuscripts (Chapters 4 and 5) are draft versions intended for submission to peer-reviewed journals. All tables and figures presented in the Chapters 3-5 are configured for journal submission. Chapter 2 is a review of the literature to-date that is relevant to the specific aims of the dissertation and Chapter 6 provides conclusions and recommendations for future research.

2 Literature Review

2.1 Manufactured Gas Plants

Before networks of natural gas pipelines were developed across the United States, MGPs were a major source of energy production and distribution for cities and towns. Every city or town of moderate size had its own MGP, with larger cities often owning several to meet their higher energy demands (1). These plants were typically constructed close to the central business district to minimize piping infrastructure and near waterways and rail lines to facilitate access to coal and other feedstock (32).

Between the early 1800s and the mid-1900s, thousands of MGPs operated nationwide to produce and distribute gas to households and businesses. The exact number of former MGP sites in the United States remains a source of debate. Estimates ranging from 1,500 to 5,000 have been reported in various publications, based on historical gas association registries, directories, and records (2, 33). More recent estimates, which include smaller on-site operations (*e.g.,* for hotels, prisons, colleges, and military facilities), are much larger, ranging from 36,000 to 55,000 across the United States (1, 32, 34, 35).

2.1.1 Gas Generation

Gas was generated through the pyrolysis of coal, oil, and other feedstock in large, closed vessels. This process liberated volatile components in the feedstock which were collected, cooled, purified, and ultimately distributed to surrounding communities. Three main processes for gas production were generally employed: 1) coal carbonization, 2) carbureted water gas, and 3) oil gas (1, 36).

Coal carbonization involved heating bituminous coal in a closed vessel (or retort) at high temperatures in the absence of oxygen. Main components of the liberated coal gas were methane and

hydrogen (33). Prior to distribution, the gas was scrubbed using lime, wood chips, or crushed iron ore to remove hydrogen sulfide, cyanide, and other impurities from the final gas stream. The main byproduct of coal carbonization was coke, a feedstock that burned hotter and cleaner than coal and was often recycled or sold to other industries. Other byproducts included coal tar, phenols, cyanides, and tar bases. Coal carbonization was exclusively used in the U.S. gas manufacturing industry until 1875 (1, 36).

The carbureted water gas process introduced steam into a closed vessel (called a generator) during heating of coal or coke at high temperatures. The steam interacted with the carbon source to produce water gas, a flammable gas mixture of hydrogen and carbon monoxide. Light oil petroleum products were injected into the water gas causing the oils to thermally crack, forming methane. Main byproducts of the carbureted water gas process were tar-water emulsions and the uncracked portion of the injected oils. Carbureted water gas was the predominant form of gas generation in the United States from 1875 until the demise of the industry (36, 37).

The oil gas process was a modification of the carbureted water gas approach that eliminated the need for coal or coke as the carbon source. Instead, oil and steam were passed through a bed of heated bricks (or checkerbricks) in the generator. Major byproducts of the oil gas process included lampblack, tar-water emulsions, and light oil (1, 36, 37). The oil gas process was primarily used on the west coast where coal and other feedstock were not easily accessible (38).

2.1.2 Waste Generation and Management

During gas generation and purification, solid and liquid waste byproducts were formed including coal tar, coke, creosote, tar-water emulsions, spent purifier waste, ash, and lampblack, depending on the gas generation process employed. Between 1880 and 1950, it is estimated that 11 billion gallons of residual tar were produced by MGPs nationwide (39). These residues contain a number of hazardous and potentially carcinogenic compounds including PAHs, benzene, ammonia, metals, cyanide, and phenols (3). Despite some waste byproducts being sold or reused (*e.g.*, coal tar,

coke), a large portion of excess residues at MGPs were simply disposed of on-site or at nearby disposal locations. Common disposal practices included on-site pits or tanks (*e.g.,* tar wells and separators), ponds, or use as fill to adjust the surface grade of the plant site (1, 2, 36). Most MGPs did not recycle water used for cooling coke or condensing tars and oils and generally released untreated water into unlined, on-site ponds or directly into adjacent water bodies (35). In a majority of cases, these past disposal practices have led to significant contamination of surrounding soils and sediments, underlying groundwater, and nearby surface water bodies (2).

Coal tar is one of the most prevalent sources of soil and groundwater contamination at former MGP sites. Following production, coal tar was generally disposed of on-site in poorly-lined tar wells and separators constructed of masonry bricks or wood (37). Over time, coal tar leaked from these "storage devices" into underlying soil and shallow groundwater. Groundwater depths at most former MGP sites are often less than 20 ft due to their close proximity to water bodies (to facilitate transport of feedstock) (39). As a dense nonaqueous phase liquid, coal tar migrates downward through an aquifer until it encounters low permeable media, creating an inaccessible long-term source for contaminant dissolution into passing groundwater (36, 40). PAHs are the most abundant class of compounds found in coal tar, constituting up to 40 wt% (41, 42). Based on their sheer abundance and toxicity (Section 2.2.1), PAHs are the main target species for remediation of soil and groundwater at former MGP sites.

2.2 Polycyclic Aromatic Hydrocarbons

PAHs are a class of several hundred organic compounds that consist of two or more benzene rings fused in linear, angular, or clustered arrangements (43). PAHs are hydrophobic in nature and do not readily dissolve in aqueous solution or volatilize to the atmosphere (with the exception of naphthalene). Their aromatic structures provide high chemical stability (*i.e.,* high resonance energy) through the delocalization of electrons between adjacent, conjugated bonds (44). Increases in the size and angularity of PAHs lead to increases in electrochemical stability and hydrophobicity (45). The

chemical stability, low water solubility, and high sorption capacity of PAHs contribute greatly to their persistence in the environment (6). PAHs can be divided into two categories: low molecular weight PAHs composed of less than four rings and high molecular weight PAHs of four or more rings. High molecular weight PAHs generally have lower water solubilities, vapor pressures, and Henry's constants and higher partitioning coefficients (*e.g.,* octanol/water and organic carbon/water) than low molecular weight PAHs. Selected properties of 16 regulated PAHs are presented in Table 2.1.

2.2.1 Toxicity

The most important property driving PAH remediation is the carcinogenic and toxic nature of some PAHs. To underline their importance as environmental contaminants, the USEPA listed 16 PAHs as 'priority pollutants' in aquatic and terrestrial ecosystems (4). Seven of these PAHs have also been classified as 'probable human carcinogens' (5), with benzo[*a*]pyrene considered the most carcinogenic of the 16-PAH family (5, 49). As a class, PAHs ranked 8th on the *2007 Comprehensive Environmental Response, Compensation, and Liability Act (CERCLA) Priority List of Hazardous Substances (PLHS)* based on their toxicity, frequency of occurrence at USEPA National Priorities List sites, and potential for human exposure (47). Individually, 13 of the 16 regulated PAHs are included on the CERCLA PLHS, with six ranked in the top 100; most notably, benzo[*a*]pyrene is ranked 9th (Table 2.1).

Regulatory guidelines or site-specific cleanup goals commonly account for PAH toxicity by assigning toxic equivalency factors (TEFs) to individual PAHs, normalized to benzo[*a*]pyrene toxicity. Multiplying the measured concentration of each PAH by its respective TEF yields an equivalent concentration of benzo[*a*]pyrene for the PAH mixture, called a benzo[*a*]pyrene equivalent (49). These adjusted values often serve as remediation goals at PAH-contaminated sites. TEFs for the regulated PAHs are provided in Table 2.1.

Table 2.1. Chemical structures and selected properties of the 16 USEPA priority pollutant PAHs [ab]

	Compound [PLHS Rank [c]]	Structure	MW	C_{iw}^{sat}	p_i^{*} [d]	$\log K_{iow}$	$\log K_{ioc}$ [d]	TEF
Low Molecular Weight PAHs	Naphthalene (NAP) [78]		128.1	31.0	1.8×10^{-2}	3.37		--
	Acenaphthylene (ACY) [NR]		152.1	16.1	2.9×10^{-2}	4.0	3.40	--
	Acenaphthene (ACE) [161]		154.2	3.80	1.6×10^{-3}	3.92	3.65	--
	Fluorene (FLU) [NR]	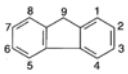	166.2	1.90	7.1×10^{-4}	4.18	3.86	--
	Phenanthrene (PHN) [246]	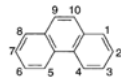	178.2	1.10	9.6×10^{-4}	4.57	4.15	--
	Anthracene (ANT) [NR]	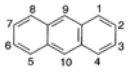	178.2	0.045	1.7×10^{-5}	4.54	4.15	--
High Molecular Weight PAHs	Fluoranthene (FLA) [110]	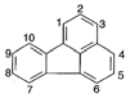	202.3	0.26	5.0×10^{-6}	5.22	4.58	--
	Pyrene (PYR) [253]	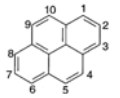	202.3	0.132	2.5×10^{-6}	5.18	4.58	--
	Benz[*a*]anthracene (BaA) [39]	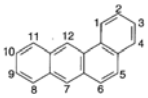	228.3	0.011	2.2×10^{-8}	5.91	6.14	0.1
	Chrysene (CHR) [137]	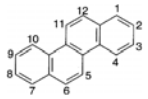	228.3	0.002	6.3×10^{-9}	5.65	5.30	0.001
	Benzo[*b*]fluoranthene (BbF) [10]	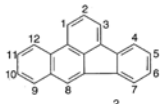	252.3	0.0015	5.0×10^{-7}	5.80	5.74	0.1
	Benzo[*k*]fluoranthene (BkF) [62]	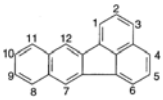	252.3	0.0008	5.1×10^{-7}	6.0	5.74	0.01
	Benzo[*a*]pyrene (BaP) [9]	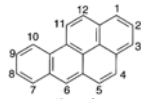	252.3	0.0038	5.6×10^{-9}	6.04	6.74	1
	Benzo[*g,h,i*]perylene (BgP) [NR]	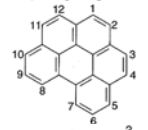	276.3	0.0003	1×10^{-10}	6.50	6.52	--
	Dibenz[*a,h*]anthracene (DBA) [15]	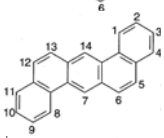	278.4	0.0006	1.0 x 10	6.75	6.20	1
	Indeno[1,2,3-*c,d*]pyrene (INP) [174]	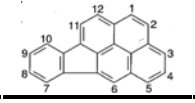	276.3	0.062	1.0×10^{-1}	7.66	6.20	0.1

[a] abbreviations: NR = Compound not ranked on PLHS; MW = molecular weight (g/mol); C_{iw}^{sat} = aqueous solubility (mg/L); p_i^{*} = vapor pressure (mm Hg); K_{iow} = octanol-water partitioning coefficient; K_{ioc} = organic carbon partitioning coefficient; TEF = toxic equivalency factor.
[b] All data are from (46) unless otherwise noted; [c] data from (47); [d] data from (48).

2.2.2 Sorption

The fate of PAHs in the soil environment is chiefly governed by PAH hydrophobicity and physicochemical properties of the soil. Natural soils and sediments are a complex mixture of SOM, humic substances, inorganic minerals, carbonaceous compounds, pyrogenic residues, pore water, and gases (50). Additional phases such as solvents, oils, tars, residues, and other nonaqueous phase liquids may be present in contaminated soils (51). Sorption of PAHs to these various soil compartments can greatly influence overall PAH transport, degradation, and bioavailability. Sorption occurs by 1) physical adsorption to a particle surface or 2) partitioning into a separate phase (absorption) such as SOM (52). Both processes involve a variety of intermolecular interactions such as van der Waals dispersive forces, dipole-dipole forces, dipole-induced dipole forces, and hydrogen bonding (44, 50). For hydrophobic organic compounds (HOCs) such as PAHs, these bonding forces are amplified by repulsive forces of the aqueous phase, driven by unfavorable free-energy costs associated with formation of a hydration shell around the HOC molecule (53).

SOM is an important reservoir for sorption of PAHs in the soil matrix (54, 55). Initially, sorption to SOM was viewed as a simple partitioning phenomenon, with SOM conceptualized as an amorphous gel-like polymer containing organo-lipophilic regions (analogous to organic liquids) (54). This model, known as the linear partitioning model, is predicated on the assumption of concentration- and competition-independent sorption (*i.e.,* unlimited sorption sites), resulting in linear sorption isotherms (Equation 2.1). The solid-water distribution coefficient (K_{id}) describes the ratio of solid (C_{is}) and aqueous phase (C_{iw}) concentrations of solute *i* under equilibrium conditions.

$$C_{is} = K_{id} C_{iw} \tag{2.1}$$

Applicability of this model was eventually challenged by evidence of non-linear behavior such as biphasic desorption kinetics, isotherm non-linearity, solute-solute competition, long equilibration times, sorption-desorption hysteresis, and limited bioremediation potential (56, 57). Alternatively, a dual-mode sorption model was proposed that treats SOM as a heterogeneous polymer of condensed

(glassy) and expanded (rubbery) regions with vastly different sorptive energies (54). Sorption to the rubbery state is dominated by linear and non-competitive absorption, a process analogous to HOC dissolution into organic solvents and described by the linear partitioning model (Equation 2.1). Equilibrium sorption is rapidly achieved in this domain, typically within minutes to hours after initial exposure (54, 58). The absorption domain of SOM consists of amorphous materials such as partially degraded biopolymers (*e.g.,* lipids, proteins, amino acids) and humic/fulvic substances (57). Sorption in the glassy domain is described by concurrent absorption and site-specific adsorption to nanometer-sized voids within the fixed-chain molecular structure. These voids or cavities are of varying shape, size, steric arrangement, and activation energy, resulting in solute-solute competition at binding sites and slow mass transfer to/from voids (54). Equilibrium sorption within the glassy domain occurs over a significantly longer time-frame than within the rubbery phase, sometimes taking years to achieve (54, 58). Consequently, many K_{id} values are not measured under true equilibrium conditions and disproportionately reflect fast sorption kinetics (52). The dual mode model, as proposed by Xing and Pignatello (54), is defined as:

$$C_{is} = K_{id} C_{iw} + \sum_{i=1}^{n} \frac{S_i^o b_i C_{iw}}{1 + b_i C_{iw}} \tag{2.2}$$

where the linear sorption term is described by the linear partitioning model (Equation 2.1) and the non-linear sorption term is represented by summed Langmuir terms, where S_i^o and b_i are capacity and affinity constants, respectively, for each of n site-limited sorption domains. The dual model has been successfully used to describe PAH sorptive behavior with a variety of natural sorbents (54, 59, 60).

Condensed aromatic materials such as coal, kerogen, coke, soot, and charcoal commonly exhibit non-linear sorption of PAHs, mirroring the physicochemical properties of the SOM glassy domain (57). These materials typically make up a small portion of the total soil/sediment mass but can be a significant component (up to 50-80 wt%) of total organic carbon (61). Khalil et al. (22) found that coal, coke, wood, and coal tar pitch originating from several MGP sediments comprised 10-20% of the total sediment mass and 70-95% of the total extractable PAHs. Further fractionation of

the condensed fraction identified coal tar pitch, a suspected waste product of MGP operations, as a major reservoir for PAH sorption.

Slow sorption kinetics (non-linear) are caused by high activation energies of sorptive bonds and solute diffusion limitations within the soil matrix (52). Large compounds, which can interact with a surface at several points, have larger activation energies than smaller compounds and are increasingly more difficult to desorb (52). For PAHs, desorption must also overcome the substantial thermodynamic gradient associated with hydrophobic expulsion of the solute from the water phase (53). Sorption kinetics are also heavily influenced by diffusion limitations within the interstitial pore network of a particle. Soil particles contain micropores (diameter, $d < 2$ nm) and mesopores (2 nm > d > 50 nm) that can trap solutes, hindering diffusion to larger macropores ($d > 50$ nm) and bulk fluid where advective transport dominates (50). Solute diffusion can be limited by sorption to pore surfaces, partitioning into SOM-coated pores, and particle tortuosity (the degree of bending, twisting, and variation in pore diameters of a particle). In homogenous soil columns, non-equilibrium sorption is identified by asymmetries in elution curves (*e.g.,* early breakthrough, peak height reduction, and tailing) relative to non-sorbing tracers (*e.g.,* tritiated water and chloride) (52). Evidence of non-equilibrium sorption in heterogeneous systems is generally less obvious. Differences in soil permeability (*i.e.,* physical non-equilibrium) can retard the migration of solutes (both sorbing and non-sorbing), also resulting in asymmetric elution curves (62).

A characteristic plateau is generally observed in PAH desorption studies with increased contact time between PAHs and soil matrix. This phenomenon is often attributed to compound 'aging', which describes the migration of compounds deep within the pore structure and subsequent binding to remote sorption sites (63). Evidence for the sequestration and aging of HOCs in soil include: 1) a decline in compound availability to microbial communities, 2) reduced toxicity in aged soils, 3) long equilibrium times for sorption and desorption, and 4) a reduction in HOC extractability with time (58). Northcott and Jones (64) observed a decline in the extractability of radiolabeled PAH-spiked microcosms with increasing abiotic incubation time. The degree of extractability appeared to be

inversely related to PAH size and hydrophobicity, with benzo[*a*]pyrene showing the lowest recovery post-incubation. Aging mechanisms can have a significant impact on PAH dissolution and bioavailability, complicating bioremediation efforts.

2.2.3 Dissolution

Dissolution of PAHs from MGP soils into passing groundwater may pose long-term health risks to surrounding receptors. To better quantify these risks, accurate prediction of aqueous PAH concentrations (particularly carcinogenic PAHs) is essential. Equilibrium dissolution of PAHs from the solid phase can be described using empirical partitioning coefficients (*i.e.,* K_{id}) derived from laboratory batch experiments. Given that SOM is the dominant sorbent in natural soils, K_{id} is often normalized to the fraction of organic carbon (f_{oc}) (redefined as the organic-carbon partitioning coefficient [$K_{ioc} = K_{id}/f_{oc}$]), for direct comparison of solute affinities (44). Regression models, known as linear free energy relationships (LFERs) (Equation 2.3), are commonly used to relate K_{ioc} values to known compound properties such as aqueous solubility and octanol-water partitioning coefficient (K_{iow}),

$$\log K_{ioc} = a \cdot \log K_{iow} + b \tag{2.3}$$

where *a* and *b* are fitting parameters unique to a given class of compounds. However, application of LFERs in natural soils and sediments is limited because sorbents must be of similar composition (*e.g.,* average molecular weight and density) (65). Brown et al. (66) reported order of magnitude differences in average molecular weight between coal tar sources. Likewise, Hawthorne et al. (67) found that K_{ioc} values for individual PAHs spanned several orders of magnitude among 114 different PAH-contaminated sediments.

Alternatively, Raoult's law has been used to estimate equilibrium aqueous PAH concentrations from a variety of contaminated sources including coal tar (41, 65, 68), former MGP soil (69), gasoline (70), and diesel fuel (71). Raoult's law describes the equilibrium partitioning of solutes in an ideal

two-phase system (*e.g.,* aqueous and organic phases) (69). At equilibrium, the chemical potential of each solute is equal among all phases (44) and can be expressed as:

$$\gamma_{iw} \cdot x_{iw} = \gamma_{io} \cdot x_{io} \tag{2.4}$$

where x_{iw} and x_{io} are the respective mole fractions of solute *i* in the aqueous and organic phases and γ_{iw} and γ_{io} are the activity coefficients of solute *i* in the aqueous and organic phases, respectively. The activity coefficient reflects how active a compound is in a given state relative to its standard state (*e.g.,* pure liquid solute) (44).

Equation 2.4 can be simplified to Equation 2.5 by applying the following assumptions (41, 69, 71, 72):

1. the solute behaves ideally in the organic phase (*i.e.,* $\gamma_{io} = 1$),
2. solute interaction in the aqueous phase is small (*i.e.,* $\gamma_{iw} = \gamma_{iw}^{sat}$, the activity coefficient of solute *i* in the aqueous phase in equilibrium with the pure liquid solute), and
3. the mole fraction of the pure liquid solute in the aqueous phase (x_{iw}^{sat}) is equal to the inverse of γ_{iw}^{sat}.

$$x_{iw} = x_{io} \cdot x_{iw}^{sat} \tag{2.5}$$

Assuming that the aqueous phase is sufficiently dilute such that its volume is approximately equal to that of pure water (41), the aqueous phase mole fraction of solute *i* can be expressed in terms of mass concentration (Equation 2.6):

$$C_{iw} = x_{io} \cdot C_{iw}^{sat}(L) \tag{2.6}$$

where C_{iw} is the mass concentration of solute *i* in the aqueous phase and $C_{iw}^{sat}(L)$ is the aqueous solubility of pure liquid solute *i*. Since many components of coal tar, including PAHs, exist as solids at ambient temperatures, pure solid aqueous solubilities ($C_{iw}^{sat}(s)$) must be adjusted for the free energy of fusion (the energy required to convert solute molecules from a pure solid state to a pure liquid state) (Equation 2.7):

$$C_{iw} = x_{io} \cdot C_{iw}^{sat}(s) \cdot \left(\frac{f_{iL}^{*}}{f_{is}^{*}} \right) \tag{2.7}$$

where $(f_{iL}^{*} / f_{is}^{*})$ is the ratio of pure fugacities in the liquid and solid phases (3, 41, 44). Pure solid aqueous solubilities for the 16 regulated PAHs are provided in Table 2.1. The mole fraction of solute *i* in the organic phase is determined by Equation 2.8:

$$x_{io} = C_{io} \cdot \left(\frac{\overline{MW_o}}{MW_i} \right) \tag{2.8}$$

where C_{io} is the mass concentration of solute *i* in the organic phase, $\overline{MW_o}$ is the average molecular weight of the organic phase, and MW_i is the molecular weight of solute *i*.

Since organic phase activity coefficients for PAHs are generally close to unity (ranging from 0.93 to 1.16 in coal tars (73) and diesel fuel (71)), the assumption of ideal solute behavior (Assumption 1) can be considered valid. However, several factors can contribute to observed deviations from ideality, including the presence of surfactants, emulsions, or cosolvents, long equilibration times, and analytical limitations (*e.g.,* quantification of poorly soluble high molecular weight PAHs) (71, 74). Under non-ideal conditions, C_{iw} is expressed as:

$$C_{iw} = \gamma_{io} \cdot x_{io} \cdot C_{iw}^{sat}(L) \tag{2.9}$$

2.2.4 Bioavailability

A variety of discipline-specific definitions of bioavailability are referenced in the literature. With respect to bioremediation, bioavailability refers to the contaminant fraction that can be effectively accessed by contaminant-degrading microbial communities (75). Bioavailability can be viewed as a series of steps describing contaminant sorption between solid and aqueous phases, transport (both dissolved and particulate-bound) within the aqueous phase, and uptake across a biological membrane where compound accumulation, metabolism, or toxicity might occur (29, 76). Semple et al. (77) reasoned that 'bioaccessibility' is a more appropriate descriptor for the above steps

over time, with 'bioavailability' reserved for instantaneous uptake at the biomembrane. To date, both terms have been used interchangeably in the literature.

Bioavailability is an important concept in soil remediation and risk assessment. Physical, chemical, and biological remedial methods have been developed that aim to increase bioavailability (*e.g.,* mixing, surfactants, cosolvents) or decrease bioavailability (*e.g.,* biostabilization, sediment capping, solidification), depending on the treatment design and site cleanup goals (29). The latter strategies reduce risk by creating a barrier between the contamination and surrounding receptors while the former must incorporate a mass removal step (*e.g.,* enhanced biodegradation, aqueous phase extraction) to minimize risk. Methods to quantify or predict bioavailability are valuable for risk assessment and for evaluating proposed and existing remediation strategies (particularly bioremediation) at contaminated sites (78). A variety of physical, chemical, and biological techniques for estimating bioavailability have been proposed, including solid-phase extraction (79-81), supercritical carbon dioxide extraction (82), surfactant extraction (83), persulfate oxidation (55), non-exhaustive solvent extraction (25, 84-87), and substrate mineralization, uptake, and toxicity (78, 85, 88).

Solid-phase extraction with polymeric adsorbent resins (*e.g.,* Tenax TA and Amberlite XAD) is a common method for estimating bioavailability in contaminated soils and sediments. The resins function as an infinite sink, maintaining a steep concentration gradient between the aqueous and solid phases for maximum desorption (89, 90). Cornelissen et al. (79) found a reasonable correlation between the rapidly desorbing fraction of PAHs and the extent of PAH biodegradation in contaminated harbor sediments. Estimation of bioavailability, however, is complicated by the fact that bioavailability is compound- and organism-specific and influenced by the physical state of the sorbent matrix (91, 92). By ignoring the effects of aging (*e.g.,* spiked incubations for mineralization) or altering the physical soil structure (*e.g.,* creating a soil slurry for solid-phase extraction), bioavailability may be overestimated compared to actual field conditions (93).

Bioavailability and degradation of PAHs in natural soils are generally biphasic, with an initial phase of rapid PAH removal followed by a longer period of limited PAH reduction. During the initial phase, bioavailability of PAHs is high and degradation rates may be limited by microbial uptake rather than mass transfer from soil particles. As available PAHs are consumed, mass transfer mechanisms (desorption and diffusion) gain importance, becoming critical factors in defining PAH bioavailability and rate of biodegradation (94). Physical exclusion of bacteria (diameter, $d > 0.2$ μm (95)) from nanometer-sized pores, particularly within SOM, exacerbates the problem of reduced bioavailability by maintaining path lengths between microbial cells and HOC-sorption sites (63). Since only dissolved compounds are believed to be accessible for microbial uptake (96), microorganisms can only control mass transfer from interstitial pores by removing substrate from the aqueous phase. To this end, some microorganisms have developed strategies such as production of biosurfactants to lower interfacial tensions and increase apparent solubilities of sorbed HOCs (97-99). Several studies have reported biodegradation rates in excess of abiotic desorption rates, suggesting the potential for microbial-facilitated desorption (24, 91, 93). Biofilm development and growth directly on sorbed HOCs are additional strategies aimed at decreasing the transport distance between the cell and substrate (99). During the slow, non-linear desorption phase, biodegradation rates can also be affected by microbial limitations. Huesemann et al. (100, 101) discovered that when PAH biodegradation ceased, it was never due to limitations in bioavailability, indicating that some PAHs (*e.g.,* five- and six-ring) may be fully or partially recalcitrant to microbial degradation.

To date, the concept of bioavailability has not received widespread consideration in devising regulatory criteria and assessing risk, with only a few sites incorporating bioavailability data (*i.e.*, *in vivo* and *in vitro* assays) in the development of site-specific soil cleanup goals (63, 102). Vigorous chemical extraction techniques that recover maximal contaminant mass from an environmental sample tend to overestimate risk by regarding contaminants as 100% available (58). Kelsey and Alexander (103) found that vigorous solvent extraction of naphthalene, phenanthrene, and atrazine in soil showed poor correlation with compound bioavailability (to earthworms and bacteria) over time.

Contrasting views exist on the role of contaminant bioavailability in remediation. If sorbed contaminants (of limited bioavailability) are truly immobile and are ultimately converted to innocuous forms, indistinguishable from SOM, it is reasonable to view sequestration as an environmental solution. However, if sorbed contaminants are not transformed or are converted to metabolites of greater toxicity, their slow release from SOM can lead to future environmental problems (104). In general, the uncertainty associated with long-term contaminant fate, the lack of standard methods for quantifying bioavailability, and fears associated with increased analytical costs, lack of regulatory guidance, legal challenges, and public disapproval have led to reduced acceptance of considering bioavailability in site remediation and risk assessment (29).

2.3 Remediation of PAHs at Manufactured Gas Plants

Remediation of former MGP sites can be challenging due to the complexity of waste residues, the often small footprint of the site, and the vicinity of the site to adjacent waterways and properties. To further complicate remedial efforts, former MGP sites that were once located on the outskirts of the business district are now often situated well within the limits of a city that has since grown. As a result, these contaminated sites are in close proximity to residential and commercial properties, municipal utilities, and roadway infrastructure (2). Approximately 30% of former MGPs and related coal tar sites are located in residential areas (1).

A variety of *ex situ* and *in situ* remediation methods have been used at former MGP sites. The most common *ex situ* practices include landfill disposal, incineration, thermal desorption, and soil washing (1, 3). Generally, these methods are expensive and can be cost-prohibitive for sites with large footprints, significant depth of contamination, and existing infrastructure. Alternatively, *in situ* treatments such as chemical oxidation, solvent and surfactant flushing, and bioremediation are available, although they are used to a lesser extent than *ex situ* methods. These remediation methods are generally less expensive but require longer treatment times to meet regulatory criteria. For this

review, discussion will focus on two *in situ* remediation technologies: chemical oxidation and bioremediation.

2.3.1 *In Situ* Chemical Oxidation

ISCO involves the transformation of an organic contaminant into less harmful intermediates or innocuous end-products (*e.g.,* carbon dioxide) by using a chemical oxidant to increase the oxidation state of the contaminant. In general, the oxidant is reduced by accepting electrons released during the oxidation of the target compound and/or other non-target species in the matrix (*e.g.* SOM, inorganic ions). Advantages of ISCO over some conventional remediation methods include reasonable treatment times, reactivity with a broad range of contaminants, and destruction of contaminants *in situ*. Drawbacks include oxidation of non-target species and limited control of oxidant delivery in heterogeneous media (105).

The most common oxidants used for ISCO are permanganate (MnO_4^-), iron-catalyzed hydrogen peroxide (H_2O_2) (*i.e.,* Fenton's reagent), ozone (O_3), and persulfate (peroxydisulfate; $S_2O_8^{-2}$) (105). Successful application of each oxidant depends upon the reactivity of the oxidant, the type and physical state of the target species, the location of the contaminant zone, the matrix of concern (soil and/or groundwater), and the subsurface properties of the field site (106). To date, laboratory and full-scale applications of ISCO have focused primarily on Fenton's reagent, ozone, and permanganate for remediation of a broad suite of organic contaminants. Persulfate is the newest and least-studied of the available oxidants, only recently receiving attention as an alternative oxidant for soil and groundwater remediation (106). The chemistry and mechanisms of persulfate ISCO will be the focus of this review; general information on other oxidants is available in (105).

The use of persulfate for ISCO originates from a wide range of industrial applications (*e.g.,* polymerization, metal surface oxidation, pulp and paper processing) and commercial laboratory instrumentation (*e.g.,* total organic carbon analyzer) (107). To date, most of the environmental research on persulfate has been performed at a bench-scale and has focused mainly on the oxidation

of chlorinated hydrocarbons. For example, the effects of oxidant concentration (108), temperature (109), pH (110), iron activation (111), and matrix interferences (*i.e.,* chloride and bicarbonate ions) (112) on trichloroethylene (TCE) oxidation have been investigated. Other environmentally relevant compounds (and classes of compounds) that have received some attention include benzene, toluene, ethylbenzene, and xylenes (BTEX) (111, 113), 1,2,4-trichlorobenzene (114), methyl *tert*-buytl ether (MTBE) (115), and lindane (116). To date, only a few studies focusing on persulfate oxidation of PAHs have been completed (55, 117, 118).

Sodium persulfate ($Na_2S_2O_8$) is the most commonly used form of persulfate for ISCO. It has a higher water solubility (55.6 g/100 ml at 20°C) than potassium persulfate and, unlike ammonium persulfate, it does not generate nitrogenous byproducts (*i.e.,* nitrate; a regulated drinking water contaminant) (105). Sodium persulfate provides greater stability and persistence in the subsurface, can be injected at higher concentrations, and has lower SOM-reactivity than other available oxidants (105, 115). In subsequent discussion, sodium persulfate will be referred to as 'persulfate'.

Persulfate chemistry involves complex chain reactions that generate a variety of reactive species for contaminant oxidation. Initially, dissociation of persulfate forms persulfate anions ($S_2O_8^{2-}$) which are strong, stable oxidants (E_h = 2.01 V) capable of oxidizing some organic contaminants (mainly BTEX and other petroleum hydrocarbons). Oxidation of organics by persulfate anions is slow, allowing for increased oxidant transport from the injection point (119). Subsequent activation of persulfate anions can produce sulfate radicals ($SO_4^{-\bullet}$) which have a greater redox potential (E_h = 2.6 V) and are reactive with a wider range of environmental contaminants (105, 120).

Activation of persulfate anions can occur under three conditions: 1) elevated temperature (30°C to 100°C) (Equation 2.10), 2) ultraviolet light exposure (photo-activation) (Equation 2.10), and 3) reaction with low-valent metal catalysts such as ferrous iron (Equation 2.11), copper, silver, manganese, cerium, and cobalt (105, 121).

$$S_2O_8^{2-} \xrightarrow{\Delta T / h\nu} 2SO_4^{-\bullet} \quad (2.10)$$

$$S_2O_8^{2-} + Fe^{2+} \longrightarrow Fe^{3+} + SO_4^{-\bullet} + SO_4^{2-} \quad (2.11)$$

Persulfate activation is generally not effective at ambient temperatures (< 20°C) (106, 115) because the activation energy ($\Delta G^{\circ\ddagger}$ = 33.5 kcal/mol) of the homolysis reaction (Equation 2.10) cannot easily be overcome (109, 120). Raising the system temperature above 30°C has shown significant improvement in persulfate anion activation and contaminant oxidation under laboratory conditions (109, 115, 121). In field applications, economical and logistical obstacles associated with raising the subsurface temperature may limit the applicability of thermally-activated persulfate, although methods to increase the subsurface temperature do exist (*e.g.,* hot air/steam injection, radio frequency heating, and electrical resistance heating). None of these technologies to-date has been used in conjunction with persulfate treatment (105).

Alternatively, ferrous iron or other metal catalysts can be used at ambient temperatures to accelerate persulfate radical formation, by reducing the overall activation energy of the reaction ($\Delta G^{\circ\ddagger}$ = 12 kcal/mol) (Equation 2.11) (122). However, ferrous iron can also act as a radical scavenger, reducing oxidant efficiency for the target species (Equation 2.12) (108). Chelators that complex with the metal catalyst (*e.g.,* citric acid and nitrilotriacetic acid) can be used to delay oxidant scavenging reactions and extend the transport distance within the aquifer, although limitations in oxidant efficiency have still been reported (121). Native iron in the soil matrix may also interfere with oxidant delivery and efficiency (105).

$$SO_4^{-\bullet} + Fe^{2+} \longrightarrow Fe^{3+} + SO_4^{2-} \qquad (2.12)$$

The generation of sulfate radicals initiates a series of complex chain reactions that form other reactive species such as the hydroxyl radical ($OH^{\bullet}$) (Equation 2.13), peroxymonosulfate (HSO_5^-) (Equation 2.14), and hydrogen peroxide (H_2O_2) (Equation 2.15) (121, 123). Like the sulfate radical, these intermediates are highly reactive (*e.g.,* $OH^{\bullet}$; E_h = 2.7 V) and can oxidize a wide variety of organic compounds. Subsequent reactions can yield secondary radicals (*e.g.,* $CO_3^{-\bullet}$) and molecular oxygen (Equation 2.16).

$$SO_4^{-\bullet} + H_2O \longrightarrow OH^{\bullet} + H^+ + SO_4^{2-} \quad (2.13)$$

$$SO_4^{-\bullet} + OH^{\bullet} \longrightarrow HSO_5^- \quad (2.14)$$

$$2OH^{\bullet} \longrightarrow H_2O_2 \quad (2.15)$$

$$H_2O_2 \longrightarrow H_2O + \frac{1}{2}O_2 \quad (2.16)$$

The balanced reaction for complete PAH oxidation (*e.g.*, phenanthrene) using persulfate is written as:

$$C_{14}H_{10} + 33Na_2S_2O_8 + 28H_2O \longrightarrow 14CO_{2(g)} + 66H^+ + 66SO_4^{2-} + 66Na^+ \quad (2.17)$$

As shown in Equation 2.17, one mole of persulfate generates two moles of sulfate (or 0.8 g of sulfate are produced for every gram of persulfate reacted). Since a substantial amount of sulfate is generated during persulfate decomposition, the implications of sulfate release into groundwater and soil matrices require consideration. With respect to human health, a study by the USEPA and Centers for Disease Control and Prevention (CDC) concluded that sulfate poses limited health risks at concentrations less than 600 mg/L in drinking waters. The study further deemed it 'unlikely that regulation of sulfate would present a meaningful opportunity for health risk reduction' (124). Other considerations such as accumulation of precipitates, as commonly observed with permanganate oxidation, are not likely to occur following persulfate injection due to the high solubility of sulfate.

A significant amount of protons is also generated from the decomposition of persulfate. Under acidic conditions, the activation of persulfate anions can be acid-catalyzed to increase production of sulfate radicals (125). The implications of lower pH on persulfate oxidation have been investigated in several studies, although conflicting results have been reported. Liang et al. (110) reported lower rates of TCE degradation at a pH of 4 versus neutral conditions for system temperatures up to 30°C. The authors attributed the decline in TCE reactivity to an increase in radical-radical ($SO_4^{-\bullet}$-$SO_4^{-\bullet}$) interactions. Conversely, Huang et al. (115) showed a decrease in the reaction rate of MTBE with increasing pH at 40°C.

2.3.2 Bioremediation

Madsen (126) defines bioremediation as 'the intentional use of biodegradation processes to eliminate environmental pollutants' by using 'the physiological potential of microorganisms to eliminate or reduce the concentration of environmental pollutants in field sites to levels that are acceptable to site owners and regulatory agencies'. Biodegradation of organic compounds, including PAHs, is dependent on 1) physical and chemical properties of the contaminant(s), 2) characteristics of the indigenous microbial community, and 3) environmental factors as listed below (7, 127, 128):

Physical/chemical:	Structure, concentration, sorption capacity, solubility, compound mixtures, and physical state.
Biological:	Size and activity of populations of relevant microorganisms, microbial adaptation, competition, predation, and growth rate.
Environmental:	Temperature, pH, soil type, organic matter, moisture content, presence of electron acceptors and donors, availability of nutrients, and salinity.

Other factors such as the availability of preferred co-substrates, the production of toxic or dead-end metabolites, and metabolite repression can also impact biodegradation (6). PAH biodegradation is complicated by the high chemical stability, hydrophobicity, and limited solubility of PAHs. These properties directly influence mass transfer and dissolution of PAHs into the aqueous phase where PAH-microbial interactions occur (129). Consequently, degradation rates tend to be inversely proportional to PAH molecular size and ring-number, leading to reduced biodegradation of high molecular weight PAHs (7, 45, 130).

Bacterial metabolism of PAHs can occur via 1) growth-related pathways where carbon from the PAH compound is used for cell growth/maintenance or 2) growth-limited pathways where the PAH is fortuitously degraded but not used as a growth substrate (*i.e.,* cometabolism) (131). Under growth conditions (and to a lesser extent growth–limited conditions), PAHs can be mineralized to non-toxic end products (*e.g.,* water and carbon dioxide) through a series of enzyme-mediated reactions. All enzymes required to catalyze the reactions of the metabolic pathway must be present, otherwise intermediate compounds will accumulate. These enzymes may be synthesized by a single bacterial

species (pure culture) or by a consortium of bacteria, each specializing in the degradation of specific intermediates within the metabolic pathway (131). Numerous bacterial species capable of utilizing two-, three-, and four-ring PAHs as sole carbon and energy sources have been identified (7, 132). Growth on PAHs of five or more rings has not been reported, although cometabolic transformation of benzo[*a*]pyrene has been shown using various co-substrates (45, 133). Known PAH degraders belong to a variety of bacterial genera, including *Acidovorax*, *Alcaligenes*, *Arthrobacter*, *Beijerinckia*, *Burkholderia*, *Flavobacterium*, *Mycobacterium*, *Pseudomonas*, *Rhodococcus*, *Sphingomonas*, and *Streptomyces* (7, 130).

For chemotrophic bacteria, energy for cellular maintenance and growth is derived from the oxidation of an electron donor via a series of electron transport (oxidation and reduction) reactions. Generally, the contaminant of interest acts as an electron donor while an external oxidizing agent serves as the electron acceptor, although this may not always be the case (*e.g.,* reductive dehalogenation of TCE). The transfer of electrons from the donor molecule (reducing agent) to the acceptor molecule (oxidizing agent) generates energy for microbial cells. Varying amounts of energy are generated depending on the available electron acceptors. Common electron acceptors, in order of decreasing energy yield, include oxygen, nitrate, manganese, ferric iron, sulfate, and carbon dioxide (134-136).

2.3.2.1 Biostimulation

Anoxic conditions are commonplace in contaminated soil/sediment environments due to the scarcity of oxygen, particularly within the contaminant source zone. Diffusion of oxygen from overlying unsaturated zones and/or groundwater recharge is slow and often insufficient to balance rapid consumption of residual oxygen by aerobes (135). Likewise, inorganic nutrients necessary for cellular activity and growth (*i.e.,* nitrogen, phosphorus, and potassium) can be rapidly depleted (137). Without sufficient recharge of oxygen and nutrients, natural attenuation (or intrinsic bioremediation)

activities can stall, even though available carbon and functional contaminant-degrading communities are present (138).

Enhanced bioremediation, or biostimulation, supplements limiting electron acceptor and/or inorganic nutrient concentrations within contaminated zones to stimulate biodegradation processes. A variety of *in situ* methods (and compounds) are available to deliver oxygen into the subsurface including air or oxygen sparging of groundwater (*i.e.,* biosparging), bioventing, groundwater recirculation, hydrogen peroxide, and commercially-available solid peroxides (*e.g.*, oxygen release compound [ORC®, magnesium peroxide] and PermeOx® [calcium peroxide]) (139-142). Nutrient addition is usually paired with groundwater recirculation systems where groundwater is extracted, amended with oxygen and nutrients, and reintroduced into the subsurface (140). The efficacy of enhanced bioremediation strategies is controlled by the rate and degree of electron acceptor and nutrient transport within contaminated zones. Subsurface heterogeneities and generation of low permeable zones by air bubble formation and entrapment (143), biofouling at the injection point (140), and precipitation of inorganic phosphate salts (143, 144) can significantly inhibit oxygen and nutrient migration.

Studies on the effects of nutrient addition on PAH biodegradation have yielded conflicting results; some have demonstrated enhanced PAH removal (24, 145) while others reported either no effect or decreased biological activity and PAH mineralization (144, 146). In general, aeration has been shown to have positive effects on the biodegradation of PAH-contaminated soils. Viñas et al. (23) reported slightly greater total petroleum hydrocarbon, chrysene, and benz[*a*]anthracene depletion after aeration without nutrient addition. Eriksson et al. (26) also observed higher degradation rates of low molecular weight PAHs in a former MGP soil following aeration.

Several studies have investigated microbial response pre- and post-nutrient amendment (147-149) and aeration (150, 151), although few have looked specifically at PAH-contaminated soil (23, 152). Viñas et al. (23) investigated the effects of aeration and nutrient addition on laboratory microcosms of slurried creosote-contaminated soil over a 200-d period. Changes in microbial

diversity and quantity were identified by denaturing gradient gel electrophoresis (DGGE) and most probable number analysis of heterotrophs and PAH-degraders, respectively. Enumeration of PAH-degraders was based on the presence/absence of color generated by partial oxidation of a spiked PAH mixture. The authors found a distinct shift in microbial diversity and an increase in microbial numbers (total and PAH-degrading), along with a concurrent decline in individual PAH concentrations. Ringelberg et al. (152) correlated a reduction in PAH levels with an increase in microbial community biomass (using ester-linked phospholipid fatty acid analysis) and genes encoding known PAH-degrading enzymes in bioreactor-treated sediment.

Despite showing a strong correlation between PAH decline and increased microbial activity, a direct link between microbial identity and metabolic function (*i.e.,* degradation of individual PAHs) was not established in the above studies. Isotopic techniques, such as stable-isotope probing (SIP), can bridge this gap and provide proof of PAH degradation by particular microbial species. To my knowledge, no study has investigated the effects of biostimulation on PAH degradation and indigenous microbial diversity while tracking SIP-identified PAH degraders under long-term continuous-flow conditions.

2.3.2.2 Anaerobic Biodegradation

Under anoxic conditions, electron acceptors other than oxygen (*e.g.,* nitrate, ferric iron, and sulfate) must be utilized by anaerobic (and facultative aerobic) microbial communities for compound oxidation and energy production. Since these electron acceptors yield less energy, rates of anaerobic PAH biodegradation are generally lower (one to two orders of magnitude) than aerobic metabolism (153-156), although exceptions have been documented (154).

Successful degradation of two- and three-ring PAHs has been documented under a variety of reducing conditions, including nitrate- (153, 154, 157-160), iron- (161), and sulfate-reducing conditions (162-168). However, anaerobic degradation of high molecular weight PAHs has demonstrated limited success, with metabolism of pyrene noted in only a few studies (154, 169) and

no reports of benzo[*a*]pyrene degradation (165). Most studies on anaerobic PAH degradation have used PAH-spiked soil and/or enriched cultures. Although these conditions can provide evidence for anaerobic PAH metabolism, they do not account for mass transfer and nutrient limitations common under field conditions. As a result, poor correlation between degradation rates of spiked and *in situ* PAHs is often observed (168).

Anaerobic conditions of various redox states can alter physicochemical properties of SOM and dissolved organic matter (DOM) and affect interactions with PAHs and other HOCs. DOM hydrophobicity, aromaticity, and molecular weight have been shown to increase under highly reducing conditions (*i.e.,* sulfate-reducing and methanogenic) relative to oxic controls, leading to increased sorption capacity for dissolved HOCs (170-173). Pravecek et al. (170) reported enhanced PAH concentrations in the aqueous phase following long-term (283 d) anaerobic incubation of MGP soil, relative to the oxic control; this observed enhancement of aqueous PAH concentrations was attributed to increased PAH-DOM associations. Furthermore, Pravacek et al. (170) found that the dissolved PAHs were subsequently available for aerobic biodegradation, suggesting that anaerobic conditions may play an important role in increasing the bioavailability and biodegradation potential of sorbed PAHs.

2.3.3 Coupling of Chemical Oxidation and Bioremediation

In many cases, implementation of ISCO at contaminated field sites does not lead to complete site closure (*i.e,* contaminant concentrations below regulatory guidelines), despite successful removal of large portions of the contaminant mass (13, 14). Insufficient oxidant delivery due to soil matrix heterogeneities, high SOM-reactivity, and gas production (*e.g.*, CO_2) can leave zones of residual contamination post-oxidation. Multiple applications of the oxidant are often made at targeted locations to reduce the potential for contaminant rebound, a phenomenon described by a steady increase in aqueous contaminant concentrations after oxidant depletion. Rebound can be attributed to slow mass transfer of residual contaminants from inaccessible micropores or low permeable zones,

resulting in continued long-term groundwater contamination (105, 174). Secondary treatment strategies such as natural attenuation or enhanced bioremediation can play an important role in reducing residual contaminant concentrations and mass transport from source zones. The goal in a combined or staged remediation effort would be to remove the bulk of the contaminant mass through aggressive treatments, in this case ISCO, while allowing biological processes to serve as a polishing step for remediation of residual contamination (12, 13).

Coupling of ISCO and bioremediation is complicated by the effects of oxidant exposure on the indigenous microbial community. Chemical oxidation can impact the activity and growth of microbes by changing biochemical conditions in the subsurface such as electron acceptor and substrate availability, temperature, and pH (105, 175). For example, low pH conditions (required to enhance the solubility of Fenton reagents or generated as a byproduct of permanganate and persulfate oxidation) can significantly reduce microbial growth and potentially affect microbial diversity following oxidant exposure (174). Oxidants and their reactive species are also highly toxic to microorganisms, directly attacking a variety of cellular components including DNA, proteins and amino acids, and membrane fatty acids (174, 176, 177). Buyuksonmez et al. (177) investigated the toxic effects of hydroxyl radicals produced during Fenton reactions on a pure culture of *Xantobacter flavus* (a known xenobiotic chemical-degrading bacterium) in aqueous systems. The results indicated that the bacterium was indeed sensitive to radical exposure; however, significant numbers of the bacterium remained following exposure. The capacity of the microbial community to rebound following oxidant injection is paramount to the long-term success of combined abiotic-biotic remediation.

Studies investigating the effects of ISCO on biological processes have focused primarily on Fenton's reagent (15-19) and permanganate (13, 14, 20, 21, 178) for the oxidation of chlorinated hydrocarbons and, to a lesser extent, PAHs. With the exception of two studies (13, 178), complete recovery or enhancement of the microbial community was observed post-oxidation. Increased microbial activity following oxidative exposure may be a function of 1) improved bioavailability of

substrates from contaminant- or SOM-oxidation, 2) reduced contaminant concentrations below toxic levels, 3) reduced microbial competition for nutrients or substrates, 4) die off of microbial predators, and/or 5) the generation of terminal electron acceptors (*e.g.,* SO_4^{2-} from $S_2O_8^{2-}$; O_2 from H_2O_2; Mn^{4+} from MnO_4^-) (105, 174). Preferential pathways and the presence of microbial microniches in heterogeneous soils also prevent direct contact between the oxidant and microbes and encourage microbial survival under harsh oxidative conditions (105).

For most of the above studies, microbial rebound was measured using biomass enumeration (*i.e.,* total bacterial counts) pre- and post-oxidation, rather than direct biological activity and the effects of ISCO on specific contaminant-degrading species and overall microbial diversity were generally not considered. To my knowledge, no study has investigated the effects of persulfate on specific PAH degraders and tracked their long-term recovery post-oxidation. Monitoring the relative abundance and activity of known PAH-degraders can provide valuable information for verifying *in situ* bioremediation before and after chemical treatment.

2.3.4 Implications of Molecular Tools on Bioremediation

A committee of the U.S. National Research Council proposed that three criteria be met to demonstrate active *in situ* bioremediation at a field site: 1) documented reduction of contaminant concentrations at the site, 2) laboratory assays confirming the presence of indigenous microorganisms capable of transforming the contaminants under expected site conditions, and 3) evidence that the biodegradation potential actually occurs in the field (179). Criteria 1 and 2 are fairly simple to demonstrate while criterion 3 is often more difficult to attain. Evidence for biodegradation potential in the field might include an increase in bacterial counts, the detection of metabolic intermediates, a decrease in electron acceptor concentrations, and agreement between theoretical and actual degradation rates. However, these analyses only provide circumstantial evidence of *in situ* bioremediation (180). Isotopic techniques such as SIP and carbon isotope fractionation have been used to provide more definitive proof of biodegradation activities at contaminated sites.

SIP is an emerging cultivation-independent technique for linking identity of microbial species to metabolic function. SIP involves the introduction of an isotopically labelled substrate (*e.g.,* ^{13}C) to a microbial community and the subsequent tracking of the heavy isotope in biomarker molecules (*e.g.,* lipids or nucleic acids) of metabolically active cells. Assimilation of the heavy isotope into new cells provides proof of substrate degradation by this particular microbial species (126, 181). Effective implementation of SIP for field-contaminated soil relies upon proper selection of incubation conditions. Maintaining field conditions as closely as possible during incubation minimizes artificial changes to the microbial community. Also, a lengthy incubation period can lead to assimilation of ^{13}C-intermediates by secondary degraders while a short incubation can result in insufficient biomarker labelling (126). Mineralization assays are often used to estimate the rate of biodegradation (*i.e.,* incubation duration) under SIP-incubation conditions. To date, SIP has been used to identify microorganisms responsible for degrading naphthalene (182, 183), phenanthrene (183), and pyrene (184, 185) in field-contaminated soils.

3 Recovery of Phenanthrene-Degrading Bacteria After Simulated *In Situ* Persulfate Oxidation in Contaminated Soil [1]

Stephen D. Richardson[2], Benjamin L. Lebron[3], Cass T. Miller and Michael D. Aitken

3.1 Abstract

A continuous-flow column study was conducted to investigate the long-term effects of persulfate oxidation on the abundance and activity of the indigenous microbial community and phenanthrene-degrading bacteria in contaminated soil from a former manufactured gas plant (MGP) site. Five pore volumes of a 20 g/L persulfate solution were introduced into the column, followed by simulated groundwater for 500 d. Soil samples were collected from the surface of the soil bed and along the column length immediately before and after persulfate injection and up to 500 d following injection. Exposure to persulfate led to a two- to three-log reduction in total bacterial 16S rRNA genes, severe inhibition of ^{14}C-acetate mineralization (as a measure of general microbial activity), and a decrease in community diversity. However, relatively rapid recovery of both bacterial gene abundance and activity was observed within 30 d after persulfate exposure. Mineralization of ^{14}C-phenanthrene was also inhibited but did not recover until 100 d post-oxidation. Known phenanthrene-degrading bacterial groups decreased to below detection limits throughout the column, with recovery times from 100 d to 500 d after persulfate injection. These findings suggest that coupling biological processes with persulfate oxidation is possible, although recovery of specific contaminant degraders may occur well after the general microbial community recovers. Furthermore, the use of total bacterial quantity or non-specific measures of activity as a surrogate for the recovery of contaminant

[1] Submitted to the journal of *Environmental Science and Technology* on July 16, 2010.
[2] Responsible for all chemical and molecular analyses of soil samples, data analysis, and manuscript preparation.
[3] Responsible for column operation, soil sample collection, and PAH extraction procedures during persulfate injection (pre-ox and t = 0).

degraders may be inappropriate for evaluating the compatibility of chemical treatment with subsequent bioremediation.

3.2 Introduction

Implementation of *in situ* chemical oxidation (ISCO) as the sole treatment strategy at contaminated field sites often does not reduce contaminant concentrations below regulatory guidelines, despite successful oxidation and transformation of large portions of the contaminant mass (13, 14). Insufficient oxidant delivery due to soil matrix heterogeneities, high oxidant reactivity with soil organic matter (SOM), and/or gas production can leave zones of residual contamination post-oxidation. Contaminant rebound, a phenomenon governed by slow mass transfer of contaminants from these residual zones, is generally responsible for continued long-term groundwater contamination after oxidant depletion (105, 174). Secondary treatment strategies such as natural attenuation or enhanced bioremediation can play an important role in reducing residual contaminant concentrations and may prove beneficial in a combined remediation scenario. The goal in a combined or staged remediation effort is to remove the bulk of the contaminant mass using aggressive treatments (such as ISCO), while allowing biological processes to serve as a "polishing" step for remediation of residual contaminant mass (12, 13).

Coupling of ISCO and bioremediation is complicated by the effects of oxidant exposure on the indigenous microbial community. Chemical oxidation can impact the activity and growth of microbes by changing conditions in the subsurface, such as the availability of an electron acceptor or substrate, temperature, and pH (105, 186). Oxidants and their reactive species can also be highly toxic to microorganisms, directly attacking a variety of cellular components (174, 176, 177).

Studies investigating the effects of ISCO on biological processes have focused primarily on Fenton's reagent (15, 17-19, 187) and permanganate (13, 14, 20, 21, 178) for the oxidation of chlorinated aliphatic hydrocarbons and, to a lesser extent, polycyclic aromatic hydrocarbons (PAHs) in spiked and field-contaminated soils. In the majority of previous studies, complete recovery or

enhancement of the overall microbial community was observed post-oxidation, in most cases within six months of oxidant exposure. Few studies, however, have investigated the effects of oxidant addition on specific contaminant-degrading microorganisms.

Persulfate is the newest and least-studied of the available oxidants, only recently receiving attention as an alternative oxidant for soil and groundwater remediation (106). The aqueous decomposition of persulfate anion ($S_2O_8^{2-}$) can be initiated by heat activation to form sulfate radicals ($SO_4^{-\bullet}$) (120, 125, 188), which react with a wide range of environmental contaminants (105), including PAHs (55, 117, 118). In soil, the resulting sulfate radicals are free to react with available contaminants, SOM, and microorganisms, and they can form other reactive species such as the hydroxyl radical ($OH^{\bullet}$), peroxymonosulfate (HSO_5^-), and hydrogen peroxide (H_2O_2) (121, 123). Subsequent reactions of $OH^{\bullet}$ and H_2O_2 ultimately yield molecular oxygen (120, 125).

Only one peer-reviewed study has examined the effects of persulfate on indigenous soil microorganisms. Tsitonaki et al. (189) exposed leachate-contaminated aquifer material to various doses of persulfate (0.02-2 g/kg) at 40°C and monitored changes in cell density and activity of the indigenous community using a standard viability assay and ^{14}C-acetate mineralization, respectively. To our knowledge, no study has investigated the effects of persulfate on specific PAH-degrading bacteria and tracked their long-term recovery post-oxidation in field-contaminated soil. We used cultivation-independent techniques to measure the quantity and activity of the total bacterial community and known phenanthrene-degrading bacteria in response to the injection of persulfate in a laboratory column packed with contaminated soil from a former manufactured gas plant (MGP) site. We focused on phenanthrene because it was the most predominant PAH in the soil.

3.3 Materials and Methods

3.3.1 Chemicals

Dichloromethane (>99.5%), acetone (>99.5%), acetonitrile (>99.9%), sodium sulfate (>99%), and sodium persulfate (>98%) were purchased from Fisher Scientific Inc. (Pittsburgh, PA).

Anthracene-d_{10} (98%) was purchased from Cambridge Isotope Laboratories (Andover, MA). [U-^{14}C] sodium acetate (97.1%; 56 mCi/mmol in ethanol) and [9-^{14}C] phenanthrene (>98%; 8.3 mCi/mmol in methanol) were purchased from Sigma-Aldrich (St. Louis, MO).

3.3.2 Soil

Contaminated soil was collected from a former MGP site in Salisbury, NC, USA. The soil was sieved through a 10-mm wire screen, mixed with sterile 40/50 grade silica sand (Unimin Corporation, Le Sueur, MN) at a 50:50 ratio (dry weight), and stored at 4°C prior to column packing. Addition of the silica sand was necessary to maintain low-pressure flow during long-term column operation; preliminary column studies with the source material yielded very high inlet pressures (>100 psi). Sand addition had minimal impact on the indigenous soil microbial community as evaluated by denaturing-gradient gel electrophoresis (DGGE; data not shown). In subsequent discussion, the final packing material is referred to as "column soil".

The column soil contained 83% sand, 14% silt, and 3% clay, with total organic matter of 8.3% as determined by a thermogravimetric method (190) and extractable organic matter of 0.64%. The total concentration of the PAHs analyzed was 295 ± 65 mg/kg dry soil (n = 33), with phenanthrene comprising 44% of the total PAH mass (129 ± 31 mg/kg). A complete list of physical properties and PAH concentrations for the column soil is presented in the Appendix A (Tables A1 and A2).

3.3.3 Simulated Groundwater

Simulated groundwater was prepared based on historical ion concentrations of groundwater in the region of the MGP site (191). The solution contained 1.83 g $CaCl_2 \cdot H_2O$, 1.01 g $MgSO_4 \cdot 7H_2O$, 2.19 g $NaHCO_3$, 1 ml of an 88 mg/L KCl solution, and 1 ml of 1 N H_2SO_4 in 20 L of sterile-filtered reagent water. New batches of groundwater were prepared weekly to limit the potential for bacterial growth in the column feed lines. The groundwater in the feed reservoir was equilibrated with the atmosphere and therefore was air-saturated when it entered the column.

3.3.4 Column Design, Operation and Analyses

The experimental apparatus consisted of a 110 cm long, 10.2 cm diameter stainless steel column containing a 100-cm bed of column soil, underlain by a 5-cm sand layer (details of the column design are in Appendix A, Figures A1 and A2). Groundwater was continuously pumped through the column at a flowrate of 1.1 L/d in a downward direction. Three evenly spaced ports (Ports A, B, and C) were positioned 30, 55, and 80 cm below the top of the column, respectively, for periodic collection of 50 g (dry wt.) soil samples. Nine additional smaller ports for monitoring porewater dissolved oxygen (DO) concentrations were located along the column length. Each DO port housed a dedicated stainless steel cannula, which spanned the column diameter and was screened along its length; each port was sealed with a septum and stainless-steel nut. The column was continuously operated at 20°C for eight months prior to persulfate injection ('equilibration phase') to allow for bed consolidation and inlet pressure stabilization.

The column was relocated to a 40ºC constant-temperature room to initiate persulfate anion activation during persulfate injection; several studies (109, 115, 121) have shown that temperatures above 30°C offer significant improvement in persulfate activation and contaminant oxidation under laboratory conditions. Five pore volumes of a 20 g/L persulfate solution were pumped through the column over a 16-d period. The selected activation temperature and persulfate dose were determined based on preliminary batch experiments (Appendix B, Figure B1). After persulfate injection, continuous pumping of simulated groundwater was resumed in a 20°C constant-temperature room. Samples from the soil-bed surface and soil sampling ports were collected at five time points: immediately before ("pre-ox") and after (t = 0) persulfate injection and 30, 100, and 500 d following persulfate injection. Samples were collected in 30-mL glass centrifuge vials and centrifuged for 15 min at 2,800 *g*, after which the supernatant was discarded. Aliquots of the centrifuged sample were used for PAH extraction and quantification, mineralization assays, DNA extraction and quantification, and moisture content determination.

Detailed information on PAH extraction and quantification and mineralization assay procedures are in Appendix B. Briefly, aliquots of centrifuged column soil (5 g wet wt. each) were transferred to triplicate 30-mL glass centrifuge vials for solvent extraction of PAHs (using dichloromethane and acetone) and subsequent PAH quantification by high-pressure liquid chromatography (HPLC). For mineralization assays, 5 g (wet wt.) of centrifuged column soil was transferred to an acid-washed 30-mL glass vial and slurried with 20 mL of sterile simulated groundwater as a source of inoculum for mineralization incubations. Assays with each sample were performed in triplicate. Each replicate consisted of a 40-mL amber EPA vial containing 1 mL of soil slurry, 4 mL of sterile simulated groundwater, a sterile glass tube containing filter paper saturated with 60 µL of 2 N KOH, and 1 µL of the radiolabelled substrate, corresponding to 20,000 disintegrations per min (dpm) for ^{14}C-acetate and 30,000 dpm for ^{14}C-phenanthrene. Triplicate killed control incubations were prepared similarly but were amended with 40 µL of phosphoric acid to reduce the pH below 2. ^{14}C-acetate was selected as a general carbon source to monitor activity of the total community (18, 189) and ^{14}C-phenanthrene was chosen to monitor phenanthrene-degrader activity.

A FOXY fiber-optic oxygen sensor system (Ocean Optics, Dunedin, FL) was used to measure DO concentrations in the column porewater (detection limit 0.1 mg/L) over the course of the experiment, except during persulfate injection. The DO sensor was inserted through a sterile hypodermic needle that was used to pierce the septum on each DO port, and it was rinsed with ethanol between measurements. Aqueous persulfate concentrations were monitored in the column effluent using a spectrophotometric method (115).

3.3.5 Molecular Analyses

DNA was extracted in triplicate using a Qbiogene (Solon, OH) FastDNA SPIN Kit according to the manufacturer's instructions. All extractions were performed immediately following column sampling to preclude the effects of soil storage on the microbial community. The mass of DNA in each replicate was quantified with a Nanodrop™ ND-3300 fluorospectrometer (Nanodrop

Technologies, Wilmington, DE) after adding Picogreen® dsDNA fluorescent indicator dye (Invitrogen; Carlsbad, CA).

Real-time quantitative PCR (qPCR) was performed to measure the abundance of total bacterial 16S rRNA genes and 16S rRNA genes from known phenanthrene-degrading bacterial groups. Primers are listed in Table B1 of Appendix B. Aliquots (1 μL) of pooled triplicate DNA (total volume 300 uL) from each sample were combined with the desired primers, SYBR® Green PCR master mix, and RNase-free water and run on a SmartCycler® qPCR system (Cepheid, Sunnyvale, CA) according to the manufacturer's instructions. Triplicate qPCR runs were performed for each primer set and the gene copy number was quantified only within the linear range of the respective standard curve.

Changes in microbial diversity after persulfate oxidation were monitored by DGGE as previously described (192), except a 6% polyacrylamide gel with a denaturant range of 35-65% was used for band separation and a non-denaturing stacking gel was used. A band that included members of a known PAH-degrading group, "Pyrene Group 1" (PG1) (183, 193), was identified by a separate DGGE analysis of clonal sequences phylogenetically related to this group.

To identify dominant bacterial groups before and after persulfate injection, clone libraries of 16S rRNA genes were constructed from surface soil DNA extracts from the pre-oxidation sample and 100 d post-oxidation. PCR amplification, cloning, and sequence analysis procedures are outlined in the Appendix B. Partial 16S rRNA gene sequences recovered from this work were submitted to GenBank with accession numbers HM622160-HM622262.

3.3.6 Statistical Analyses

Cohen's maximum likelihood estimator method (194) was used to estimate mean and standard deviations for qPCR samples where one or more replicates were below detection. All other statistical analyses were performed using JMP® 7.0.1 (SAS Institute Inc., Cary, NC).

3.4 Results

3.4.1 Persulfate Breakthrough

Based on the persulfate breakthrough data (Appendix B, Figure B2), approximately 37% of the injected persulfate mass was consumed within the column, which corresponds to an oxidant demand of 9.9 mg persulfate per g dry column soil. Batch experiments yielded a higher persulfate demand (14.5 ± 0.9 mg/g, n = 6) under continuously mixed, slurried conditions (Appendix B). Effluent pH gradually decreased from 7.0 to 3.2 after 16 d of continuous persulfate injection but returned to neutral after persulfate was flushed from the column.

3.4.2 DO Profile

A DO front formed during the eight-month equilibration phase (prior to persulfate injection) that extended to Port A (Appendix B, Figure B3a), 30 cm below the top of the column and approximately 25 cm below the original top of the soil bed. Oxygen concentrations were ≤ 0.1 mg/L in the remainder of the column. Oxygen was detected throughout the column within 12 d after persulfate injection, most notably in the former anoxic region, at concentrations ranging from 2.8 to 6.9 mg/L (Appendix B, Figure B3b). In subsequent measurements (75, 137, 220, and 495 d post-oxidation), DO concentrations gradually decreased in this region, presumably as oxygen was consumed by the recovering community.

3.4.3 Microbial Activity

Pre-oxidation mineralization experiments with the surface soil revealed a community capable of mineralizing both ^{14}C-acetate and ^{14}C-phenanthrene extensively within 15 d (75% and 60%, respectively) (Figure 3.1). Substantial mineralization (48-52%) of ^{14}C-acetate was also observed at Ports A, B, and C, while less than 10% of ^{14}C-phenanthrene was mineralized by samples from these ports. Immediately after persulfate injection, mineralization of both compounds was strongly inhibited at all sample locations. After 30 d, ^{14}C-acetate mineralization recovered to near pre-oxidation levels, while ^{14}C-phenanthrene mineralization remained low (<5%). Full recovery of ^{14}C-

phenanthrene mineralization activity was not observed until 100 d post-oxidation in the surface soil, along with enhanced mineralization at Ports A, B, and C (where pre-oxidation activity was negligible).

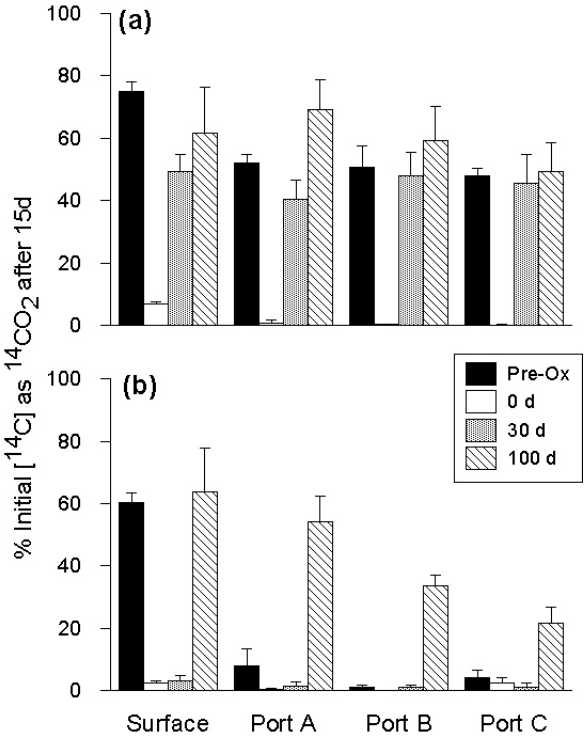

Figure 3.1. Mineralization of ^{14}C-acetate (a) and ^{14}C-phenanthrene (b) by the soil microbial community at each column sampling location before persulfate injection, immediately after injection (0 d) and 30 and 100 d post-injection. Values represent the means and standard deviations of triplicate incubations.

In supplemental batch experiments neither an increase in temperature from 20°C to 40°C nor addition of SO_4^{2-} (which would be generated from $SO_4^{-\bullet}$ decomposition) inhibited mineralization of ^{14}C-acetate or ^{14}C-phenanthrene (Appendix B, Figure B4).

3.4.4 Molecular Analyses

Clone libraries of 16S rRNA genes were constructed to identify dominant bacterial groups in DNA extracted from the surface soil before and 100 d after persulfate injection (corresponding to recovery of phenanthrene mineralization activity). A total of 109 partial 16S rRNA gene sequences were obtained from the two libraries (44 pre-oxidation and 65 post-oxidation). Five suspected chimeric sequences were excluded from further analyses. Clones were grouped at the >99% similarity

level to define 13 operational taxonomic units (OTUs), with an additional 17 singleton clones. Phylogenetic relationships among the OTUs and select singleton clones are illustrated in Figure 3.2. A phylogenetic tree showing all sequences is provided in Appendix B (Figure B5).

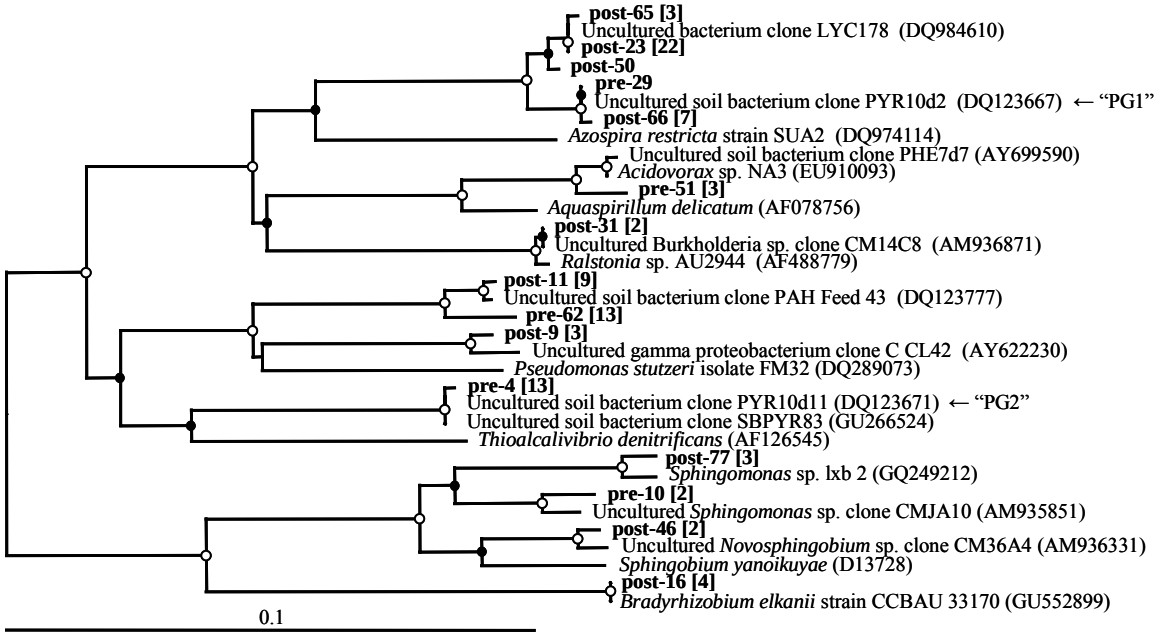

Figure 3.2. Neighbor-joining phylogenetic tree of 16S rRNA gene sequences recovered pre- and post-oxidation (100 d) from the column surface soil and selected close relatives. Clones from this study (in bold) follow the naming scheme of "pre" (pre-oxidation) and "post" plus an assigned number for identification purposes. Square brackets (in bold) include the number of sequences within an OTU represented by the clonal sequence shown. GenBank accession numbers are shown in parentheses for the selected reference sequences. Bootstrap values are indicated on nodes with an open (○) and closed (●) circle representing ≥95 and ≥50% bootstrap support, respectively. *Thermus aquaticus* YT-1 (L09663) was used as an outgroup (not shown). Sequences associated with groups PG1 and PG2 are indicated with an arrow.

Before persulfate addition, the majority of cloned sequences (62%, 26 of 42) were associated with γ-Proteobacteria. Two of the OTUs each accounted for 31% (13 of 42) of the total clones in the pre-oxidation sample. One OTU (represented by clonal sequence "pre-4") was closely related to members of uncultivated "Pyrene Group 2" (PG2), a group of bacteria previously implicated in pyrene (183) and phenanthrene (193) degradation in a bioreactor treating a different MGP soil. The second OTU (represented by clonal sequence "pre-62") was closely related to an uncultivated bacterial group (clonal sequence "PAH-Feed-43") found in untreated MGP soil from an earlier study

(183). Members of other known PAH-degrading groups were present, including *Acidovorax* spp. and *Sphingomonas* spp., but each were minor members of the total community.

Post-oxidation, cloned sequences were predominantly β-Proteobacteria (59%, 36 of 61). An OTU (represented by clonal sequence "post-23') containing sequences closely related to the uncultivated clone LYC178 (GenBank entry DQ984610) from oil-contaminated soil comprised 41% (25 of 61) of the clones in the post-oxidation library. Unfortunately, no published information on Genbank entry DQ984610 is available for comparative purposes. Sequences related to PG1 (represented by clonal sequence "post-66"), another uncultivated group of organisms associated with pyrene (183) and phenanthrene (193) degradation, comprised 11% (7 of 61) of the post-oxidation clone library. The dominant members of the pre-oxidation library appeared adversely affected by the addition of persulfate. The relative abundance of clones related to clone PAH-Feed-43 decreased to 15% (9 of 61) in the post-oxidation community, while no clones related to PG2 were recovered. Other genera associated with PAH degradation were identified in low abundances 100 d after persulfate injection, including members of the *Sphingomonas*, *Novosphingobium*, and *Ralstonia* genera.

The 16S rRNA gene copy numbers of total bacteria and groups PG1 and PG2 were tracked for all sample locations and time points by qPCR. Pre-oxidation, total bacterial abundance was greatest at the soil-bed surface ($6.2 \pm 2.4 \times 10^8$ genes/g dry soil) and declined with depth (Figure 3.3). Following persulfate injection, a two- to three-log reduction in total bacteria was observed at all sample locations, with surface soil abundance below the detection limit of 3×10^5 genes/g. By 30 d post-oxidation, the bacterial community had recovered substantially, approaching pre-oxidation levels (10^7-10^8 genes/g) at all sample locations. Quantification of DNA mass yielded a similar recovery pattern within 30 d post-oxidation (Appendix B, Figure B6).

The 16S rRNA genes associated with the known PAH-degrading groups PG1 and PG2 were most abundant in the upper section of the column pre-oxidation, with surface soil concentrations of $7.6 \pm 0.7 \times 10^7$ and $1.2 \pm 0.2 \times 10^8$ genes/g, respectively (Figure 3.3). Group PG2 sequences were more abundant at Ports A and B than were group PG1 sequences. Immediately following persulfate

injection, PG1 and PG2 sequences were not detected at any sample location and remained below detection at 30 d, even though recovery of total bacteria had been established. Recovery of PG1 organisms was first observed at 100 d post-oxidation in the surface soil and at Ports A and B, with concentrations above the respective pre-oxidation levels, and they were eventually detected at Port C 500 d post-oxidation. Group PG2 organisms required additional time to re-establish, achieving near pre-oxidation levels or greater at all sample locations 500 d post-oxidation.

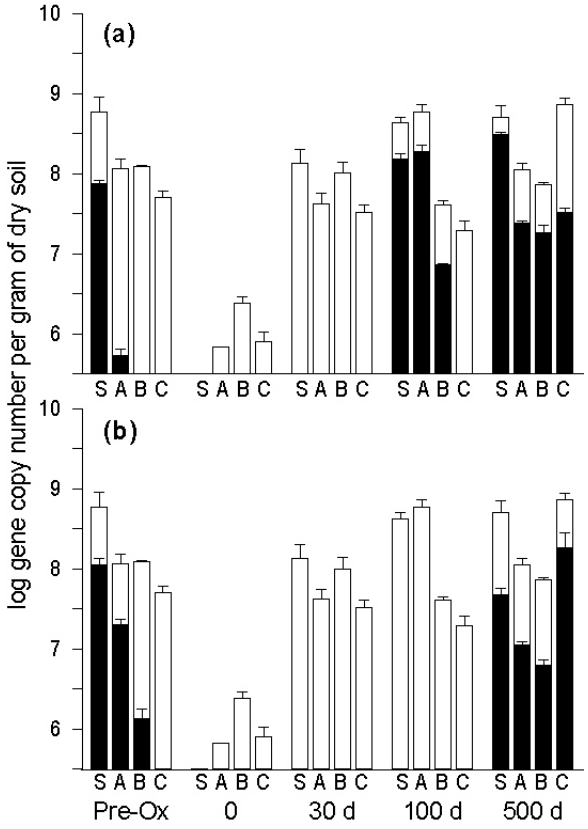

Figure 3.3. Abundance of 16S rRNA gene sequences representing groups PG1 (a) and PG2 (b) in the column soil pre- and post-oxidation (black bars), relative to total bacterial abundance (white bars). Values represent the log-transformed mean and standard deviation of triplicate qPCR runs of pooled DNA extracts. The minimum value on the y-axis is the average quantification limit for all primer sets (3 x 10^5 genes/g). Samples from the soil bed surface and column sampling ports are designated S, A, B and C, respectively.

Microbial community profiles as determined by DGGE analysis of 16S rRNA genes are illustrated in Figure 3.4. Clear differences in the pre-oxidation community (lanes 1-4) were observed over the column depth. Consistent with the data shown in Figure 3.3, the intensity of the DGGE band associated with group PG1 decreased between the surface and Port A, and was not observed at Ports

B and C. It was not possible to identify a single band associated with group PG2 because sequence variations among PG2-related clones resulted in two distinct DGGE bands (not shown). The transitional community observed at Port A (Figure 3.4, lane 2) coincided with the boundary of the pre-oxidation DO front (Appendix B, Figure B3a). Immediately after persulfate injection, DGGE profiles (Figure 3.4, lanes 5-8) were similar with depth but appeared less diverse than in the pre-oxidation samples, exhibiting only a few strong bands. At 30 and 100 d post-oxidation, community diversity increased and some differences among sample locations were re-established. Of particular note was the rebound of group PG1 in the surface soil and at Port A (Figure 3.4, lanes 13 and 14) and its appearance at Port B (lane 15), which corresponds well with qPCR results (Figure 3.3a).

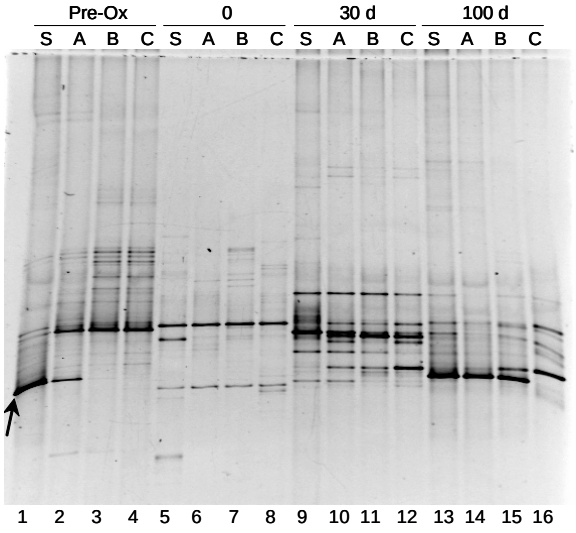

Figure 3.4. Negative image of DGGE gel delineating 16S rRNA genes pre- and post-oxidation (0, 30, and 100 d) at the surface soil (S) and Ports A, B, and C. Gel lanes were arranged according to column depth for each time point as follows: pre-oxidation (lanes 1-4), immediately post-oxidation (lanes 5-8), 30 d post-oxidation (lanes 9-12) and 100 d post-oxidation (lanes 13-16). The location of the band corresponding to group PG1 sequences is indicated with an arrow.

3.4.5 Soil PAH Concentration

Significant reductions (p <0.05) in PAH concentrations (mainly three- and four-ring PAHs) were observed at the surface soil (59% of total PAHs) and Port A (26% of total PAHs) during the column equilibration phase, as a result of continuous dissolution and aerobic biodegradation within the DO front (Appendix B, Figure B7). Phenanthrene concentrations were reduced by 74% and 28%

in the surface soil and at Port A, respectively, although the reduction was not statistically significant (p >0.05) at Port A. No significant differences (p >0.05) in PAH concentrations were noted at Ports B and C (within the anoxic zone of the column). The injection of persulfate, however, had little impact on PAH concentrations at all sample locations, with only acenaphthene and anthracene (at Port B) exhibiting significant reductions in concentration after the persulfate injection period (Appendix B, Figure B7). This observation is in contrast to the results of batch efficacy tests, in which up to 47% of total PAHs were removed over a 16-d incubation (Appendix B, Figure B2). Phenanthrene concentrations were not statistically different (p >0.05) pre- and post-oxidation at all sample locations.

3.5 Discussion

Exposure to persulfate had a major impact on the total microbial community in the column soil, as evidenced by a two- to three-log reduction in total bacterial abundance, inhibition of ^{14}C-acetate mineralization, and a decrease in community diversity after injection. However, this adverse effect was short-lived, with near-complete recovery (both in bacterial 16S rRNA gene abundance and acetate-mineralization activity) observed at all sample locations within 30 d after persulfate exposure. Chapelle et al. (18) reported similar results in a field-scale application of Fenton's reagent, where bacterial counts and ^{14}C-acetate mineralization declined and subsequently recovered within six months of oxidant injection. Other microbial exposure studies with Fenton's reagent (15, 187), permanganate (178), ozone (195), and steam injection (12) reported substantial reductions in bacterial counts with moderate to complete recovery following treatment. Explanations for the observed microbial recovery (105, 174, 196) have included improved bioavailability of intermediate substrates from the oxidation of contaminants or SOM; introduction of new organisms from upgradient groundwater; reduced contaminant concentrations below toxic levels; die-off of microbial predators; and/or the generation of terminal electron acceptors. Preferential flow pathways and the presence of microbial microniches in heterogeneous soils can also reduce direct contact between the oxidant and

microbes, allowing microbial survival under harsh oxidative conditions (105). In contrast, Tsitonaki et al. (189) found little effect of heat-activated persulfate (0.02-2 g/kg) on cell density, with reductions in ^{14}C-acetate mineralization activity observed only at the highest persulfate dose. The decrease in activity was attributed to a drop in pH following persulfate addition, which may have interfered with acetate metabolism. Persulfate doses used in their work were also much lower (one to three orders of magnitude) than in this study, which might explain the differences in microbial response to persulfate exposure.

Phenanthrene mineralization activity and the abundances of known PAH-degrading bacterial groups, PG1 and PG2, were greatly impacted by persulfate exposure, requiring additional time to recover in comparison to the overall microbial community. This lag in recovery might reflect lower initial PG1 and PG2 concentrations in the pre-oxidation community, resulting in quicker recovery for those bacterial groups with larger initial populations. However, the fact that PG1 and PG2 organisms recovered at different times (despite having similar initial abundances in the surface soil) suggests that recovery time might also be a function of group-specific tolerance (or degree of sensitivity) to oxidative conditions and radical exposure.

3.5.1 Effects of Oxygen on the Microbial Community

Establishment of a DO front in the upper section of the column (due to continuous influx of air-saturated groundwater) appeared to influence community diversity with depth in the pre-oxidation soil, as evidenced by variations in DGGE banding patterns (Figure 3.4) and a decrease in PG1 and PG2 sequence abundance with depth (Figure 3.3). After persulfate injection, oxygen detected in the former anoxic region of the column (Appendix B, Figure B3b) may be attributed to persulfate decomposition and/or a decrease in oxygen demand due to microbial inactivation. The formation or penetration of oxygen may have helped stimulate post-oxidation recovery of groups PG1 and PG2, although variations in time between soil sampling events and DO measurements make it difficult to pinpoint this effect.

3.5.2 PAH Removal

The lack of PAH removal observed after persulfate injection may be attributed to reduced PAH availability compared to the preliminary, continuously mixed batch experiments. Bioavailability of PAHs may have been particularly low in the surface soil and Port A as a result of continuous dissolution and aerobic biodegradation of the most readily available fraction of the PAHs during the eight-month equilibration phase. An earlier study (55) found that persulfate was capable of oxidizing only the bioavailable fraction of PAHs in a variety of field-contaminated soils and sediments. These findings call into question the applicability of persulfate for the oxidation of highly weathered contaminants, as typically encountered at former MGP sites.

3.5.3 Implications for Field Applications

This study has illustrated that persulfate oxidation is compatible with subsequent bioremediation with respect to recovery of the overall microbial community and, more importantly, specific PAH-degrading bacterial groups in the soil matrix. A key finding was that complete recovery of phenanthrene-degrading bacteria took longer relative to the overall community, suggesting that rates of recovery of individual bacterial species are not equivalent. Differences in initial abundance, oxidative-stress resistance, and availability of preferred substrate and/or electron acceptors can impact microbial recovery, and hence diversity, post-oxidation. In terms of field application, these results suggest that the quantity or activity of total bacteria may be inappropriate as a surrogate measure of contaminant degrader recovery. Previous studies investigating coupled chemical-biological treatment have, in general, overlooked the effects of oxidation on specific contaminant-degrading bacteria.

3.6 Acknowledgments

We thank Randall Goodman and Glenn Walters for their help in the design and construction of the column apparatus and David Singleton for the reverse primer for group PG2. We also thank Maiysha Jones and David Singleton for their invaluable advice on molecular techniques. This work

was supported by the National Institute of Environmental Health Sciences (grant number 5 P42 ES005948).

4 Long-term Simulation of *In Situ* Biostimulation of Polycyclic Aromatic Hydrocarbon-Contaminated Soil

Stephen D. Richardson[1], Maiysha D. Jones[2], David R. Singleton[3] and Michael D. Aitken

4.1 Abstract

A continuous-flow column study was conducted to evaluate the long-term effects of *in situ* biostimulation on the biodegradation of polycyclic aromatic hydrocarbons (PAHs) in soil from a manufactured gas plant (MGP) site. Simulated groundwater amended with oxygen and inorganic nutrients was introduced into the column, and a second column receiving unamended groundwater served as a control. PAH and dissolved oxygen concentrations and microbial community profiles were monitored along the column length immediately before and at selected intervals up to 534 d after biostimulation commenced. Biostimulation resulted in significantly greater PAH removal than in the control condition (73% vs. 34%, respectively), with dissolution accounting for a minor amount of the total mass loss (~6%) in both columns. Dissolution was most significant for naphthalene, acenaphthene, and fluorene, accounting for >20% of the total mass removed for each. A known group of PAH-degrading bacteria, 'Pyrene Group 2' (PG2), was identified as a dominant member of the microbial community and responded favorably to biostimulation. Spatial and temporal variations in soil PAH concentration and PG2 abundance were strongly correlated to dissolved oxygen advancement, although there appeared to be transport of PG2 organisms ahead of the oxygen front. At an estimated oxygen demand of 6.2 mg O_2/g dry soil and a porewater velocity of 0.8 m/d, it took between 374 and 466 d for oxygen breakthrough from the 1-m soil bed in the biostimulated column.

---

[1] Responsible for column operation, sample collection, all chemical and molecular analyses of soil samples, data analysis, and manuscript preparation.

[2] Responsible for sample collection, DNA extraction, identification of dominant PAH-degrading bacterial groups (using stable-isotope probing) and associated primer design.

[3] Developed PG2 primer set and contributed to experimental design.

This study demonstrated that the presence of oxygen was the limiting factor in PAH removal, as opposed to the abundance and/or activity of PAH-degrading bacteria once oxygen reached a previously anoxic zone.

4.2 Introduction

Soil and sediments contaminated with polycyclic aromatic hydrocarbons (PAHs) are complex systems with multiple compound- , microbial- , and matrix-specific factors that can ultimately impact the success of bioremediation strategies (197, 198). For bioremediation to be effective, an adequate supply of bioavailable carbon (PAHs and other substrates), macro- and micro-nutrients, electron acceptors, and a well-established contaminant-degrading community must be present in the subsurface (26). However, PAH-contaminated field sites such as former manufactured gas plant (MGP) sites are frequently nutrient- and oxygen-limited (199). PAHs are also partitioned in various domains that limit their bioavailability, including soil organic matter (SOM), nonaqueous phase liquids such as oil or tar, pitch, and black carbon such as coal, coke, and soot (22, 200). These limitations lead to reduced PAH biodegradation and continued long-term dissolution and transport of PAHs in the saturated subsurface (199, 201).

Enhanced bioremediation strategies such as biostimulation can be used to supply nutrients, oxygen, and other amendments to the subsurface for stimulation of indigenous microbial activity and contaminant biodegradation (137, 202, 203). The benefits of adding oxygen and/or nutrients on PAH biodegradation have been well-documented in laboratory studies of former MGP and wood-preserving site soils (24, 26, 145, 204-206); however, only a few studies have focused on the direct effects of biostimulation on the indigenous microbial community and PAH-degrading bacteria (23, 152). Viñas et al. (23) used denaturing gradient gel electrophoresis (DGGE) and most-probable number analyses to detect distinct shifts in microbial diversity and an increase in PAH-degrading bacteria, respectively, along with a concurrent decline in individual PAH concentrations after 200 d of nutrient amendment and aeration in slurried creosote-contaminated soil. Likewise, Ringelberg et al.

(152) correlated a reduction in PAH levels with an increase in microbial community biomass (using ester-linked phospholipid fatty acid [PLFA] analysis) and genes encoding known PAH-degrading enzymes in bioreactor-treated MGP sediment. Although such *ex situ,* continuously-mixed slurry systems can improve PAH bioavailability and the distribution of oxygen and/or nutrients, the costs and space requirements associated with soil excavation can preclude their use at field sites. Numerous column studies have been conducted to investigate *in situ* PAH biodegradation, dissolution, and bioavailability, as well as transport of PAH-degrading bacteria (25, 207-214); however, artificially-contaminated soils and/or cultured PAH-degrading bacteria were used in most of these studies.

To our knowledge, no study has investigated the long-term efficacy of biostimulation for PAH removal and its effect on the indigenous microbial community and PAH-degrading bacteria in weathered MGP soil under *in situ* conditions. We operated two continuous-flow columns packed with soil from a former MGP site to monitor concurrent changes in soil- and aqueous-phase PAH concentrations and abundances of indigenous PAH-degrading bacteria for over 500 d; one column was subjected to continuous biostimulation and the other served as a control. Monitoring of dissolved oxygen (DO) over the column length permitted spatial and temporal correlation of soil PAH concentration and PAH-degrader abundance to DO advancement over time. Overall oxygen demand and transport of desorbed PAHs in the column effluents were also quantified.

A separate column experiment was conducted concurrently with the above study to investigate the long-term effects of imposed anaerobic conditions on PAH mobilization and bioavailability. Anaerobic incubation has shown promise in laboratory studies for potentially increasing PAH transport and bioavailability in weathered MGP soils (170, 213, 215). However, in the current study, no significant increase in aqueous PAH concentration or improved PAH removal and bioavailability was observed relative to the control column. To simplify the discussion, methods and results of the anaerobic column experiment are not presented in this chapter, but are included in Appendix C.

4.3 Materials and Methods

4.3.1 Chemicals

Dichloromethane (>99.5%), acetone (>99.5%), acetonitrile (>99.9%), and sodium sulfate (>99%) were purchased from Fisher Scientific Inc. (Pittsburgh, PA). Anthracene-d10 (98%) was purchased from Cambridge Isotope Laboratories (Andover, MA).

4.3.2 Soil

Contaminated soil was collected from a former MGP site in Salisbury, NC, USA and processed according to the method outlined in Appendix A. The processed soil contained 83% sand, 14% silt, and 3% clay, with total organic matter of 8.3% and extractable organic matter of 0.64%; physical properties of the processed soil are summarized in Appendix A. Total PAH concentration (sum of 14 of the 16 USEPA-regulated PAHs (4)) was 295 ± 65 mg/kg dry soil, with phenanthrene comprising 44% of the total PAH mass (Table 4.1). In subsequent discussion, the processed soil is referred to as 'column soil'.

Table 4.1. PAH concentrations in the column soil

PAH		No. of Rings	Concentration (mg/kg) [a]
Naphthalene	NAP	2	9.5 ± 4.2
Acenaphthene	ACE	3	11.9 ± 2.7
Fluorene	FLU	3	9.5 ± 2.0
Phenanthrene	PHN	3	129 ± 31
Anthracene	ANT	3	10.5 ± 2.2
Fluoranthene	FLA	4	25.2 ± 5.0
Pyrene	PYR	4	40.9 ± 7.8
Benz[*a*]anthracene	BaA	4	13.8 ± 3.0
Chrysene	CHR	4	14.0 ± 3.6
Benzo[*b*]fluoranthene	BbF	5	6.9 ± 1.7
Benzo[*k*]fluoranthene	BkF	5	4.2 ± 1.1
Benzo[*a*]pyrene	BaP	5	13.5 ± 4.2
Benzo[*g,h,i*]perylene	BgP	6	5.3 ± 1.6
Total			295 ± 65

[a] Values are presented as mean ± standard deviation (n = 33).

4.3.3 Simulated Groundwater

Groundwater for the biostimulated column was prepared by adding 1 ml of a nutrient stock solution, containing 59.4 g/L of NH_4NO_3 and 29.2 g/L of K_2HPO_4, to the recipe outlined in Section 3.3.3, yielding final nitrogen and phosphorus concentrations of 1.0 mg/L and 0.3 mg/L, respectively. The final feed solution for the biostimulated column was continuously sparged with pure oxygen. Unamended groundwater was continuously pumped through the control column. The control groundwater was equilibrated with the atmosphere and therefore was air-saturated when it entered the column. New batches of groundwater were prepared weekly to limit the potential for bacterial growth in the feed solutions.

4.3.4 Experimental Design

Details of the column design are presented in Appendix A. Briefly, each column was 110 cm long, 10.2 cm in diameter, and constructed of stainless steel. Each column contained a 100-cm bed of column soil underlain by a 5-cm bed of clean sand. The columns were operated for ~780 d in a constant-temperature room at 20°C, receiving a continuous supply of simulated groundwater in a downward flow direction. A flowrate of 2.1 L/d (corresponding to a porewater velocity [v] of 0.8 m/d) was maintained for ~630 d and subsequently reduced to 1.4 L/d (v = 0.5 m/d) to stabilize rising inlet pressures. Tracer tests using tritiated water were conducted to estimate the porosity, pore volume, and mean retention time for each column and to confirm the absence of flow short-circuiting (Appendix A, Table A5). Three soil sampling ports (Ports A, B, and C) were positioned 30, 55, and 80 cm below the top of each column, respectively, along with nine additional smaller ports for monitoring porewater DO concentrations. Both columns were operated under control conditions for eight months (‘equilibration phase’) to allow for bed consolidation, initial DO advancement, and stabilization of inlet pressures before biostimulation was initiated in one of the columns. Baseline data from the equilibration phase (inlet pressure, effluent pH, and flowrate) are provided in Appendix A (Table A3).

Soil samples were collected from the surface soil and Ports A, B, and C of the biostimulated and control columns at six time points: at the end of the equilibration phase (t = 0) and 31, 93, 184, 380, and 534 d after initiation of biostimulation. During each sampling event, approximately 170 g (dry wt.) and 50 g (dry wt.) of column soil were collected from the surface soil and each sample port, respectively, using dedicated stainless-steel core sampling devices, for extraction of PAHs and DNA. Sampling accounted for removal of approximately 15% of the initial soil mass from each column over the duration of the study.

4.3.5 PAH Analyses

Soil samples for PAH analysis were collected in 30-ml glass centrifuge vials, stored at 4°C, and extracted the following day using the extraction and quantification method outlined in Appendix B, except 3 g (wet wt.) aliquots of column soil were extracted and 5 g of sodium sulfate was added to each extraction vial. Of the 16 USEPA-regulated PAHs, acenaphthylene was not detected using this quantification method; dibenz[*a,h*]anthracene and indeno[1,2,3-*c,d*]pyrene were detected at concentrations near their respective method detection limit and are excluded from subsequent analyses. Total mass of PAHs remaining in each column after treatment was calculated by linear interpolation of t = 534 d PAH concentrations between sample locations and summing the resulting PAH masses from each column section. PAH concentrations at Port C were assumed to be representative of the soil between the port and the bottom of the soil bed.

Aqueous-phase PAH concentrations were monitored in the column effluents over time to estimate the contribution of dissolution to overall PAH removal. Samples were collected in 1-L acid-washed glass vessels and extracted using 47 mm C18 solid-phase extraction (SPE) disks (Empore™, 3M Inc., St. Paul, MN) according to USEPA Method 3535 (216). Prior to extraction, an internal standard (0.1 ml of 100 mg/l anthracene-d_{10} in acetonitrile) was added to each sample to measure the recovery efficiency of the extraction procedure. A 0.7 μm pore-size glass-membrane pre-filter (Whatman® GF/F, Sigma-Aldrich, St. Louis, MO) was placed above the C18 disk to retain any

suspended solids in the sample. After filtration of the 1-L effluent samples, the C18 disks and pre-filters were placed in separate 30-ml glass centrifuge vials with Teflon-lined caps and extracted with dichloromethane and acetone (10 ml each) per the PAH extraction method outlined in Appendix B, except sodium sulfate and glass beads were not added and the combined extracts were brought up to 100 ml with acetonitrile. PAHs were not detected in the pre-filter extracts for all sample locations and time points.

4.3.6 Oxygen Monitoring

A FOXY fiber optic oxygen sensor system (Ocean Optics, Dunedin, FL) was used to measure DO concentrations in the porewater of the biostimulated and control columns. The DO sensor was inserted through a sterile hypodermic needle that was used to pierce the septum on each DO port, and it was rinsed with ethanol between measurements. The oxygen demand of the column soil was calculated using oxygen breakthrough curves at DO ports where oxygen saturation corresponding to the introduced gas (oxygen or air) had been established. Specifically, the total oxygen mass advancing beyond a given port was subtracted from the oxygen mass influx and divided by the mass of dry soil above the selected port (see Appendix D for calculations).

4.3.7 Molecular Analyses

DNA extraction was performed on triplicate 0.5-0.7 g (wet wt.) aliquots of soil from each sample location using the same procedure outlined in Section 3.3.5. All extractions were performed immediately following column sampling to eliminate the effects of soil storage on the microbial community. Mass of DNA in the replicate extracts was measured using a NanoDrop ND-3300 Fluorospectrometer (ThermoScientific; Waltham, MA) and Quant-iT Picogreen dsDNA Kit (Invitrogen; Carlsbad, CA). Since DNA masses were similar among replicates, the triplicate extracts were pooled for subsequent molecular analyses. DGGE and qPCR were conducted, as previously described in Section 3.3.5, to monitor spatial and temporal changes in microbial diversity and specific PAH-degrading groups, respectively, in response to DO advancement within the columns. For qPCR,

the abundance of 16S rRNA genes from dominant naphthalene-, phenanthrene-, and pyrene-degrading groups previously identified in the processed Salisbury MGP soil by stable-isotope probing (SIP) (Maiysha Jones, personal communication) were measured. Primer sets used in this study are presented in Appendix B (Table B3). To limit the number of qPCR runs, detection of SIP-identified groups was first confirmed in Port A DNA extracts at select time points (0, 93, 380, and 534 d). If at least one cycle threshold (Ct) value for a given group-specific primer was within the linear range of the respective standard curve, duplicate qPCR runs were conducted for all sample locations and time points. However, if the Ct values for a given group fell outside of the linear detection range over all the time points, the SIP-identified group was considered below detection.

4.3.8 Statistical Analyses

The nonparametric Spearman rank statistical test (JMP® 7.0.1, SAS Institute Inc., Cary, NC) was used to identify pairwise correlations between three experimental variables: DO concentration, individual soil PAH concentration, and 16S rRNA gene copy number of a known PAH-degrading bacterial group, "Pyrene Group 2" (PG2) (183, 193). Spearman rank order analysis tests the hypothesis of no association between population datasets and indicates if any significant monotonic relationship (either increasing or decreasing) exists among the variables. The Spearman rank order coefficient (r_s) falls between -1 (perfectly negative correlation) and +1 (perfectly positive correlation). To account for the small number of data points (n=6) in the PAH and PG2 datasets, coefficients corresponding to p-values < 0.15 were considered to be significant. DO concentrations measured closest (in time) to each soil sampling event (n=6) were used for comparison to PAH and PG2 time-series data.

Outlier tests were performed on replicate soil extracts that contained any PAH concentration well above the respective concentration in the column soil (Table 4.1). Suspect values greater than the upper quartile of the initial column soil concentration by more than three times the interquartile range (the difference between the upper and lower quartiles) were deemed to be outliers and were excluded

from the data set; 20 out of 216 replicates were identified as outliers. Other statistical analyses (*i.e.*, Student *t*-test and, Tukey-Kramer Honestly Significant Difference [HSD] test) were performed using JMP® 7.0.1 (SAS Institute Inc., Cary, NC).

4.4 Results and Discussion

4.4.1 DO Profile

After the eight-month equilibration phase, DO fronts in the biostimulated and control columns were similar, extending 15-20 cm below the top of the column; oxygen concentrations were ≤ 0.1 mg/L in the remainder of the columns (Figure 4.1). Once oxygen-saturated groundwater was introduced (t = 0), DO concentrations in the biostimulated column rose sharply and advanced at a greater rate than in the control column, achieving breakthrough between 374 and 466 d. The DO front in the control column did not advance beyond 45 cm from the top of the column over the course of the study (Figure 4.1).

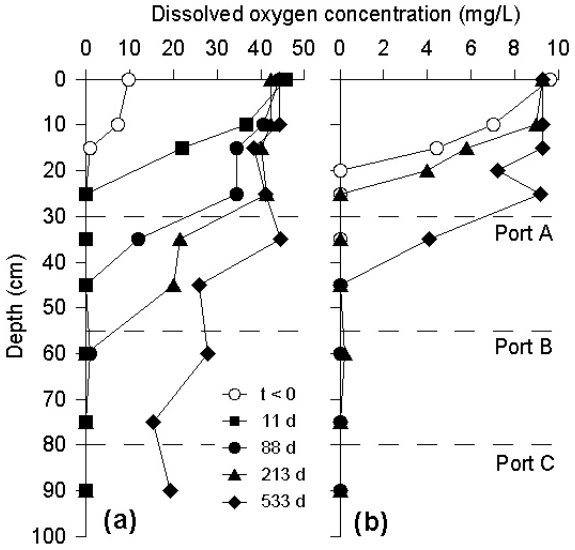

Figure 4.1. DO profiles of the biostimulated (a) and control (b) columns over time. Oxygen measurements at the end of the equilibration phase (t < 0) are denoted with open circles. Oxygen concentrations at the top of each column (depth = 0) were measured in the feed groundwater reservoir. Data for time points other than those shown are omitted for clarity. Note the different scales on the x-axes for the two panels.

Based on the DO penetration data, the oxygen demand of the column soil was estimated to be 6.2 ± 0.2 mg O_2/g dry soil in the biostimulated column and 4.9 ± 0.7 mg/g in the control column

(Appendix D). The theoretical oxygen demand of the 13 detectable PAHs accounts for 14% of the total oxygen demand exhibited in the biostimulated column soil.

4.4.2 Soil PAH Concentration

After 534 d, 73 ± 28% of the total PAH mass in the biostimulated column was removed as compared to 34 ± 24% in the control column (Figure 4.2). PAH mass remaining after treatment was significantly lower (p <0.05) in the biostimulated column for all PAHs except benzo[*g,h,i*]perylene. The majority of PAH mass removed during biostimulation consisted of three- and four-ring PAHs (86% and 66%, respectively), although 41% of the five-ring PAH mass was removed (Table 4.2). In the control column, total mass removals for three-, four- and five-ring PAHs remained below 40% (Appendix D, Table D1). Error associated with the percent removal values was the result of sample variability of the column soil and propagation of error in calculating total mass and percent removal of each PAH in the columns. PAH mass loss due to sampling ranged from 4-23% for all PAHs in both columns.

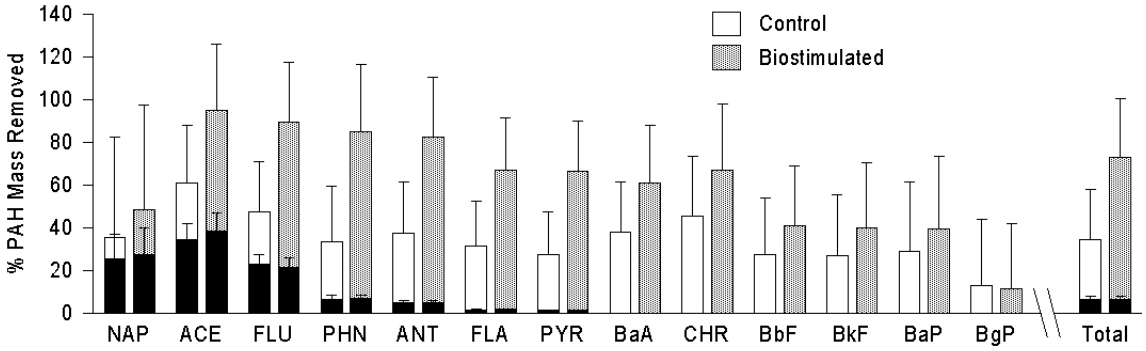

Figure 4.2. Percentage of PAHs removed from the biostimulated and control columns. Removal of a PAH by dissolution is represented by the black bars.

Time-series graphs of soil PAH concentration at all sample locations are summarized in Appendix D (Figures D2-5), with selected PAHs from Port A presented in Figure 4.3. PAH removal decreased with increasing depth in both columns, with greater removal observed in the biostimulated column at all sample locations. The greatest reduction in total PAH concentration occurred at Port A of the biostimulated column (80%), where three-, four-, and five-ring PAH concentrations were

significantly lower (p <0.05) than their respective initial column soil values after 534 d. At Ports B and C, PAH removal was lower (73% and 55%, respectively) and significant reductions (p <0.05) in concentration were limited to the three- and four-ring PAHs. In the control column, total PAH concentration at Port A decreased by 37%, with three-ring PAHs comprising the majority of the total PAH reduction. At Ports B and C, concentrations for all but two PAHs (acenaphthene and anthracene at Port C) were not statistically different than initial column soil values. PAH concentrations in the surface soil were highly variable for both columns, possibly due to soil heterogeneity resulting from the larger soil mass removed at each sampling event relative to the soil sampling ports; therefore, further discussion is limited to PAH results from Ports A, B, and C.

Table 4.2. Percentage of PAH mass removed by dissolution, sampling, and biodegradation in the biostimulated column after 534 d.

	Percent of PAH Mass Removed			
PAH [a]	Total	Dissolution	Sampling	Biodegradation [b]
NAP	48.5 ± 49.0	27.5 ± 12.1	12.9 ± 5.7	8.1 ± 50.8
ACE	95.1 ± 31.1	38.3 ± 8.6	4.3 ± 1.1	52.5 ± 32.3
FLU	89.3 ± 28.1	21.5 ± 4.5	5.8 ± 1.3	62.0 ± 28.4
PHN	84.9 ± 31.8	6.6 ± 1.6	7.1 ± 1.8	71.2 ± 31.9
ANT	82.4 ± 27.9	4.9 ± 1.0	7.4 ± 1.7	70.1 ± 28.0
FLA	67.1 ± 24.5	1.6 ± 0.3	10.5 ± 2.2	55.0 ± 24.6
PYR	66.6 ± 23.5	1.2 ± 0.2	10.3 ± 2.1	55.1 ± 23.6
BaA	60.9 ± 27.1	[c]	12.5 ± 2.9	48.5 ± 27.3
CHR	67.0 ± 31.2	[c]	14.6 ± 3.8	52.3 ± 31.4
BbF	40.8 ± 27.9	[c]	16.0 ± 4.1	24.7 ± 28.2
BkF	40.1 ± 30.2	[c]	15.7 ± 4.4	24.4 ± 30.5
BaP	39.2 ± 34.1	[c]	16.1 ± 5.1	23.0 ± 34.5
BgP	11.0 ± 31.0	[c]	22.6 ± 6.9	NA
Total	73.0 ± 27.7	6.5 ± 1.4	9.5 ± 2.2	56.9 ± 27.8
3-ring [d]	85.7 ± 31.4	9.7 ± 2.3	6.8 ± 1.7	69.1 ± 31.5
4-ring [d]	66.0 ± 24.5	[c]	11.3 ± 2.4	54.6 ± 24.7
5-ring [d]	40.7 ± 32.0	[c]	15.8 ± 4.7	24.8 ± 32.3

[a] See Table 4.1 for definitions of abbreviations.
[b] Calculated by subtracting percent dissolution and percent sampled from the percent total and accounting for error propagation; NA = calculated value was negative.
[c] Value was below detection.
[d] Represents the sum of the mass removed for PAHs with the same number of rings (Table 4.1); NAP and BgP are not included in these values.

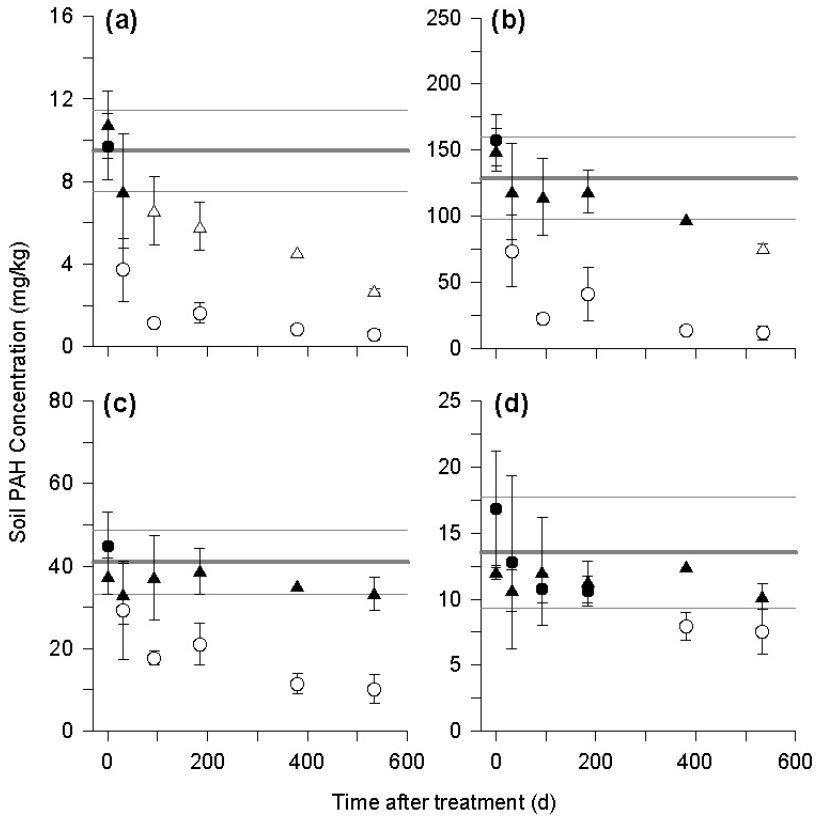

Figure 4.3. Time courses of fluorene (a), phenanthrene (b), pyrene (c), and benzo[a]pyrene (d) concentrations for soil samples collected from Port A of the biostimulated (●,○) and control (▲,Δ) columns. Each point represents the mean value of duplicate or triplicate samples and the error bars are the range or standard deviation, respectively. An open symbol represents an analyte concentration that is significantly different ($p < 0.05$) from the column soil concentration. Gray lines represent the mean and standard deviation of the PAH in the original column soil (Table 4.1).

Biostimulation also resulted in faster rates of PAH removal. At Port A, significant reductions ($p < 0.05$) in all three-ring PAHs, fluoranthene, and pyrene were observed after only 31 d of biostimulation (Figure 4.3 and Appendix D). Chrysene, benzo[*a*]anthracene, and the five-ring PAHs required longer treatment times (up to 184 d and 380 d, respectively) before concentrations significantly declined; no significant change in benzo[*g,h,i*]perylene concentration was observed. In the control column, only acenaphthene and fluorene significantly declined ($p < 0.05$) during early time (within 31 d and 93 d, respectively), while significant reductions of other three-ring and all four-ring PAHs were not observed until the last sampling event (534 d). Five- and six-ring PAH concentrations at Port A of the control column were not significantly different ($p > 0.05$) than respective initial column soil values over the course of the study (Figure 4.3 and Appendix D). At Ports B and C of

both columns, longer treatment times (relative to Port A) were generally required before reductions in PAH concentration were observed. PAH concentrations at Port C of the control column during the 380 d time point decreased unexpectedly (in some cases, lower than the respective biostimulated values) but subsequently returned to higher concentrations after 534 d; this decrease was attributed to soil heterogeneities.

Concentrations of all three-ring PAHs, fluoranthene, and pyrene at Port A of the biostimulated column appeared to 'plateau' after their initial rapid decline (Figure 4.3 and Appendix D). This biphasic pattern for PAH removal is frequently reported in field-contaminated soils and reflects variations in PAH bioavailability over time within various soil domains (200). The decreased rate of PAH removal associated with the 'plateau' region is indicative of mass transfer limitations and sequestration of less labile PAHs (63, 199).

4.4.3 Aqueous-Phase PAH Concentrations

Effluent PAH concentrations were monitored over time to estimate the contribution of PAH dissolution to overall PAH removal in each column. Naphthalene, acenaphthene, fluorene, phenanthrene, anthracene, fluoranthene, and pyrene were detected in the effluent samples, while higher-molecular-weight PAHs remained below detection in the effluent, consistent with other studies on PAH transport from MGP soils (217-219).

Time-series graphs of aqueous-phase PAH concentrations are provided in Appendix D (Figure D6), with selected PAHs presented in Figure 4.4. Of the detectable PAHs, phenanthrene was the most abundant in the column effluents during the equilibration phase. Aqueous-phase PAH concentrations gradually decreased in the column effluents over time, with naphthalene and fluorene concentrations below detection after 534 d; effluent naphthalene concentrations for the biostimulated column remained above the respective North Carolina Department of Environment and Natural Resources (NCDENR) groundwater standard of 6 μg/L (220) for up to 466 d. Although PAH concentrations in the biostimulated effluent were somewhat lower than in the effluent from the control column at later

time points, the total PAH mass leached from each column was essentially the same (6.5 ± 1.4% and 6.2 ± 1.4%, respectively) over the course of the study (Figure 4.2). Dissolution accounted for removal of >20% of naphthalene, acenaphthene, and fluorene in both columns. Overall, PAH dissolution generally decreased with increasing molecular weight of the compound, with the exception of naphthalene for both columns. The observed lower naphthalene percentage is likely due to its weathered state in the original MGP soil and subsequent volatilization during soil processing.

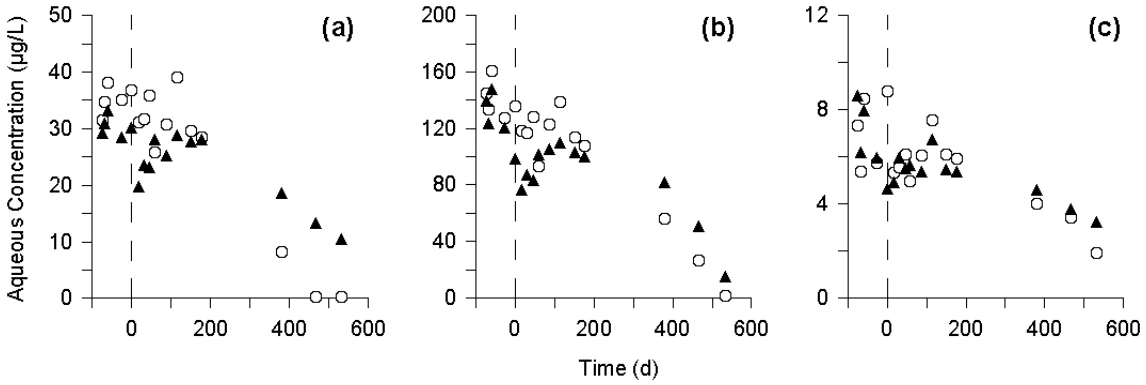

Figure 4.4. Fluorene (a), phenanthrene (b), and pyrene (c) concentrations in effluent samples collected from the biostimulated (○) and control (▲) columns over time. Time 0 (depicted with the vertical dashed line) refers to the time that biostimulation commenced. Data shown before t = 0 were from samples collected during the equilibration phase. Concentrations of BaA, CHR, BbF, BkF, BaP, DBA, and BgP were below detection.

Accounting for PAH losses due to sampling and dissolution, biodegradation appeared to be the primary mechanism of mass removal for all PAHs except naphthalene in the biostimulated column (Table 4.2). In the control column, however, dissolution accounted for greater mass loss of naphthalene, acenaphthene, and fluorene than did biodegradation (Appendix D, Table D1).

4.4.4 Effect of DO on PAH Removal

Reduction of PAH concentrations in the column soil corresponded well with advancement of the DO front in both columns. By the end of the eight-month equilibration phase, three-ring PAH removal was observed within the oxic zone of both columns, likely due to continuous dissolution and aerobic biodegradation (Appendix D, Figure D2). After biostimulation, significant correlations were identified between DO levels and individual PAH concentrations with depth using Spearman rank order analyses, as presented in Table 4.3. At Port A, the observed rise in DO concentration was

negatively correlated with concentration reductions for most of the PAHs. Rank coefficients (r_s) were higher for three- and four-ring PAHs because ranking analyses were skewed by variability associated with the 'plateau' regions of PAH and DO concentrations after 93 d. At greater depths, strongly negative correlations (r_s < -0.76; p <0.1) were identified for anthracene and all four-ring PAHs at Port B and all three- and four-ring PAHs at Port C. In the control column, negative correlations between DO and PAH concentrations were also identified at Port A; however, r_s values were not significant for most PAHs (data not shown). Rank order analyses were not performed on Port B and C datasets because oxygen was not detected at these depths in the control column. PAH and DO concentrations were poorly correlated at the surface soil of both columns since oxygenated conditions were well-established and significant removal of some PAHs had already occurred during the equilibration phase. Overall, these results suggest a strong correlation between the presence of oxygen in the porewater and reductions in PAH concentrations in the column soil. Other column studies have reported similar spatial distribution of contaminants with respect to oxygen presence/absence after short-term biosparging (221, 222).

Table 4.3. Spearman rank coefficients (r_s) representing significant correlations between individual PAH concentrations (mg/kg) and DO concentration (mg/L) in the biostimulated column.

	Spearman rank coefficients (r_s) with DO concentration [a]		
PAH [b]	Port A	Port B	Port C
ACE			**-0.85**
FLU	*-0.71*		**-0.78**
PHN	*-0.71*		**-0.78**
ANT	*-0.71*	**-0.76**	**-0.78**
FLA	*-0.71*	**-0.88**	**-0.78**
PYR	*-0.71*	**-0.76**	**-0.78**
BaA	**-0.83**	**-0.76**	**-0.82**
CHR	**-0.83**	**-0.76**	**-0.85**
BbF	*-0.71*		
BaP	**-0.83**		
BgP	**-0.77**		

[a] Only r_s values representing correlations with p < 0.15 are reported (p <0.05 in bold and underlined; 0.05< p <0.1 in bold; 0.1< p <0.15 in italics); r_s values with p > 0.15 are omitted for clarity; no significant correlations were identified in the surface soil.

[b] Spearman rank coefficients for NAP, BkF, and DBA were not significant at all sample locations and are, therefore, omitted from the table; see Table 4.1 for definitions of abbreviations.

4.4.5 Microbial Abundance and Diversity

Profiles of total bacterial 16S rRNA genes were obtained by DGGE analysis of DNA extracts from the biostimulated and control columns to identify any gross differences in the overall microbial community over time (Figure 4.5). Prior to biostimulation (t = 0), community profiles appeared more diverse in the surface soil of both columns (Figure 4.5; lane 1), each containing more prominent bands than respective communities at Ports A, B, and C (Figure 4.5; lanes 8, 15, and 22, respectively). After biostimulation, the surface soil community remained similar over time in both columns, with no major differences in the intensity or position of prominent bands (Figure 4.5; lanes 2-6). However, clear shifts in community profiles were observed at Ports A, B, and C in both columns at various time points. In the biostimulated column, a number of new bands that were prominent in the surface soil community appeared at Ports A, B, and C after 31, 93, and 184 d, respectively (Figure 4.5; lanes 9, 17, and 25). More subtle shifts in the control column communities occurred after 31 d at all sample ports (Figure 4.5, lanes 9, 16, and 23).

At the time this study was conducted, bacteria in the column soil that were capable of degrading naphthalene, phenanthrene and pyrene had been identified by SIP. Of these, only the group of organisms identified as the major pyrene-degrading bacteria in the soil (M. Jones, personal communication), referred to as PG2, was a significant component of the column soil community. All other SIP-identified PAH degraders were below the qPCR quantification limits (~3 x 10^5 genes/g). Prior to biostimulation, the quantity of 16S rRNA genes of PG2 organisms was greatest in the surface soil of both columns, with concentrations of 3.7 ± 1.2 x 10^7 and 3.4 ± 0.4 x 10^7 genes/g, respectively (Figure 4.6). Concentrations were lower at Port A and were near or below detection at Ports B and C in both columns. Total bacterial abundance was also greatest in the surface soil during the equilibration phase (~2 x 10^8 genes/g), up to an order of magnitude higher than in samples collected from Ports A, B, and C (Figure 4.6). During biostimulation, temporal trends in PG2 abundance in the surface soil and at Port A of both columns were generally consistent with those observed for the total bacterial community. In the biostimulated column (Figure 4.6a), concentrations of PG2 organisms in

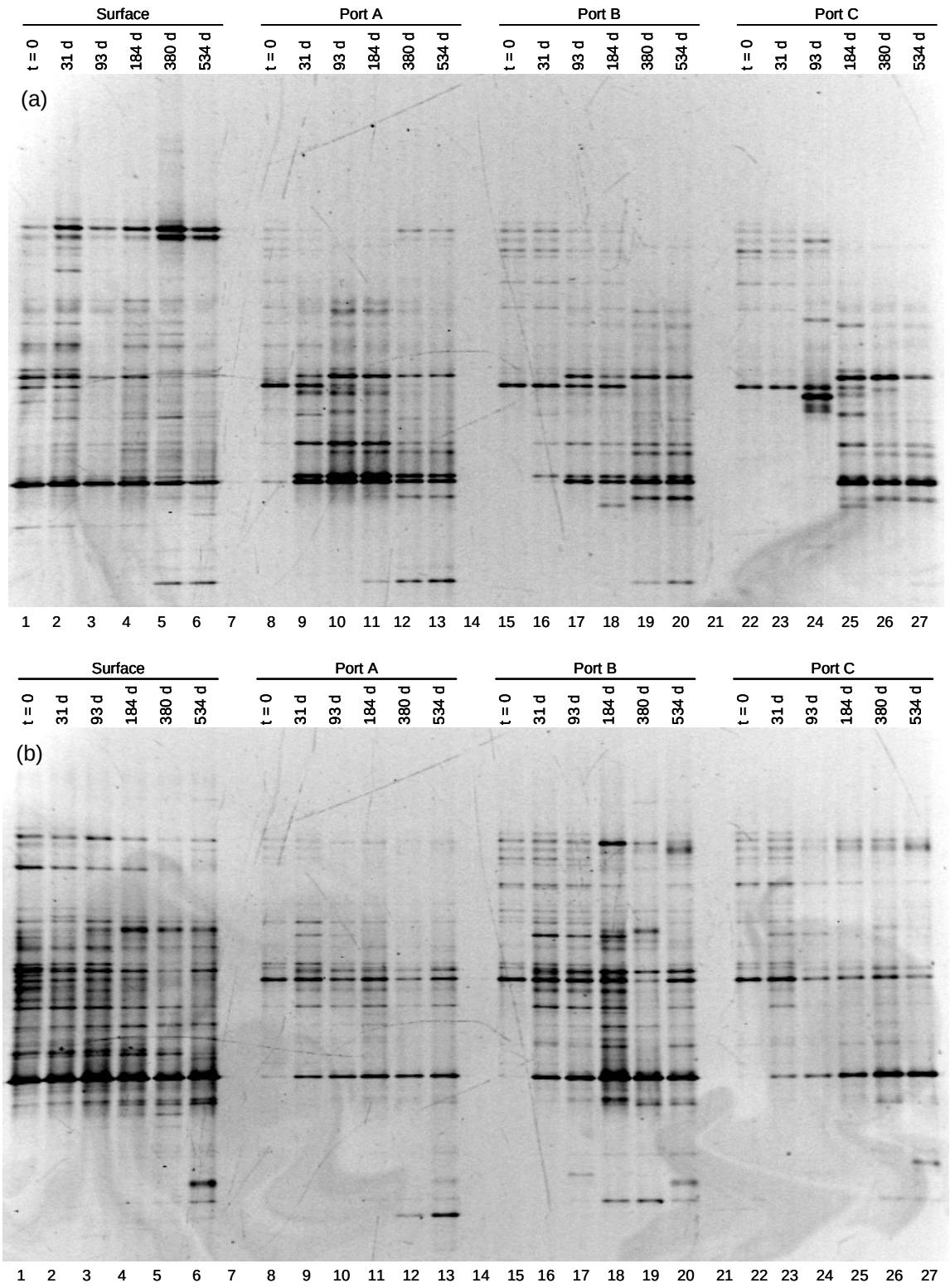

Figure 4.5. Negative image of DGGE gels for the biostimulated (a) and control (b) columns delineating 16S rRNA genes before (t = 0) and at the indicated sampling times after treatment at the surface soil (lanes 1-6), Port A (lanes 8-13), Port B (lanes 15-20) and Port C (lanes 22-27). Gel lanes 7, 14, and 21 were left blank for clarity.

the surface soil gradually decreased with time, whereas at Port A, PG2 organisms increased by 1.2-log over the first 93 d and subsequently decreased by an order of magnitude during the remainder of the experiment. In the control column (Figure 4.6b), PG2 abundances remained steady in the surface soil and increased by 1.3-log over time at Port A. The most significant changes in PG2 organisms, however, were observed in the lower section of the columns, at Ports B and C. In the biostimulated column, PG2 increased by at least two orders of magnitude at both ports after 534 d, with a delay of up to 184 d in PG2 detection at Port C. In the control column, PG2 was detected within 31 d at Ports B and C at concentrations substantially higher than those observed in the biostimulated column. After 534 d, PG2 concentrations in the biostimulated column were greater at Ports B and C than in the upper section (surface soil and Port A). In the control column, the abundance of PG2 organisms remained highest in the surface soil.

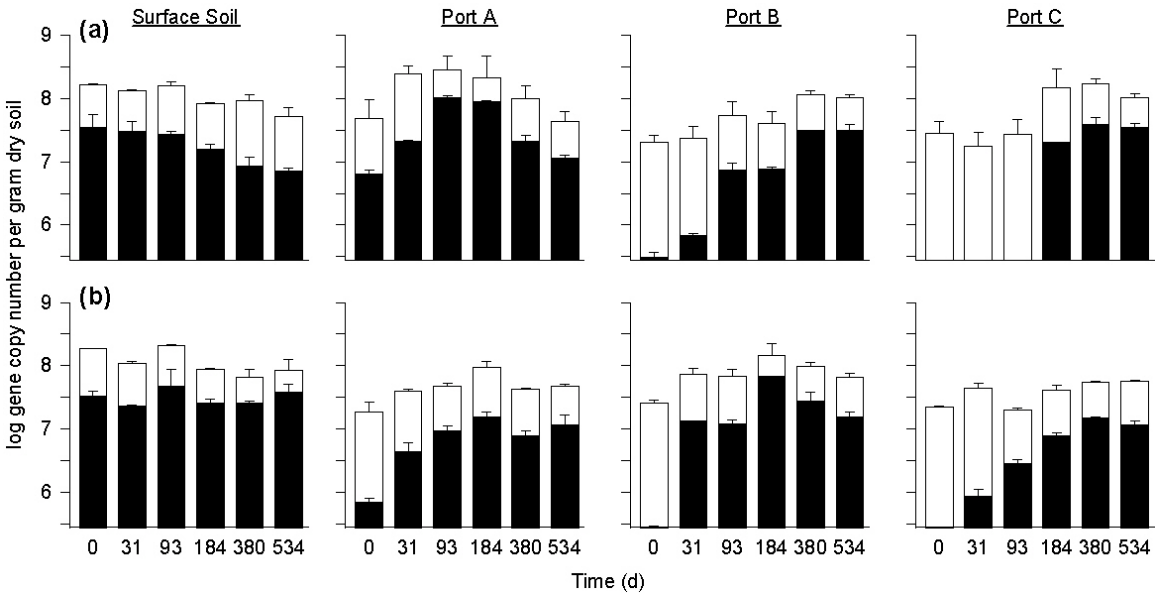

Figure 4.6. Abundances of 16S rRNA genes for total bacteria (white bars) and group PG2 (black bars) in the surface soil and at Ports A, B, and C for the biostimulated (a) and control (b) columns over time. Values represent the log-transformed mean and range of duplicate qPCR runs of pooled DNA extracts. The minimum value on the y-axis is the average detection limit for all primer sets (3 x 10^5 genes/g). Absent values were below detection.

4.4.6 Effect of DO on the Microbial Community

Establishment of a DO front during the equilibration phase appeared to influence community diversity in the columns, as evidenced by variations in DGGE banding patterns between the surface soil and ports (Figure 4.5) and a decrease in PG2 abundance with depth (Figure 4.6). After biostimulation, variations in PG2 abundance corresponded well with the advancing oxygen front and consumption of oxygen demand in the upper region of the biostimulated column. Based on an average oxygen demand of 6.2 mg O_2/g, oxygen demand of the soil above Port A was exhausted after ~200 d, which coincides with the initial decline in PG2 concentration after 184 d (Figure 4.6). Likewise, the gradual decrease in PG2 abundance in the surface soil might reflect a lack of available carbon to sustain growth (223, 224). In desorption studies reported in Chapter 5, PAHs were found to be significantly less available in the biostimulated soil than in the control at Port A after 534 d.

DO concentration was positively correlated to increases in PG2 abundance at Ports A, B, and C of the biostimulated column (Appendix D, Table D2), although PG2 was detected ahead of the advancing DO front at these ports. This suggests that bacterial transport from the upper region of the column may be a contributing factor to PG2 establishment with depth. Transport is also a likely explanation for the early detection (within 31 d) and subsequent increase in PG2 abundance at Ports B and C of the control column, given that this region was anoxic over the course of the study. Alternatively, oxygen introduced from extrusion of soil samples at these ports may have stimulated PG2 growth between sampling events; however, this seems unlikely since a similar rise in PG2 abundance was not observed at Port C of the biostimulated column. Anaerobic metabolism of other available substrates or biodegradation intermediates by PG2 bacteria is also a potential explanation for their detection at greater depths, although we would have expected substantial amounts of these organisms to be present during the equilibration phase if this were the case. Nevertheless, no representative of PG2 has yet been isolated in pure culture and, therefore, its physiology remains unknown.

Spearman rank analyses also identified a number of significant correlations between PG2 abundance and individual PAH concentrations in both columns (Appendix D, Table D3). In the biostimulated column, increases in PG2 abundance were negatively correlated to PAH reductions at Ports A, B and C, with significant correlations (r_s <-0.77, p <0.1) identified for three- and four-ring PAHs at Ports B and C. Significant correlations were identified at Port C in the control column for most PAHs (except naphthalene); however, these results were influenced by the unexpected drop in PAH concentration during the fifth sampling event (380 d) (Appendix D, Figure D5). Ringelberg et al. (152) also identified significant relationships (using Spearman rank analyses) between individual PAH concentrations and PAH-degrading bacteria in bioreactor-treated sediment. Specifically, reductions in three-ring PAHs correlated well with variations in abundance of PLFA-defined genera and genes encoding PAH-degrading enzymes over the three-month treatment period.

Phenanthrene and pyrene have been previously identified as growth substrates for PG2 organisms (183, 193) and recent SIP analyses of the original MGP soil have also implicated PG2 in the degradation of fluoranthene and benzo[*a*]anthracene (M. Jones, personal communication). Although Spearman rank analyses support a strong relationship between PG2 abundance and PAH concentrations, the exact role of PG2 organisms in the degradation of any single PAH cannot be directly inferred from the available data. Along with PG2 organisms, other PAH-degrading bacteria in the mixed column soil community may also be capable of growth on a given PAH.

4.4.7 Conclusions

In this study, spatial and temporal variations in the quantity of a group of bacteria known to be PAH degraders and soil PAH concentrations were strongly correlated to oxygen advancement over time, which underlines the importance of maintaining oxygenated conditions for PAH biodegradation. Bacterial transport was also implicated as a factor in the establishment of PAH-degrading bacteria ahead of the oxygen front. The potential for migration of PAH-degrading bacteria and their rapid

response to oxygen are important findings relevant to the biodegradation of mobilized PAHs within zones of subsurface contamination.

Even though substantial PAH degradation was achieved in this study as a result of continuous biostimulation, time scales for significant PAH removal were generally long, greater than 380 d for some four- and five-ring PAHs. Significant reductions in six-ring benzo[*g,h,i*]perylene were not observed even after 534 d of biostimulation. Despite the presence of an established PAH-degrading community and available oxygen and nutrients, PAH concentrations appeared to plateau over time, reflecting limitations in PAH mass transfer and bioavailability. Oxygen transport was also governed by the oxygen demand of the column soil, resulting in slow DO penetration into deeper regions of the column. It is clear from these results that careful consideration of matrix-specific factors such as oxygen demand, PAH bioavailability, and the quantity of PAH-degrading bacteria is essential for the successful design and implementation of *in situ* bioremediation strategies in weathered contaminated soils.

4.5 Acknowledgements

We thank Randall Goodman and Glenn Walters for their help in the design and construction of the columns. We also thank Dr. Wei Sun and Joe Rigdon of the UNC Department of Biostatistics for assistance with statistical analyses. This work was supported by the National Institute of Environmental Health Sciences (grant number 5 P42 ES005948).

5 Bioavailability of Polycyclic Aromatic Hydrocarbons in Density-Based Soil Fractions after Long-Term *In Situ* Biostimulation of Contaminated Soil

Stephen D. Richardson and Michael D. Aitken

5.1 Abstract

The distribution and potential bioavailability of polycyclic aromatic hydrocarbons (PAHs) in soil from a former manufactured-gas plant (MGP) site were examined before and after long-term biostimulation under simulated *in situ* conditions. Treated soil was collected from the oxygenated zones of two continuous-flow columns, one subjected to biostimulation and the other serving as a control, and subjected to density-based separation. In the original soil, over 50% of the total PAH mass was associated with lower-density particles, which comprised < 2% of the total soil mass. However, desorbable fractions of PAHs were much lower in the low-density material than in the high-density material. After over 500 d of biostimulation, significant removal of total PAHs occurred in both the low- and high-density materials (53% and 77%, respectively), with three- and four-ring PAHs accounting for the majority of the observed mass loss. Total PAHs that desorbed over a 28 d period were substantially lower in treated soil from the biostimulated column than in the original soil for both the high-density material (63% vs. 23%) and low-density material (20% vs. 5%). The fast-desorbing fractions quantified by a commonly used two-site desorption model ranged from 0.1 to 0.5 for most PAHs in the unfractionated original soil but were essentially zero in the biostimulated soil. The fast-desorbing fractions in the original soil underestimated the extent of PAH biodegradation observed in the biostimulated column, and thus was not a good predictor of PAH bioavailability under long-term, simulated *in situ* biostimulation conditions.

5.2 Introduction

Polycyclic aromatic hydrocarbon (PAH)-contaminated soils at former manufactured gas plant (MGP) sites are a complex mixture of soil organic matter (SOM), humic substances, inorganic minerals, and various waste residues from past gas operations including pyrogenic residues, oils, tars, and other nonaqueous phase liquids (3, 51). Sorption of PAHs to these various compartments can greatly influence overall PAH transport, degradation, and bioavailability and, therefore, ultimately governs the success of bioremediation strategies (29, 225). PAH bioavailability is commonly equated with the amount of a given PAH that can be desorbed relatively rapidly from a solid-phase or nonaqueous compartment to the aqueous phase, where the compound can be accessed by indigenous PAH-degrading bacteria (79). However, the distribution and bioavailability of PAHs varies among the soil compartments, reflecting differences in compound hydrophobicity and sorption capacities of the soil domains. SOM and other natural and anthropogenic domains (such as residual coal tar, pitch, coke, soot, coal, and lampblack) have been identified as important reservoirs for sorption of PAHs in MGP soils (22, 226-228) and tend to exhibit significantly lower PAH availability than mineral particles (31).

Desorption of PAHs in natural soils is generally biphasic, with an initial phase of rapid PAH release followed by a longer period of slow PAH desorption. During the initial phase, the bioavailability of PAHs is high and degradation rates may be limited by microbial processes; however, as available PAHs are consumed, mass transfer mechanisms such as desorption and diffusion gain importance, becoming critical factors in defining PAH bioavailability (229, 230). PAHs associated with compartments characterized by slow release to the aqueous phase have been regarded as largely unavailable for microbial activity (88, 231), although evidence of repartitioning from slow- to fast-desorbing domains has been documented (232). A number of physical (79-82), chemical (25, 55, 84-87), and biological (78, 85, 88) techniques have been proposed for estimating the bioavailability of PAHs and other hydrophobic organic chemicals in field-contaminated soils. Solid-phase extraction is one of the more common estimation methods, in which polymeric adsorbent

resins (such as Tenax TA® and Amberlite XAD®) function as an infinite sink, maintaining a steep concentration gradient between the aqueous and solid phases for maximum desorption (89, 90).

An empirical model is most commonly used to quantify the biphasic nature of PAH desorption (233), which assumes that desorption occurs from two compartments (or two sites) in the soil defined by fast and slow rates, each following first-order kinetics (79, 234, 235). The rapidly desorbing fraction is often defined as the "bioavailable fraction" and has been used successfully to predict the extent of PAH degradation in field-contaminated sediments (78, 81, 82); however, other studies have found that the rapidly desorbing fraction underestimates the extent of biodegradation (24, 79). Although the two-site model output parameters are empirical and have no direct mechanistic relationship with physical compartments of the soil matrix (79), they have proven valuable in quantifying variations in PAH bioavailability between different soils and sediments (215, 236) and under different treatment conditions (79, 82, 215).

The effects of bioremediation on PAH distribution and bioavailability in field-contaminated soils and sediments has been well-documented in a variety of *ex-situ* treatment systems (25, 79, 82, 205, 227, 237-241). However, only a few of these studies have examined variations in PAH bioavailability among different soil fractions after treatment (205, 227) and even fewer have investigated these effects under *in situ* treatment conditions (25). In this study, we examined the effects of long-term *in situ* biostimulation on PAH distribution and bioavailability in contaminated soil from a former MGP site. Two continuous-flow columns packed with MGP soil were operated for over 500 d; one column was subjected to continuous biostimulation and the other served as a control. Samples of the original and treated soils were density-separated into primarily carbonaceous (lower-density) and primarily mineral (higher-density) fractions to evaluate the impact of biostimulation on PAH distribution within these fractions and to estimate the contribution of each fraction to overall PAH desorption.

5.3 Materials and Methods

5.3.1 Chemicals

Acetone (>99.5%), acetonitrile (>99.9%), dichloromethane (>99.5%), methanol (>99%), cesium chloride (>99%), sodium azide, and sodium sulfate (>99%) were purchased from Fisher Scientific Inc. (Pittsburgh, PA). Anthracene-d_{10} (98%) was purchased from Cambridge Isotope Laboratories (Andover, MA).

5.3.2 Soil

Contaminated soil was collected from a former MGP site in Salisbury, NC, USA and processed according to the method outlined in Appendix A. The processed soil contained 83% sand, 14% silt, and 3% clay, with total organic matter of 8.3% and extractable organic matter of 0.64%. Total PAH concentration (sum of 13 of the 16 USEPA-regulated PAHs (4)) was 295 ± 65 mg/kg dry soil (n = 33), with phenanthrene comprising 44% of the total PAH mass (Figure 5.1). In subsequent discussion, the processed soil is referred to as 'column soil'.

5.3.3 Experimental Design

Two 110-cm long, 10.2-cm diameter stainless-steel columns, each containing a 100-cm zone of column soil, were operated for ~780 d at 20°C, receiving a continuous supply of simulated groundwater (Appendix A) in a downward flow direction. The columns were operated at a flowrate of 2.1 L/d for ~630 d that was subsequently reduced to 1.4 L/d to stabilize rising inlet pressures near the end of the experiment. One of the columns was subjected to biostimulation by amending simulated groundwater with pure oxygen and inorganic nutrients; the second column served as a control, receiving air-saturated, unamended groundwater. New batches of groundwater were prepared weekly to limit the potential for bacterial growth in the feed solutions. Initially, both columns were run under control conditions for eight months ('equilibration phase') to allow for bed consolidation and stabilization of inlet pressures before biostimulation was initiated. Each column was equipped with three ports (Ports A, B, and C) positioned 30, 55, and 80 cm below the top of each column,

respectively, for periodic soil sample collection, along with nine additional smaller ports for monitoring porewater dissolved oxygen (DO) concentrations. Detailed information on the design and operation of the columns is provided in Appendix A.

As part of a larger study (Chapter 4), soil samples were collected from the surface soil and Ports A, B, and C of the control and biostimulated columns immediately after the equilibration phase (t = 0) and 31, 93, 184, 380, and 534 d after biostimulation commenced. Note that all sample time points are referenced to the time that biostimulation was initiated in one of the columns (*i.e.*, "day 534" refers to 534 d after biostimulation began). For this study, desorption experiments, soil extraction, and quantification of PAHs were conducted on the column soil (untreated) and treated soil from Port A of the control and biostimulated columns on day 534. Port A was selected because the dissolved oxygen concentration was saturated at this depth (30 cm) in both columns at the time of sampling. Additional soil was collected from both columns at day 593 for density separation into two soil fractions: carbon-rich particles and the bulk mineral fraction (30), defined as "low-density" and "high-density" material.

5.3.4 Desorption

Tenax TA® polymeric adsorbent beads (Alltech, Deerfield, IL) were used as an infinite sink to continuously uptake dissolved PAHs and establish a steep concentration gradient between the soil and aqueous phases. Prior to use, Tenax beads were cleaned in 50:50 acetone:hexane for 12-16 hr (Soxhlet extraction), rinsed with methanol, and air-dried overnight. Five-gram (wet wt.) aliquots of the column soil and treated samples (day 534) were distributed into triplicate 30-ml glass centrifuge vials for both desorption and initial PAH analyses (*i.e.*, six vials per condition). To each desorption replicate was added 20 ml of unamended simulated groundwater, 0.2 ml of 330 g/L sodium azide to inhibit biological activity, and 0.1 g of clean Tenax beads. The vials were sealed with screw-top caps (with Teflon-lined septa), covered in aluminum foil to eliminate light exposure, and placed on a wrist-action shaker at room temperature (19-23°C). After 1, 3, 6, 14, and 28 d of continuous shaking, the

vials were centrifuged for 15 min at 2,800 *g* and allowed to stand for 1-2 hr for separation of the beads and soil particles. The beads were removed by raising the water surface in each vial with sterile-filtered reagent water to access the floating beads. Once the beads were removed, the supernatant was carefully decanted and the vial replenished with simulated groundwater, sodium azide, and new beads and returned to the shaker. The 28-d desorption period is beyond the time frame (7-12 d) recommended (242) to capture the fast-desorbing fraction of PAHs in field-contaminated soils and sediments.

For each time point, the beads were retrieved using a stainless-steel spatula, transferred to a clean centrifuge tube with reagent water, and vortexed briefly to detach any residual soil particles from the beads; any settled material collected during this bead washing step was returned to the original desorption vial. The beads were then transferred to 15 ml amber screw-top vials containing methanol and shaken for 24 hr. Each methanol extract was filtered through a 0.2 μm pore-size nylon filter (Millipore; Burlington, MA) and transferred to a 25-ml volumetric flask for subsequent HPLC analysis. In preliminary experiments, bead mass recovery for this method was 96 ± 2 %. Following the last time point (t = 28 d), the residual PAH concentration in the desorbed soil replicates was determined to evaluate total PAH recovery at the end of the desorption experiment. A mass balance for each analyte was assessed by comparing the initial PAH mass of the soil sample to the sum of the residual mass and cumulative mass desorbed.

The same desorption procedure described above was used for the high-density material of the column soil and treated soil samples (day 593). For the low-density material, only 0.2 g (dry wt.) was added to duplicate desorption incubations, along with 1 g of Tenax beads to account for the higher organic content of this fraction (30). Desorption studies on the low-density column soil were extended to 58 d to determine the effect of longer desorption time periods on overall PAH release.

5.3.5 Density Separation

Density separation with a cesium chloride solution (specific gravity 1.8) was used to separate the low-density carbonaceous particles and wood fragments (22) from the high-density, bulk mineral fraction of the column soil and treated soils removed from the columns on day 593 (30). Aliquots (10 g wet wt.) of each soil sample were distributed into nine 30-ml centrifuge vials and combined with 20 ml of the cesium chloride solution. Contents of the vials were vigorously shaken for 24-48 hr and centrifuged for 15 min at 2,800 g to divide the soil into the high- and low-density fractions. The floating, low-density material was transferred to a 0.2 μm pore-size nylon filter using a stainless-steel spatula, rinsed several times with reagent water to remove residual cesium chloride, and placed in a desiccator to dry; volatilization of PAHs during sample storage was minimal (< 0.03% of total PAH mass), as determined with a Tenax trap placed in the desiccator. The above steps were repeated 3-5 times or until low-density material was no longer visible at the top of the vial after centrifugation. All low-density material collected on the filters was combined in an aluminum pan and weighed to determine the mass of low-density material in each soil sample. Prior to desorption and PAH analyses, the low-density material for each sample was lightly ground using a mortar and pestle to ensure uniformity among replicates. The remaining high-density material was also rinsed with reagent water, vigorously mixed, and centrifuged several times to remove residual cesium chloride. Subsamples of the high-density material were used to calculate moisture content by loss of weight at 105°C for 24 hr for quantification of PAHs on a dry mass basis. Moisture content of the low-density material was not determined due to low overall mass recovery; however, it is reasonable to assume that water content was minimal after extended desiccation. For the column soil and treated soils, PAH mass recovered in the whole samples removed from the columns on day 534 was compared to the sum of the respective PAH masses in the low- and high-density materials in the samples obtained on day 593.

5.3.6 Chemical Analyses

Extraction and quantification of PAHs in the column soil and treated soil, along with their respective low- and high-density material, were conducted according to the method outlined in Appendix B, with the following exceptions: sodium sulfate was not added to the low-density extractions because solvent-water interferences were expected to be minimal following desiccation; and residual low-density material (after the desorption period) was dried at 60°C overnight to eliminate water prior to extraction. A third extraction step (with an additional 10 ml each of dichloromethane and acetone) was performed for the low-density material to account for the higher PAH and organic carbon content; however, the improvement in PAH mass recovery beyond the first two extractions was marginal (< 2% of total mass). Where necessary, treated soil extracts were concentrated to improve detection of low-molecular weight PAHs. Of the 16 USEPA-regulated PAHs, acenaphthylene was not detected using this quantification method; dibenz[*a*,*h*]anthracene and indeno[1,2,3-*c*,*d*]pyrene were detected at concentrations near their respective method detection limit and are excluded from subsequent analyses.

5.3.7 Data Analysis

An empirical two-compartment model (Equation 5.1) (79, 82, 215, 234, 236, 243, 244) was used to describe the biphasic (fast- and slow-desorbing) desorption data for each PAH in the whole, low-density, and high-density fractions of the column soil and treated soil samples:

$$\frac{C_t}{C_0} = 1 - f \cdot e^{(-k_1 t)} - (1 - f) \cdot e^{(-k_2 t)} \tag{5.1}$$

where t is time (hr), C_t is the concentration of PAH desorbed after time t (mg/kg dry soil), C_0 is the initial concentration of PAH in the soil, f is the fast-desorbing fraction, and k_1 and k_2 are the first-order rate constants for fast and slow desorption, respectively (hr^{-1}). Best-fit values of f, k_1, and k_2 were determined by non-linear regression of duplicate (low-density material) and triplicate (column soil and high-density material) data points of PAH desorbed at each time point using ProStat® 4.02 (Poly

Software International, Pearl River, NY). The fraction of mass desorbed for a given PAH at each time point was normalized to the respective initial PAH concentration.

For samples where biphasic desorption behavior was not observed and unique values of f, k_1, and k_2 could not be obtained from the two-site model, a simplified form of Equation 5.1 (where f and k_1 were set to 0) was used to fit the data:

$$\frac{C_t}{C_0} = 1 - e^{(-k_2 t)} \tag{5.2}$$

To ensure the most appropriate model was selected, the simple first-order model (Equation 5.2) was also fit to all datasets and the resulting r^2 values compared to the two-site model fit. Student t-tests and the Tukey-Kramer HSD test were performed using JMP® 7.0.1 (SAS Institute Inc., Cary, NC). Differences between experimental conditions are noted as significant if $p < 0.05$.

5.4 Results

5.4.1 PAH Removal and Distribution

PAH concentrations in the column soil and treated soil samples from Port A (day 534) are presented in Figure 5.1. After continuous biostimulation, significant reductions in concentration were observed for all PAHs with the exception of benzo[*g,h,i*]perylene. In the control column, significant reductions were limited to three-ring PAHs. Total PAH removal at Port A of the biostimulated and control columns was 80% and 37%, respectively, and generally decreased with increasing molecular weight of the PAH (Section 4.4.2).

Low-density material constituted < 2% of the total mass of the original column soil, but contained more than 50% of the total PAHs (Figure 5.2). Low-density material similarly accounted for a small fraction of the total soil mass in samples removed from the biostimulated and control columns (1.7% and 1.5% of the total soil mass, respectively) but total PAH mass was comparable to that in the high-density material (Figure 5.2); however, poor mass balances on PAHs in the treated soils removed from the columns (which we attribute to the small mass of material to work with and

the high PAH concentrations) made it difficult to accurately quantify the fraction of total PAHs in the low-density material. Total PAH concentrations in the low- and high-density fractions of the treated soils obtained at day 593 were lower than the respective column soil fractions (Figure 5.2). For the high-density material, PAH removal was greater in the biostimulated soil than the in control condition, with average total PAH concentrations of 29 mg/kg and 81 mg/kg, respectively. Significant reductions in three- and four-ring PAH concentrations accounted for the majority of PAH removal following biostimulation, while only acenaphthene, phenanthrene, and pyrene decreased significantly in the control soil (Appendix E, Figure E1a). No significant reductions in five- and six-ring PAH concentrations were observed in the high-density material of either the biostimulated or control soils (Figure E1a).

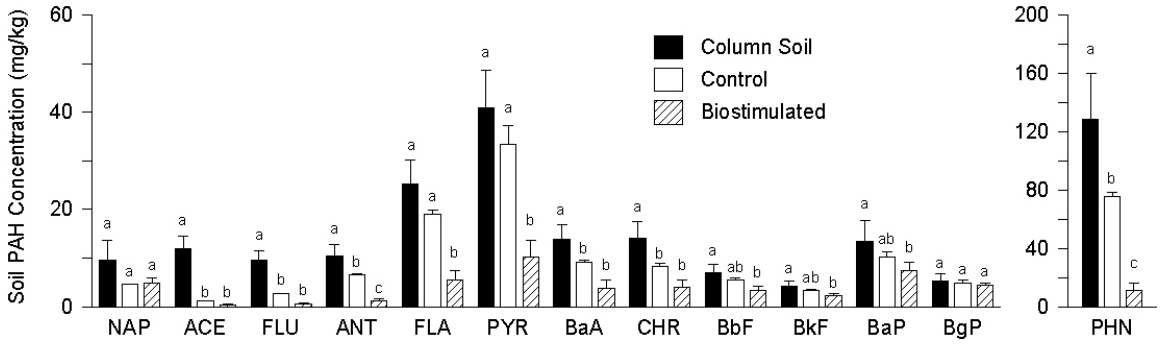

Figure 5.1. PAH concentrations in the column soil and in samples collected from Port A of the control and biostimulated columns at day 534. Note that phenanthrene concentration is plotted separately. Error bars represent one standard deviation. The letters above the error bars represent the results of significance analyses using the Tukey-Kramer HSD test. For each analyte, conditions sharing a common letter are not significantly different.

For the low-density material, average total PAH concentration was reduced from 6,140 mg/kg in the original column soil to 3,890 mg/kg and 3,220 mg/kg in the control and biostimulated soils, respectively (Figure 5.2 inset). All three- and four-ring PAHs were significantly reduced in the low-density fraction following biostimulation, while no significant removal of five- and six-ring PAHs was noted; similar results for the control low-density material were observed, except the four-ring compounds benz[*a*]anthracene and chrysene were not removed as well (Appendix E, Figure E1b).

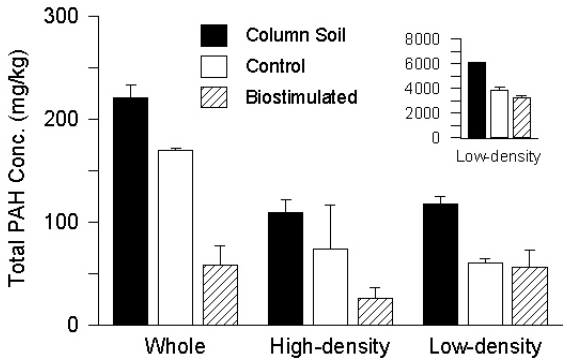

Figure 5.2. Total PAH mass per unit dry mass of the whole (unseparated) soil for the whole soil itself and the high-density and low-density materials in the original column soil and soil collected from the control and biostimulated columns. The inset shows the actual total PAH concentration in the low-density material (mg/kg dry material) of the original column soil and the treated soils.

5.4.2 PAH Desorption from Whole (Unfractionated) Soil

Desorption curves for all PAHs in the column soil and treated soils are presented in Appendix E (Figure E2), with selected PAHs shown in Figure 5.3. Recovery of the initial PAH mass was generally good, ranging from 79% to > 100%, for all PAHs except naphthalene, which is consistent with observations from other desorption studies (79, 215, 232). Poor mass recoveries for naphthalene were attributed to volatilization losses.

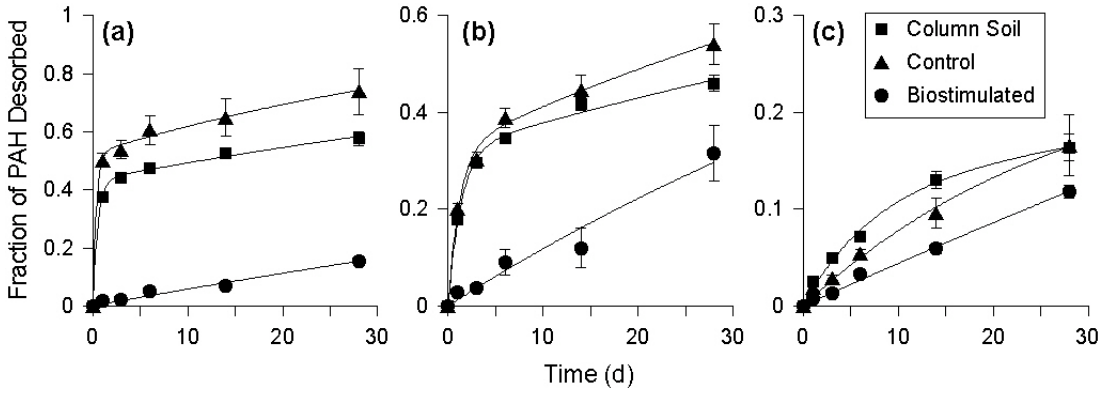

Figure 5.3. Desorption curves for phenanthrene (a), pyrene (b), and benzo[*a*]pyrene (c) for the original column soil and for soil collected from the control and biostimulated columns at day 534. Symbols are the mean values of duplicate analyses from triplicate vessels. Error bars represent the standard deviation and are within the size of the symbol if not visible. The solid lines are the best-fit curves from the simple first-order (biostimulated) or two-site desorption models (column soil and control). Note the different scales on the y-axes.

After the 28-d desorption period, the amount of PAH desorbed generally decreased with increasing PAH molecular weight in the column soil, with average desorbable fractions of 59% for

three-ring PAHs, 43% for four-ring PAHs, and 16% for five- and six-ring PAHs. Similar results were observed for the control soil obtained at day 534, for which there was no significant difference in the fraction desorbed between the control condition and column soil for most PAHs (Appendix E, Figure E2). For the biostimulated soil obtained at day 534, the amount of PAH desorbed was generally lower than for the control condition and column soil for most PAHs, with significant differences noted for all three- and four-ring PAHs (Appendix E, Figure E2). The trend of decreasing desorbable fraction with increasing PAH molecular weight was not evident in the biostimulated soil, with fractions of PAH desorbed remaining below 33% for all PAHs.

Best-fit parameters of the two-site desorption model (Equation 5.1) for the data in Figures 5.3 and E2 are summarized in Appendix E (Table E1). For the column soil and control data, unique values of the three model parameters were obtained for all PAHs except benzo[*g,h,i*]perylene, for which the simple first-order model (Equation 5.2) was used. The simple first-order model also provided better fits than the two-site model for the biostimulated soil desorption data, suggesting that the more labile (fast-desorbing) fraction of the PAHs had already been removed by biodegradation.

The fast-desorbing fraction (f) of PAHs in the column soil and control soil ranged from 0 to 0.85 and, like total PAH fraction desorbed, decreased with increasing PAH molecular weight (Appendix E, Table E1). Depletion of the fast-desorbing fraction occurred within 2-4 d for three- and four-ring PAHs and within 9-15 d for five- and six-ring PAHs, consistent with observations from other desorption studies (79, 215, 242). Average f values for the control soil were significantly lower than those for the column soil for higher molecular-weight PAHs. Rate constants for the fast-desorbing fraction (k_1) were higher in the control column soil than the original column soil for all PAHs, although the differences were not significant.

Rate constants for the slow-desorbing fraction (k_2) for all PAHs ranged from 0.003 – 1.2 x 10^{-3} hr^{-1} for all samples, which falls within the range of reported literature values (233). For the column soil and control soil, k_2 values were generally smaller for higher molecular-weight PAHs than for three-ring PAHs, which was not the case for k_2 values for the biostimulated soil. Values of k_2 were

one to two orders of magnitude lower than k_1 for all PAHs in the column soil and control soil, consistent with other studies in which the two-site desorption model was used (245).

5.4.3 PAH Desorption from Density-Separated Materials

PAH desorption data for the high- and low-density material of the original column soil and treated soils are presented in Appendix E (Figures E3 and E4), with selected PAHs shown in Figure 5.4. Mass recoveries for all PAHs in the high-density materials were comparable to the whole soil (65% to > 100%); however, mass recoveries were much lower for the low-density material, ranging from 35% to 89%, with the majority of PAH recoveries between 50% and 70%. Desorption experiments with the low-density material involved very small quantities of material (< 0.2 g) that were dried at 60 ºC before PAH extraction at the end of the desorption period, with the corresponding potential for PAH loss.

The amount of PAH desorbed after 28 d from the column soil and treated soil samples was greater in the high-density material than the respective low-density material for all PAHs (Figure 5.4). For the column soil, desorbable fractions in the high-density material ranged from 6 to 86% while in the low-density material, desorbable fractions were less than 37% for all PAHs. For the control and biostimulated soils, up to 46% and 32%, respectively, of PAHs were desorbed from the high-density material while up to 22% and 13%, respectively, were desorbed from the low-density material. For most PAHs, the total fraction desorbed was significantly lower in the treated soil samples than the column soil for the high-density material (Appendix E, Figure E3). In the low-density material, desorbable fractions of three- and four-ring PAHs were significantly lower in the treated soils than those of the column soil; no significance difference was noted among the soil samples for five- and six-ring PAHs (Appendix E, Figure E4). These results differ from the whole soil data, for which the fractions desorbed were similar between the column soil and control soil for most PAHs. Soil heterogeneities and/or the amount of time elapsed between collection of the whole soil samples (day

534) and the low- and high-density materials (day 593) may have contributed to these observed differences.

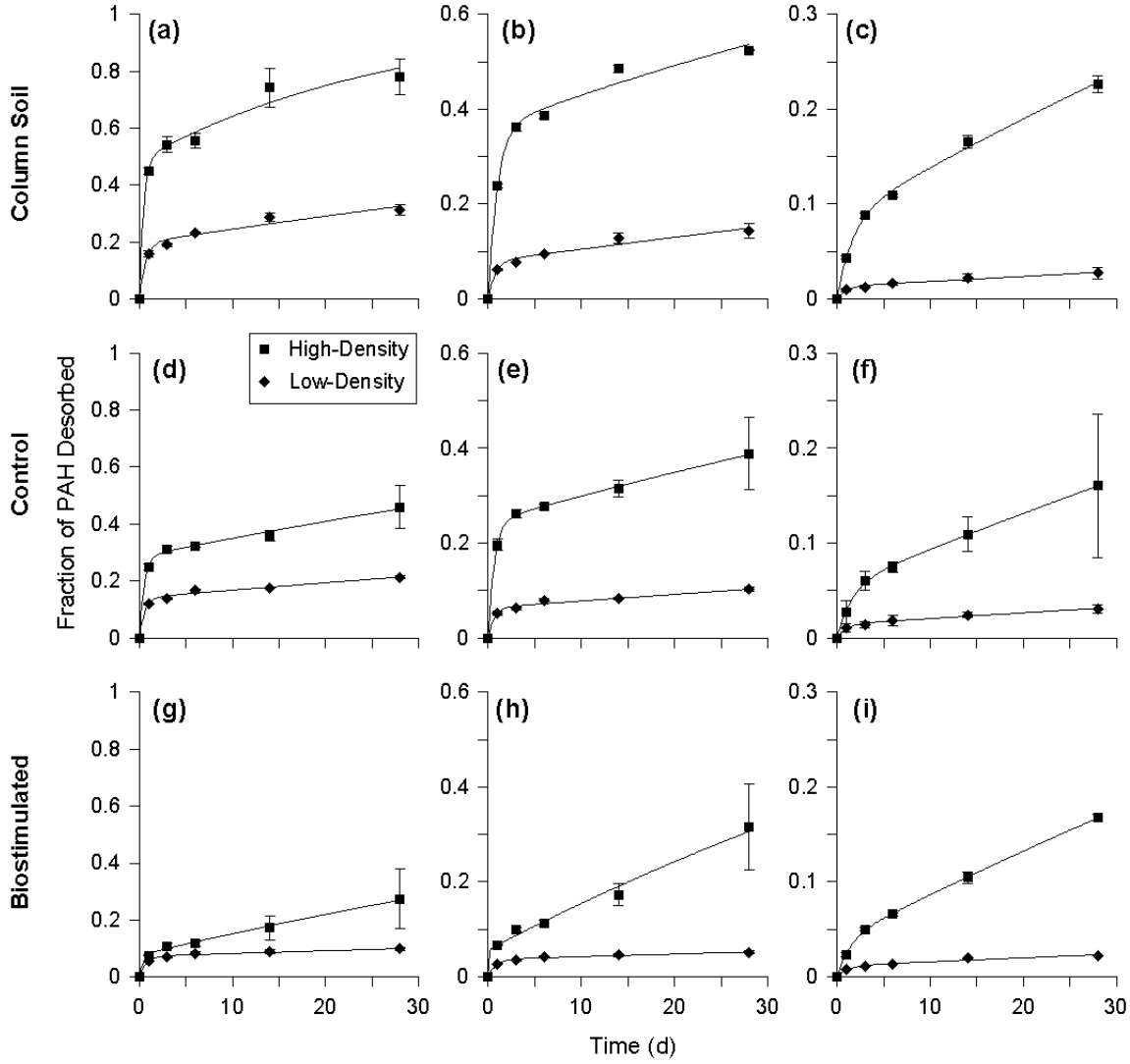

Figure 5.4. Desorption curves for phenanthrene, pyrene, and benzo[*a*]pyrene for the low-density and high-density materials from the original column soil (a-c, respectively) and soil collected from the control column (d-f, respectively) and biostimulated column (g-i, respectively) at day 593. Symbols are the mean values of duplicate analyses from duplicate or triplicate vessels. Error bars represent the range or standard deviation and are within the size of the symbol if not visible. The solid lines are the best-fit curves from the two-site desorption model. Note the different scales on the y-axes.

The two-site desorption model provided the best fits for the low- and high-density desorption data for the column soil and the treated soils. Best-fit parameter values for the low- and high-density material in the column soil and treated soils are presented in Appendix E (Tables E2 and E3). Fast-desorbing fractions (*f*) for the column soil ranged from 0 to 0.56 in the high-density material and 0 to

0.25 in the low-density material, while *f* values in the control soil were much lower (less than 0.28 and 0.14 in the high- and low-density materials, respectively); significant differences were noted for all PAHs in the high-density material and for three-ring PAHs in the low-density material. For the biostimulated soil, *f* values for most PAHs in the low- and high-density material were significantly lower than those of the original column soil and the control.

No major differences in the rate constants for the fast-desorbing fraction (k_1) were observed between the high- and low-density materials. Likewise, no significant differences were found in k_1 values among the column soil and treated samples for both the high- and low-density materials. For most PAHs, k_2 values were an order of magnitude higher in the high-density material than the low-density material, as evidenced by steeper slopes of the model fits in Figure 5.4. Among experimental conditions, k_2 values for the high-density material were significantly lower for the treated soils than for the original column soil for all PAHs, while for the low-density material, significant differences were observed only for three- and four-ring PAHs between the treated soils and column soil.

5.5 Discussion

Over 50% of the PAH mass in the original column soil was distributed in the low-density, carbonaceous fraction (Figure 5.2), consistent with observations in previous studies on density-based separation of PAH-contaminated sediments (30, 205, 246). Khalil et al. (22) further separated the low-density fraction of a variety of PAH-contaminated sediments by particle type (wood, charcoal, coal/coke, cenospheres, coal tar pitch), revealing that coal tar pitch, a suspected waste product of former MGP operations, was a major reservoir for PAHs (> 90% of PAH mass in the low-density material). We did not fractionate the low-density material further in this study.

Long-term biostimulation under simulated *in situ* conditions resulted in significant PAH removal, particularly for three- and four-ring PAHs, in both the low-density and high-density materials of the original column soil (Appendix E, Figure E1). These results are in contrast to an earlier study (205) in which aerobic bioslurry treatment of PAH-contaminated sediment was found to

reduce PAH concentrations only in the high-density material. However, in a companion study by the same group (227), significant reductions were also reported for PAHs associated with low-density material recovered from different contaminated sediments. The authors attributed the observed differences between sediments to the differences in carbon composition in the low-density material, suggesting that PAHs associated with coal tar pitch (a softer, semi-solid domain) were more bioavailable than those bound to highly aromatic, coal-derived particles (227). Their hypothesis was supported by differences in PAH desorption from the low-density material between sediments. Although the presence of coal tar pitch in the low-density material of the column soil was not confirmed in the present study, it is clear from our results that PAHs in the low-density material were amenable to desorption and biodegradation.

Although long-term biostimulation removed the rapidly desorbing fractions of PAHs, up to 30% of the remaining PAHs in soil from the biostimulated column continued to be desorbable over a 28-d period (Figures 5.4g-i). The fast-desorbing fractions of the five-ring PAHs were generally low (0.13-0.14) in the original column soil, but long-term biostimulation reduced this fraction to effectively zero (Appendix E, Table E1). In contrast, Cornelissen et al. (79) reported significant reductions in the fast-desorbing fractions of only the two-, three- and four-ring PAHs after aerobic bioreactor treatment of field-contaminated sediment, while the fast-desorbing fraction of five- and six-ring PAHs remained unchanged after treatment.

For all experimental conditions, model fits for the whole soil (Figure 5.3) and the high-density material (Figure 5.4) did not reach an asymptote, so the extent to which desorption may have continued beyond 28 d is unknown. For the low-density material, slopes of the model fits generally approached an asymptote after 28 d, particularly in the biostimulated soil. This suggests that there is a very slow (or effectively irreversible) desorption domain present in the low-density material. After extending the desorption period to 58 d, additional mass released from the low-density material of the column soil accounted for less than 3% of the total PAH mass desorbed (data not shown).

5.6 Implications of the Two-Site Model

Several studies (78, 81, 82) have found that the fast-desorbing fraction can be used as a predictor of PAH bioavailability and, correspondingly, the extent of PAH degradation over time. For the present study, we compared the fraction of each PAH removed after 534 d of biostimulation and control conditions versus respective fast-desorbing fractions in the column soil for the whole soil and the low- and high-density materials (Figure 5.5). For the control soil, the fractions of each PAH removed were mostly near or below the respective *f* values of the original column soil in both the whole soil and the high-density material (Figures 5.5a and b). In contrast, for all PAHs in the whole soil and the high-density material from the biostimulated column, the fraction removed was greater than the respective *f* values of the original column soil. The fast-desorbing fraction was, therefore, not predictive of PAH biodegradation under long-term, simulated *in situ* biostimulation conditions. Other studies have also reported that *f* values from the two-site desorption model underestimated the extent of PAH degradation in field-contaminated soils and sediments (24, 79). Birdwell et al. (232) recently suggested that PAHs partitioned into apparently slow-desorbing compartments are capable of re-partitioning to a more bioaccessible domain.

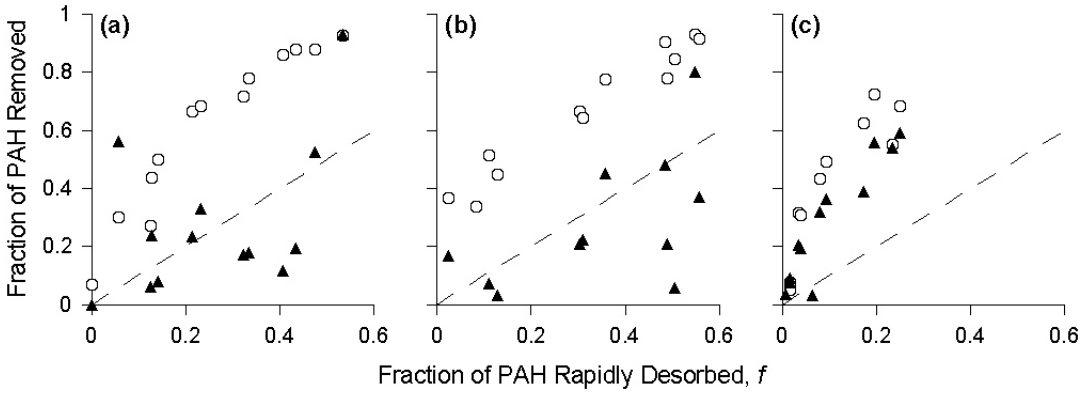

Figure 5.5. Fractions of PAH removed in the control (▲) and biostimulated (○) columns versus the fraction of PAH rapidly desorbed (*f*) in the original column soil for the whole soil (a), the high-density material (b), and the low-density (c) material. Each point represents the mean value for an individual PAH. Standard deviations have been omitted for clarity. The dashed line represents a 1:1 correlation. NAP, BaP, and BgP are not included in plot (c) because no removal was observed.

In the low-density material (Figure 5.5c), the fractions of PAH removed under both the biostimulated and control conditions were up to six times greater than the respective *f* values of the

original column soil. Although the *f* values for the low-density material were much lower than the corresponding values for the whole soil or the high-density material, these results reinforce that the fast-desorbing fraction of a PAH is not necessarily predictive of long-term biodegradation.

Using the best-fit model parameters in Tables E1-E3 of Appendix E extrapolation of Equation 5.1 to a desorption period of 534 d results in PAH concentrations well below those actually observed in either of the column systems. Such overestimation of PAH removal by extrapolation of the two-site model suggests that there may be a third effective domain characterized by very slow desorption that is not captured over the time frames (28 d) used in our desorption experiments; similarly short desorption periods have been used in a number of other studies (79, 215, 227, 236). Ghosh et al. (30) found that, even after a 100-d desorption period with PAH-contaminated sediment, the desorption curve for the high-density material had not reached an asymptote. It appears, therefore, that longer desorption periods may be necessary to accurately predict the long-term extent of PAH biodegradation in field-contaminated soils.

5.7 Acknowledgements

We thank Randall Goodman and Glenn Walters for their help in the design and construction of the columns. We also thank Dr. Wei Sun of the UNC Department of Biostatistics for assistance with statistical analyses. This work was supported by the National Institute of Environmental Health Sciences (grant number 5 P42 ES005948).

6 Conclusions and Recommendations

The overall goal of this dissertation was to investigate the effects of biological and coupled chemical-biological remediation strategies on the concentration, distribution, availability, and biodegradation of PAHs in weathered MGP soil. Specific attention was paid to the direct impact of treatment strategies on the quantity and activity of known PAH-degrading bacteria. Overall, this work has shown that inclusion of molecular tools as part of site assessment activities can provide valuable information for the design and implementation of *in situ* bioremediation technologies at former MGP and other contaminated sites. Furthermore, knowledge of PAH distribution and bioavailability within various soil domains can improve decision-making regarding remediation selection and quantification of risk. Conclusions and recommendations for the specific aims of this research project are outlined below:

1. Determine the effects of persulfate oxidation on soil PAH concentration and the abundance and activity of the indigenous microbial community and specific phenanthrene-degrading bacteria in weathered MGP soil.

Exposure to persulfate led to a two- to three-log reduction in total bacterial 16S rRNA genes, severe inhibition of ^{14}C-acetate mineralization, and a decrease in community diversity. However, relatively rapid recovery of both bacterial gene abundance and activity was observed within 30 d after persulfate exposure. Mineralization of ^{14}C-phenanthrene was also inhibited but did not recover until 100 d post-oxidation. Known phenanthrene-degrading bacterial groups decreased to below detection limits throughout the column, with recovery times from 100 d to 500 d after persulfate injection. These findings suggest that coupling biological processes with persulfate oxidation is possible, although recovery of specific contaminant degraders may occur well after the general microbial community recovers. Furthermore, the use of total bacterial quantity or non-specific measures of

activity as a surrogate for the recovery of contaminant degraders may be inappropriate for evaluating the compatibility of chemical treatment with subsequent bioremediation.

The implications of sulfate release into groundwater and soil matrices after persulfate oxidation and its effects on indigenous sulfate-reducing bacteria (SRB) require further consideration. Injection of significant amounts of persulfate at field sites could raise groundwater sulfate concentrations above the USEPA secondary drinking water standard of 250 mg/L (247). However, this effect may be temporary owing to intermittent persulfate injection, dilution and dispersive transport of sulfate from the injection point, and reduction of sulfate to sulfide by SRB. Although the USEPA standard is non-enforceable, some states may choose to incorporate it into site-specific remediation guidelines (247), increasing the importance of maintaining acceptable groundwater sulfate levels. Understanding the inhibitory effects of persulfate oxidation and sulfide production on SRB activity may be valuable in assessing the fate of sulfate over time. Cassidy (248) reported that SRB in a PAH-contaminated sediment recovered within six months of exposure to Klozur®, a commercially-available form of persulfate. The effects of sulfide production on subsequent PAH biodegradation in field-contaminated soils and sediments have not been investigated to date.

2. Examine the long-term effects of in situ biostimulation on a) soil PAH concentration and b) the indigenous microbial community and specific PAH degraders in weathered MGP soil.

Biostimulation resulted in significantly greater PAH removal than in the control condition (73% vs. 34%, respectively), with dissolution accounting for a minor amount of the total mass loss (~6%) in both columns. Dissolution was most significant for naphthalene, acenaphthene, and fluorene, accounting for > 20% of the total mass removed for each. The effluent naphthalene concentration for the biostimulated column remained above the respective NCDENR groundwater standard of 6 μg/L (220) for up to 466 d, highlighting the importance of this compound for long-term groundwater contamination and off-site migration. A known group of PAH-degrading bacteria, 'Pyrene Group 2' (PG2), was identified as a dominant member of the microbial community and responded favorably to

biostimulation. Spatial and temporal variations in soil PAH concentration and PG2 abundance were strongly correlated to dissolved oxygen advancement, although there appeared to be transport of PG2 organisms ahead of the oxygen front. At an estimated oxygen demand of 6.2 mg O_2/g dry soil and a porewater velocity of 0.8 m/d, it took between 374 and 466 d for oxygen breakthrough from the 1-m soil bed in the biostimulated column. This study demonstrated that the presence of oxygen was the limiting factor in PAH removal, as opposed to the abundance and/or activity of PAH-degrading bacteria once oxygen reached a previously anoxic zone.

Further research on the transport of indigenous PAH-degrading bacteria would be a beneficial extension to the current study, particularly the rate and extent of bacterial migration from contaminated source zones and the potential for recolonization in "downstream" uncontaminated soils. Although evidence for transport of PG2 organisms was obtained in this study, the presence of PAH-degrading bacteria in the column porewater and effluent was not confirmed. Incorporation of secondary "downstream" columns, packed with clean material and receiving the effluent from the current treatment columns, would enable long-term monitoring of PAH-degrader reestablishment with respect to the transport of dissolved PAHs, particularly naphthalene, acenaphthene, and fluorene. Solid phase media such as Bio-Sep® beads could be used to trap and concentrate free-flowing bacteria from the secondary column for subsequent microbial identification and quantification (249).

3. Determine the impact of in situ biostimulation on PAH distribution and bioavailability among various compartments of weathered MGP soil.

In the original soil, over 50% of the total PAH mass was associated with lower-density particles, which comprised < 2% of the total soil mass. However, desorbable fractions of PAHs were much lower in the low-density material than in the high-density material. After over 500 d of biostimulation, significant removal of total PAHs occurred in both the low- and high-density materials (53% and 77%, respectively), with three- and four-ring PAHs accounting for the majority of the observed mass loss. Total PAHs that desorbed over a 28-d period were substantially lower in

treated soil from the biostimulated column than in the original soil for both the high-density material (63% vs. 23%) and low-density material (20% vs. 5%). The fast-desorbing fractions quantified by a commonly used two-site desorption model ranged from 0.1 to 0.5 for most PAHs in the unfractionated original soil but were essentially zero in the biostimulated soil. The fast-desorbing fractions in the original soil underestimated the extent of PAH biodegradation observed in the biostimulated column, and thus was not a good predictor of PAH bioavailability under long-term, simulated *in situ* biostimulation conditions. Better methods need to be developed to estimate long-term bioavailability of PAHs under in situ conditions in which oxygen availability is not the limiting factor.

A key finding of this work was that PAHs were bioavailable in the low-density, carbonaceous fraction of the column soil. In earlier studies, Talley et al. (205) and Ghosh et al. (227) came to different conclusions regarding the bioavailability of PAHs in the low-density material of different MGP sediments, pointing to variations in the carbon composition (specifically, coal tar pitch content) as the driver for the observed differences. Petrography analyses of the low-density material are recommended as an extension to the current study to identify the major sorption reservoirs for PAHs in this MGP soil. Provided enough material can be obtained from each carbon fraction, subsequent desorption and PAH biodegradation analyses may be beneficial in quantifying respective rates of PAH release and degradability over time. Since MGP wastes are a function of the original operational practices of the plant (coal carbonization, carburetted water gas, and oil gas), samples from a variety of former MGP sites might be warranted. This work would compliment the equilibrium partitioning research by Hawthorne et al. (67) where K_{ioc} values were measured for 114 sediment samples from six MGP sites over a 3-year period. The overall goal would be to gain a broad understanding of PAH distribution and bioavailability at MGP sites and incorporate this information into risk assessment and site remediation decision-making.

Appendix A. Column Design and Operation

Field Site Description and Soil Preparation

Source material for the columns was collected from a former MGP site in Salisbury, North Carolina. This site is one of 27 former MGP sites identified across the state of North Carolina (33). The former Salisbury MGP is located on a 2.5 acre lot and was established in 1901, continuing gas operations until 1960 (250). Based on this time frame, the plant likely employed carburetted water gas technology.

Samples were collected from the site on July 18, 2006 during active site remediation initiated by the site owner. The remedial program involved excavation and transport of approximately 9,000 tons of contaminated soil from the site to a licensed waste management facility (250). The excavation area encompassed locations of former MGP infrastructure including the retort house, oil tank, and tar well and extended to depths ranging from 6 to 10 ft below ground surface. Prior to remediation activities, boreholes were advanced to delineate the extent of soil contamination at the site. The highest PAH concentrations were detected in boreholes located between the former retort house and tar well. Soil samples for the research project were collected from this region at a depth of approximately 4 ft and stored at 4°C prior to processing.

Processing of the Salisbury MGP soil was conducted on July 20, 2006. The soil was initially screened through a 10-mm wire screen to break up large clay aggregates and remove rocks, brick fragments, and other debris. Random portions of the screened soil were repeatedly mixed in a commercial cement mixer to create a homogenous soil stock. The homogenized soil was then mixed with sterile 40/50 grade silica sand (Unimin Corporation, Le Sueur, MN) at a 50:50 ratio (dry weight) to promote low-pressure flow through the columns. Previous column tests with the whole soil yielded elevated inlet pressures (50-100 psi) over a short time period (2-3 weeks). This final packing material is referred to as ‘column soil’. The column soil was prepared in 11 smaller batches (1-2 kg) to facilitate column packing; triplicate subsamples from each batch were collected for subsequent PAH extraction and quantification.

Column Soil Characterization

Physical properties and PAH characterization of the column soil are summarized in Tables A1 and A2, respectively. The porosity and particle density of the 30/40 silica sand support layer are 0.35 and 2.67 g/cm^3, respectively (251).

Table A1. Properties of the column soil

Property	Unit	Value (mean ± std. dev.)	No. of Replicates	Method (reference)
Sand content	%	82.9	1	(252)
Silt content	%	13.8	1	(252)
Clay content	%	3.3	1	(252)
Moisture content	%	7.50 ± 0.01	6	(253)
Soil pH		7.56 ± 0.11	3	(254)
Inorganic carbon	%	7.0 ± 1.6	6	(190)
Organic matter (375°C)	%	8.3 ± 1.2	6	(190)
Black carbon (550°C)	%	0.88 ± 0.26	3	(190)
Soil particle density	g/cm^3	2.62 ± 0.04	3	(255)
Bulk density	g/cm^3	1.65 ± 0.03	3	

Table A2. PAH concentrations in the column soil

Analyte	Abbreviation	Concentration (mg/kg) [a]
Naphthalene	NAP	9.5 ± 4.2
Acenaphthene	ACE	11.9 ± 2.7
Fluorene	FLU	9.5 ± 2.0
Phenanthrene	PHN	129 ± 31
Anthracene	ANT	10.5 ± 2.2
Fluoranthene	FLA	25.2 ± 5.0
Pyrene	PYR	40.9 ± 7.8
Benz[*a*]anthracene	BaA	13.8 ± 3.0
Chrysene	CHR	14.0 ± 3.6
Benzo[*b*]fluoranthene	BbF	6.9 ± 1.7
Benzo[*k*]fluoranthene	BkF	4.2 ± 1.1
Benzo[*a*]pyrene	BaP	13.5 ± 4.2
Dibenz[*a,h*]anthracene	DBA	1.0 ± 0.5
Benzo[*g,h,i*]perylene	BgP	5.3 ± 1.6
TOTAL		295 ± 65

[a] Values are presented as mean ± standard deviation (n = 33).

Design and Operation of Column System

Column Design

The columns were constructed of 10.2 cm (4 in.) diameter (O.D.) 304 stainless steel (SS) pipe with a total length of 110 cm (43.3 in.) (Figures A1 and A2). Each column housed a 100-cm (39.4 in.) zone of column soil, underlain by a 5-cm sand bed support. Flow through the columns was in a downward direction to facilitate collection of surface soil samples from the top of each column. Dedicated 316 SS single-piston metering pumps (Eldex Laboratories, Inc., Napa, CA) delivered flow to each column at a design rate of 2.1 L/d. Each column was equipped with three sampling ports for periodic collection of soil cores and nine smaller ports for monitoring of dissolved oxygen (DO) and redox profiles along the column length. All columns were pressure tested (up to 50 psi) to identify any leaks prior to column packing. Columns were operated at 20°C for the duration of the experiment, except for the persulfate column during thermal activation at 40°C (~16 d).

The inlet end of the column was constructed of two 15 x 15 cm (5.9 in.) plates: a 0.64 cm (0.25 in.) thick aluminum plate (located below the flange) and a 1.27 cm (0.5 in.) thick clear acrylic top plate. The clear top plate enabled visual observation of the surface column soil during operation. A 0.16 cm (1/16 in.) thick butyl rubber gasket was secured between the two plates with eight bolts to achieve a pressure-tight seal. During sampling events, the bolts were loosened and the top plate removed for collection of surface soil samples. Influent groundwater was delivered via 0.16 cm (1/16 in.) diameter (O.D.) SS tubing connected to the center of the clear acrylic top plate. A pressure gauge was positioned at the top of each column to monitor inlet pressure. Increases in inlet pressure are often indications of soil bed consolidation (pore space reduction), fines migration (blockage of pore throats), and bioclogging over time.

The outlet end of the column was constructed of the following 15 x 15 cm (5.9 in.) components: two 0.64 cm (0.25 in.) thick aluminum plates (one located above the outlet flange), a 0.16 cm (1/16 in.) thick SS outlet plate, two 0.16 cm (1/16 in.) thick butyl rubber gaskets, a Mesh 325 (43-micron opening) SS wire cloth (for fines retention), and a Mesh 8 (2-mm opening) SS wire screen (for bed support). The wire cloth and screen were permanently sealed between the gaskets using silicone glue to create a leak-tight wire-gasket assembly. The outlet plate and wire-gasket assembly were positioned between the aluminum plates and secured to the bottom flange of the column by eight bolts. A two-valve SS assembly was installed to the outlet plate of the column to facilitate effluent sampling and flow control.

Each column was equipped with three evenly-spaced sampling ports along the column length for collection of soil samples. The sampling ports were constructed of 1.27 cm (0.5 in.) diameter threaded SS Swagelok® fittings (Swagelok Corporation, Solon, OH), positioned 30, 55, and 80 cm below the top of the column. A device analogous to a split-spoon sampler was used for collection of soil samples. The device was made of two 14.6 cm (5.7 in.) long SS tubes of slightly different diameters (1.3 cm [0.5 in.] vs. 1.1 cm [7/16 in.] O.D.), placed one inside the other. Voids left by the sampling device were displaced by tapping or vibrating the column wall in the vicinity of the sampling point. Each port was sealed between sampling events with a SS ferrule, rod, and nut assembly.

Nine smaller ports were located along each column length to facilitate monitoring of DO and redox conditions within the column. The ports were constructed of 0.64 cm (0.25 in.) diameter SS Swagelok® fittings (Swagelok Corporation, Solon, OH), and located 10, 15, 20, 25, 35, 45, 60, 75, and 90 cm below the top of each column. The positions of the ports were alternated 45° and 315° from center to minimize fluid short-circuiting during column operation. Distance between ports was

shorter at the inlet end of the column to improve monitoring of oxygen advancement during early time. Each port housed a dedicated 13.8 cm (5.4 in.) long, 0.6 cm (0.2 in.) diameter (O.D.) SS probe, screened with six 0.025 cm (0.01 in.) slits along its length to promote groundwater infiltration (Figure A2). Screened sections were located at the base end, mid-point, or tip end of the probe. These different screen configurations were alternated along the length of the column to further minimize fluid short-circuiting. A Mesh 325 (43-micron opening) wire cloth was wrapped around the inner wall of the probe to prevent fines infiltration. A smaller SS, perforated tube (12.3 cm [4.3 in.] long, 0.3 cm [0.1 in.] O.D.), called a DO sensor sleeve, was placed within each probe to provide protection for the fiber optic DO sensor (Figure A3). The sleeve could be removed from the probe for periodic maintenance. Each DO port was sealed with two 0.64 cm (0.25 in.) diameter silicone rubber septa.

A FOXY fiber optic oxygen sensor system (Ocean Optics, Dunedin, FL) was used to measure DO concentrations in the pore water of the persulfate, biostimulated, and control columns. The system consists of a miniature spectrometer, a 470 nm excitation source, a 200 μm bifurcated optical cable, and a 1 m long, 300 μm aluminum-jacketed fiber optic fluorescence sensor (FOXY-AL300). The tip of the sensor houses a proprietary oxygen-sensing coating that contains a fluorophore formulation (ruthenium) entrapped in a sol-gel matrix. Light from the excitation source (~475 nm) travels through the fiber optic cable assembly and excites the ruthenium complex, causing it to fluoresce and release energy at 600 nm. The excess energy is transferred to oxygen molecules (if present) resulting in a decreased fluorescence signal. This phenomenon is known as dynamic fluorescence quenching. The degree of fluorescence quenching is proportional to the number of oxygen-fluorophore collisions and therefore the concentration of oxygen in the pore water. The fluorescence signal from the spectrometer is related to the partial pressure of oxygen using the Stern-Volmer equation (256):

$$\frac{I_o}{I} = 1 + k \cdot p_{O_2} \tag{A1}$$

where I_o is the fluorescence intensity recorded at zero oxygen pressure, I is the intensity at oxygen pressure p_{O2}, and k is the Stern–Volmer constant. The linear relationship in Equation A1 is only valid up to partial pressures of 30 kPa (30%) (257). For higher oxygenated environments, the following second order polynomial equation is used:

$$\frac{I_o}{I} = 1 + k_1\left(p_{O_2}\right) + k_2\left(p_{O_2}\right)^2 \tag{A2}$$

where k_1 and k_2 are first- and second-order coefficients of best-fit, respectively (256).

A three-standard calibration curve was used for quantification of DO concentrations in the column system. Zero, air-saturated (~9 mg/L), and oxygen saturated (~44 mg/L) standards were prepared by sparging compressed nitrogen, air, and pure oxygen, respectively, into sterile distilled water. To accommodate high oxygen concentrations (*i.e.,* biostimulated column), Equation A2 was selected as the fit model for the calibration curve. All standards were prepared at the operating temperature of the column system (20°C).

Redox conditions within the anaerobic column were monitored using a platinum-band oxidation-reduction potential (ORP) electrode (Cole-Parmer, Vernon Hills, IL). Aqueous samples were collected from the column by inserting a 10 ml sterile syringe into each port while the effluent valve of the column was closed. Flow was diverted through the port and into the syringe barrel, minimizing introduction of air into the aqueous sample. All ORP measurements were made

immediately after sample collection. The ORP probe was calibrated using two standards, 86 mV and 263 mV, which were prepared by adding a small quantity of quinhydrone powder to pH 7 and pH 4 buffer solutions, respectively (185, 258).

Column Packing

The columns were packed over a period of two days (August 21-22, 2007) to allow adequate time for consolidation and saturation of the column soil. A 5-cm bed support of oven-dried, autoclaved 30/40 sand (Unimin Corporation, Le Sueur, MN) was added to each column prior to column soil addition. The column soil was then introduced in 3 to 5 cm lifts; each lift was followed by vibration of the column walls (using a pneumatic vibrator) and gentle rodding to ensure amalgamation of the lift layers. The water surface was maintained 3 cm above each newly added lift to minimize air entrainment. Approximately 14 kg (wet wt.) of column soil was added to each column. Operation of the columns (*i.e.*, continuous-flow of simulated groundwater) commenced immediately following the packing procedure.

Column Operation

Prior to initiation of experimental conditions (*i.e.,* biostimulation, chemical oxidation, anaerobic conditions), all columns were run under the same operating conditions for eight months. The goal of this 'equilibration phase' was to 1) allow for consolidation of the packed column soil, 2) gather baseline data (*i.e.,* inlet pressure, effluent pH, and flowrate), 3) monitor initial DO advancement in the pore water, and 4) conduct tracer tests to characterize flow properties within each column. Measured flowrates, effluent pH, and inlet pressures for all columns were similar over the equilibration phase, providing justification to proceed with the experimental conditions (Table A3).

Table A3. Column baseline operating data

Parameter [a]		Persulfate	Anaerobic	Biostim.	Control
Flowrate	(ml/min)	1.50 ± 0.10	1.47 ± 0.13	1.41 ± 0.23	1.51 ± 0.08
pH		7.41 ± 0.11	7.45 ± 0.12	6.75 ± 0.22	7.44 ± 0.11
Pressure	(psi)	20.5 ± 7.5	13.8 ± 4.2	32.3 ± 17.1	7.4 ± 2.7

[a] Includes data collected from August 22, 2007 to April 26, 2008.

Flowrate, inlet pressure, and pH data collected after initiation of the treatment conditions are summarized in Figures A4-6.

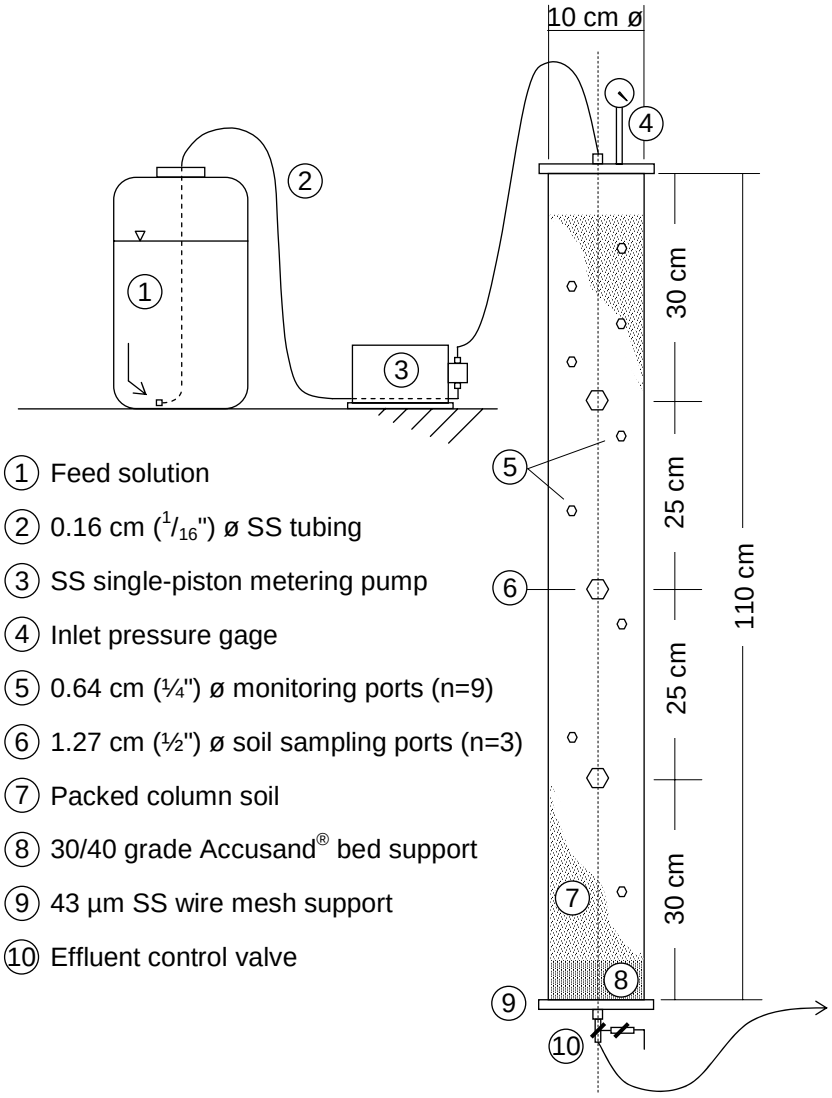

Figure A1. Schematic of the column system. SS, stainless steel.

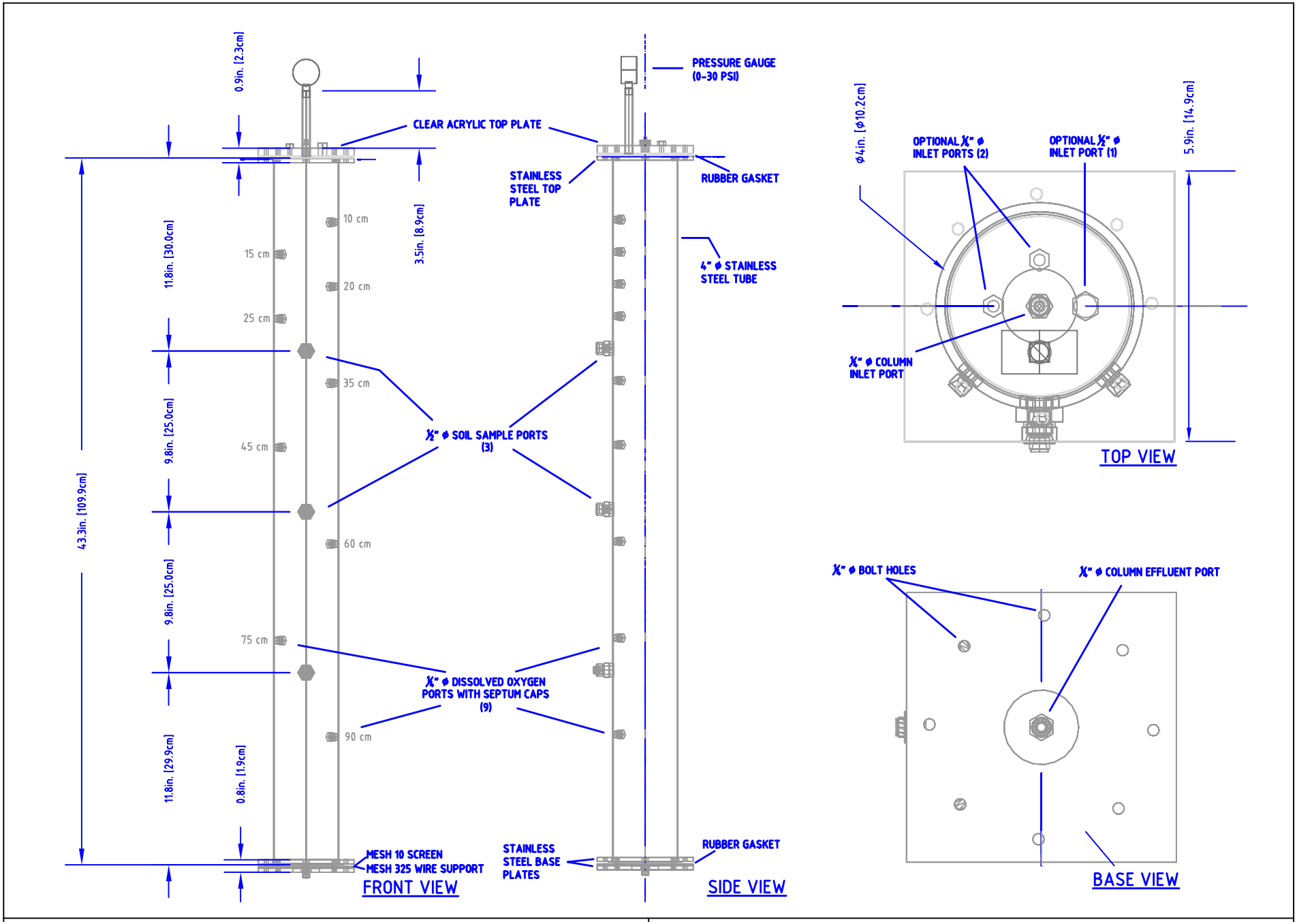

Figure A2. Column design and specifications

D.O. PROBE

Each column is equipped with nine stainless steel D.O. probes.
The D.O. probe serves as a conduit for groundwater collection, monitoring, and sampling.
Each D.O. probe is permanently installed across the diameter of the column.
Three slit configurations exist on the D.O. probes: base end, mid-point, and tip end (as shown).
Probes of differing slit positions are alternated along the length of the column to minimize fluid short-circuiting.

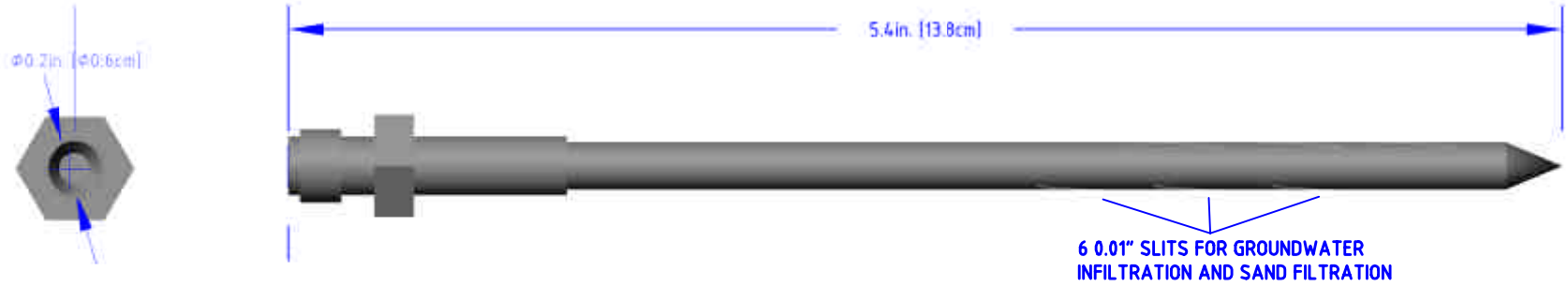

D.O. SENSOR SLEEVE

The D.O. sensor sleeve serves to protect the fibre optic D.O. probe from damage.
Each sleeve is placed within the D.O. probe and can be removed for maintenance.
The outside of each sleeve is wrapped in Mesh 325 screen to prevent fines infiltration.

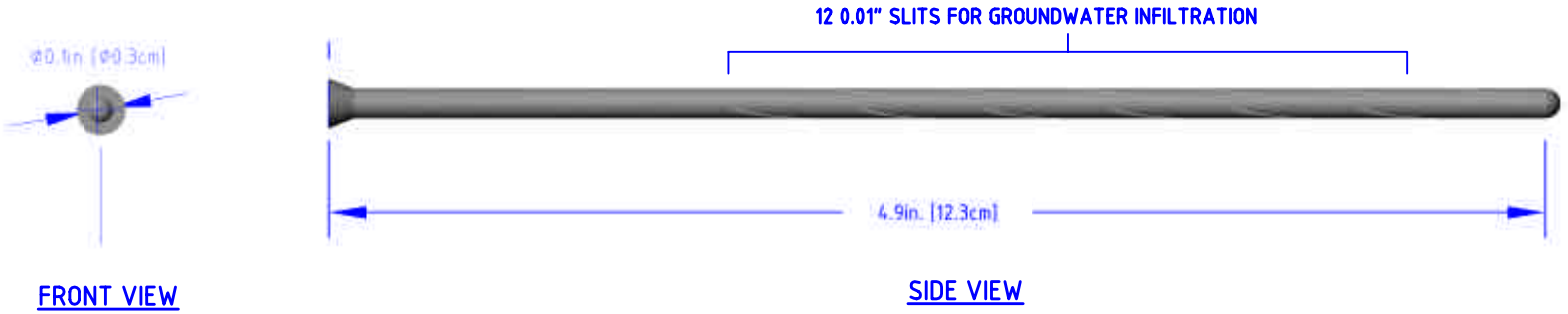

Figure A3. Dissolved oxygen probe design and specifications

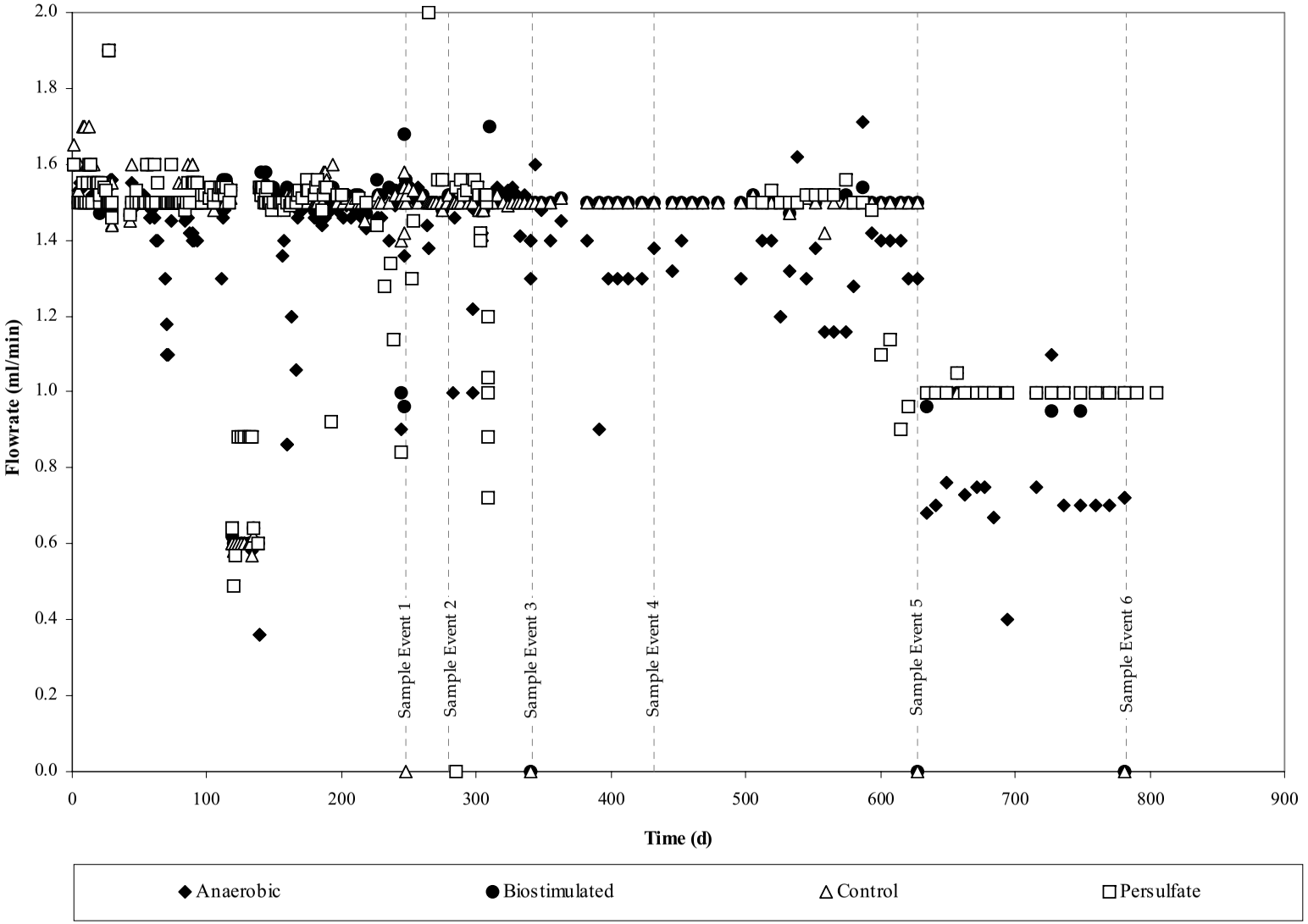

Figure A4. Effluent flowrate data for all columns, 'Sample Event 1' is also denoted as t = 0.

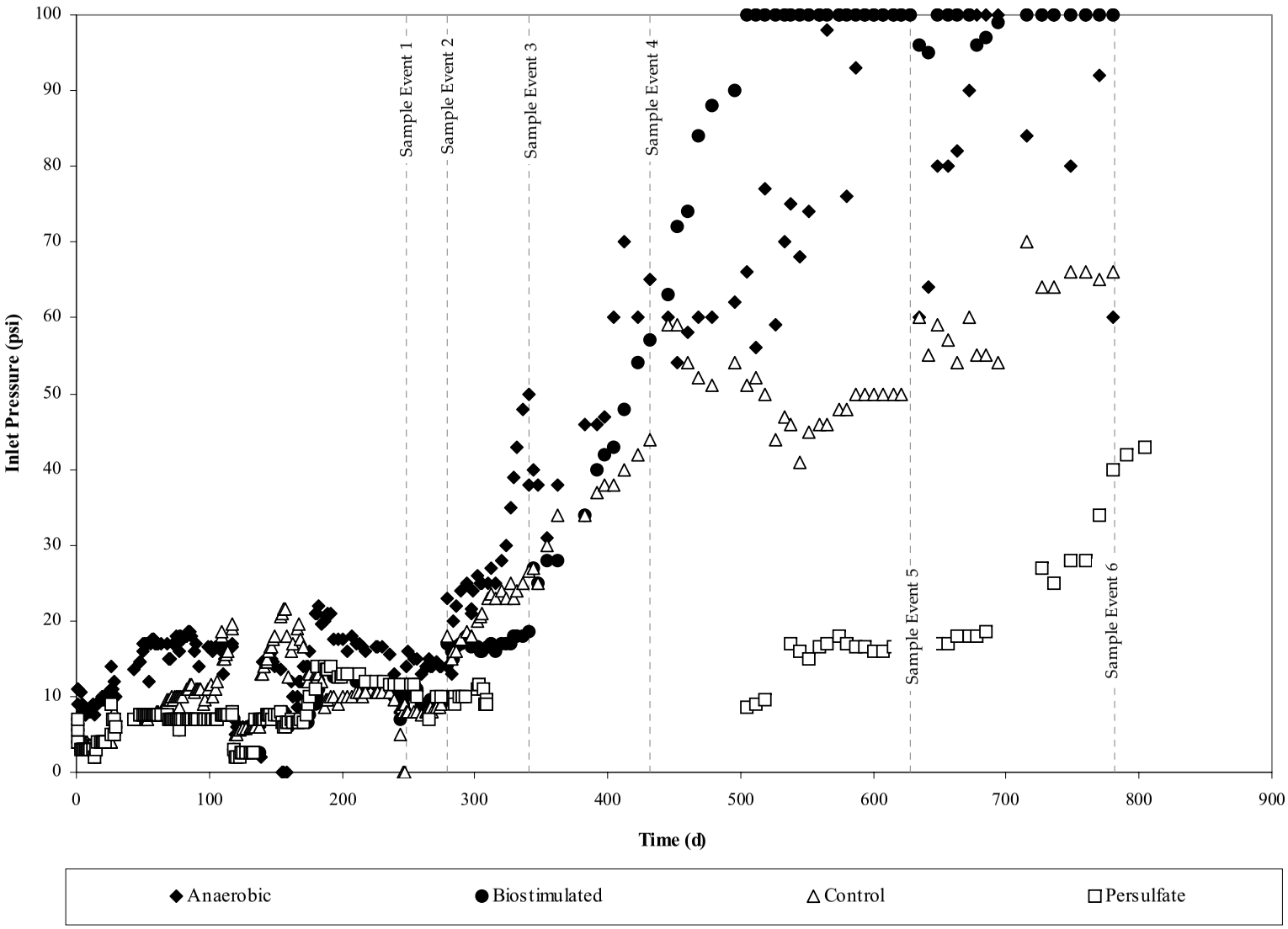

Figure A5. Inlet pressure data for all columns, 'Sample Event 1' is also denoted as t = 0.

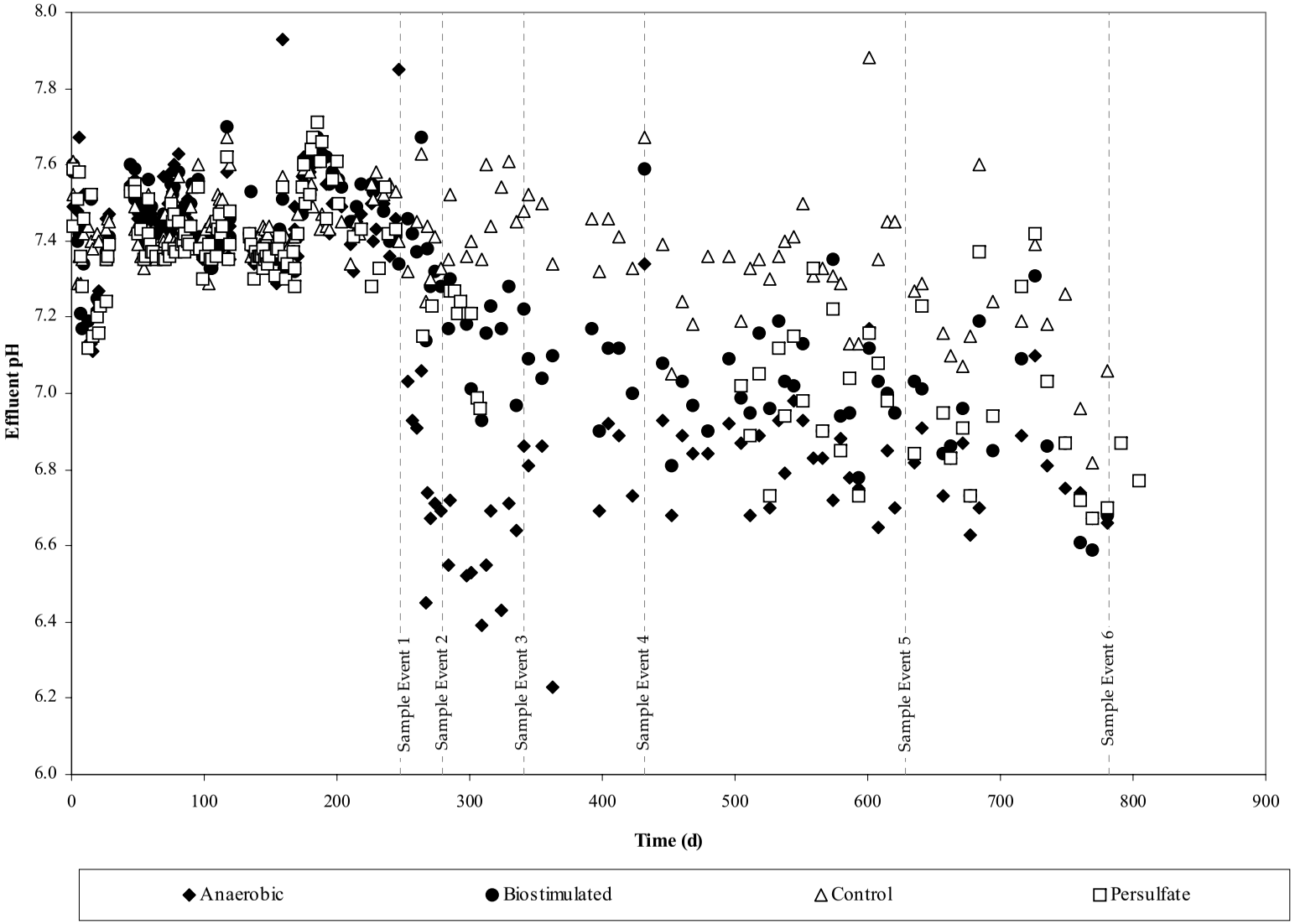

Figure A6. Effluent pH data for all columns, 'Sample Event 1' is also denoted as t = 0.

Simulated Groundwater

A simulated groundwater recipe was developed based on historical ion concentrations in groundwater wells surrounding Salisbury, North Carolina (191). Ion composition of the simulated groundwater is summarized in Table A4.

Table A4. Ion composition of the simulated groundwater

Cation	Conc. (mg/L)	Anion	Conc. (mg/L)
Calcium	25	Bicarbonate	80
Magnesium	5.0	Chloride	46
Potassium	2.3	Sulfate	22
Sodium	30		

Groundwater was prepared by adding 1.83 g of $CaCl_2 \cdot H_2O$, 1.01 g of $MgSO_4 \cdot 7H_2O$, 2.19 g of $NaHCO_3$, 1 ml of an 88 mg/L KCl solution, and 1 ml of 1 N H_2SO_4 to approximately 20 L of sterile-filtered deionized water. Sterile filtration was achieved using a 0.1 μm flow-through hollow-fiber membrane water filter (Sawyer Products, Safety Harbor, FL). Simulated groundwater was stored in autoclaved polypropylene carboys (Fisher Scientific, Pittsburgh, PA) dedicated to specific columns. New batches of groundwater were prepared weekly to limit the potential for bacterial growth.

Nutrient-amended groundwater for the biostimulated column was prepared by adding 1 ml of a nutrient stock solution, containing 59.4 g/L of NH_4NO_3 and 29.2 g/L of K_2HPO_4, to the recipe outlined above, yielding final nitrogen and phosphorus concentrations of 1.0 mg/L and 0.3 mg/L, respectively. The final feed solution for the biostimulated column was then continuously sparged with pure oxygen.

Groundwater for the anaerobic column was prepared by adding 100 ml of a 100,000 mg/L chemical oxygen demand (COD) molasses stock solution to the nutrient-amended groundwater recipe. The final amended groundwater was designed to have a COD of 500 mg/L. At this concentration, an ample supply of labile carbon is available in the influent groundwater to encourage consumption of DO, maintaining anaerobic conditions within the column. The final feed solution was sparged with a continuous nitrogen stream to displace residual oxygen.

Flow Characterization

Tracer tests were conducted to determine flow characteristics (*e.g.,* mean retention time, pore volume, and porosity) and to identify any flow short-circuiting or stagnant regions within each column. Tritiated water was selected as the tracer because it is 1) non-reactive, 2) not subject to density effects, and 3) easily detectable in the column effluent (259). A 16 nCi/ml tracer solution was prepared by combining a stock solution of tritiated water with simulated groundwater. Approximately half of one pore volume (1,580 ml) of tritiated groundwater was pumped into each column at a flowrate of 2.1 L/d, followed by continuous flushing with non-tritiated groundwater at the same flowrate. Effluent samples were collected in glass scintillation vials, combined with a commercially-available scintillation cocktail, and analyzed on a Packard Tri-Carb Liquid Scintillation Analyzer (Meriden, CT; Model 1900 TR). Normalized effluent tracer concentrations were analyzed using a method of moments to calculate pore volume and mean retention time for each column. A summary of flow properties is presented in Table A5 for all four columns.

Table A5. Tracer-derived flow properties

Pore Volume	(ml)	$3{,}454 \pm 40$
Mean Retention Time	(hr)	39.3 ± 0.7
Soil Bed Porosity	(%)	36.1 ± 0.3
Pore Velocity	(cm/d)	76.9 ± 0.9

To identify flow short-circuiting, average column pore volumes were determined gravimetrically and compared to the tracer-derived values (Table A5). The average pore volume obtained by the tracer tests corresponded well with the calculated pore volume, indicating that limited bypassing of flow was present. Average mass recovery of the tracer was 99.3 ± 0.7 % among the columns.

Appendix B. Recovery of Phenanthrene-Degrading Bacteria after Simulated *In Situ* Persulfate Oxidation in Contaminated Soil

Procedures for Chemical and Molecular Analyses

PAH Analysis

Aliquots of centrifuged column soil (5 g wet wt. each) were transferred to triplicate 30-mL glass centrifuge vials for extraction. To each vial was added sodium sulfate (6-7 g), 5-mm glass beads to improve mixing, and 10 mL each of dichloromethane and acetone. An internal standard, 0.2 mL of 100 mg/L anthracene-d_{10} in acetonitrile, was also included to evaluate the recovery efficiency. All vials were sealed with screw-top caps with Teflon-lined septa, vigorously shaken for 24 hr, and centrifuged for 15 min at 3,500 rpm. The supernatant from each vial was filtered through a 0.2 µm pore-size nylon filter (Millipore, Burlington, MA) and transferred to a 50-mL volumetric flask. The vials were replenished with dichloromethane and acetone (10 mL each), returned to the shaker for 24 hr, and centrifuged as described above. The second-day extracts were filtered and combined with the initial extract in the volumetric flask. The combined extracts were brought up to volume, transferred to amber serum vials, and stored in the dark at 4°C prior to HPLC analysis. The HPLC system included a Waters (Milford, MA) 600E system controller, a Waters 717 Plus autosampler, and a Perkin Elmer (Beaconsfield, UK) LS40 fluorescence detector. Samples were injected through a 3-µm particle-size Supelcosil™ LC-PAH column (Sigma-Aldrich, St. Louis, MO) using a gradient mobile phase of filtered acetonitrile and reagent water. Initial conditions consisted of 60% acetonitrile and 40% filtered water at a flowrate of 1 mL/min. The proportion of acetonitrile was increased linearly to 100% during the first 10 min of each sample run, followed by a flowrate increase to 2 mL/min at 12.5 min. Analyte standards were prepared from an EPA 610 Polynuclear Aromatic Hydrocarbons Mixture stock (Sigma-Aldrich, St. Louis, MO) and used to create a four-point calibration curve for sample quantification. Of the 16 USEPA-regulated PAHs, acenaphthylene and indeno[1,2,3-*cd*]pyrene were not detected using this method. Moisture content was measured in triplicate for each sample to normalize PAH concentrations on a dry mass basis. Recovery of anthracene-d_{10} was ≥90%.

Mineralization Assay

Approximately 5 g (wet wt.) of centrifuged column soil was transferred to an acid-washed 30-mL glass vial and slurried with 20 mL of sterile simulated groundwater as a source of inoculum for mineralization incubations. Assays with each sample were performed in triplicate. Each replicate consisted of a 40-mL amber EPA vial containing 1 mL of soil slurry, 4 mL of sterile simulated groundwater, a sterile glass tube containing filter paper saturated with 60 µL of 2 N KOH, and 1 µL of the radiolabeled substrate, corresponding to 20,000 disintegrations per min (dpm) for ^{14}C-acetate and 30,000 dpm for ^{14}C-phenanthrene. Triplicate killed control incubations were prepared similarly but were amended with 40 µL of phosphoric acid to reduce the pH below 2. Each incubation vial was sealed with an aluminum foil-lined septum and screw-top cap and shaken continuously (60 rpm) at room temperature for 15 d. At designated time points, the filter paper CO_2 trap was removed and replaced, combined with Ultima Gold™ XR scintillation cocktail, and analyzed on a Packard Tri-Carb Liquid Scintillation Analyzer (Meriden, CT; Model 1900 TR). After 15 d, all vials were acidified with phosphoric acid and incubated for an additional 48 hr to collect any residual $^{14}CO_2$. For all incubations, there was negligible recovery of residual $^{14}CO_2$ following acidification. To quantify unmineralized radiolabeled compound in the incubations, 2 mL of ethyl acetate was added to each slurry, shaken overnight, and the activity in the extract quantified by scintillation counting. Total recovery of the radiolabeled compounds as $^{14}CO_2$ plus extractable ^{14}C ranged from 82% to 132% in the live incubations.

16S rRNA Clone Libraries

To identify dominant bacterial groups before and after persulfate injection, clone libraries of 16S rRNA genes were constructed from surface soil DNA extracts from the pre-oxidation sample and 100 d post-oxidation. PCR amplification was performed using primers 8f (260) and 1492r (261) as described elsewhere (185). PCR products were cloned into an Invitrogen TA cloning kit (Carlsbad, CA) per the manufacturer's instructions and resulting inserts were partially sequenced with primer 8f by Functional Biosciences, Inc. (Madison, WI). The resulting partial 16S rRNA sequences were trimmed using Sequencher 4.7 (Gene Codes; Ann Arbor, MI) and close relatives identified by BLASTN searches of GenBank (262). Using ClustalX (263), sequences were aligned and a neighbour-joining phylogenetic tree was constructed (bootstrapped 1,000 times without considering gaps). Chimeras were resolved using the Bellerophon server (264) and confirmed with BLAST analyses. Partial 16S rRNA gene sequences recovered from this work were submitted to GenBank with accession numbers HM622160-HM622262.

Persulfate Batch Experiments: Demand and Efficacy

Batch Persulfate Demand

To ensure a sufficient dose of persulfate was added to the column (to overcome the oxidant demand of the soil), batch experiments were conducted to determine the persulfate demand of the column soil. In general, the procedure for measuring soil oxidant demand involves exposing the test soil to varying oxidant dosages over a period of time and subsequently quantifying the amount of oxidant remaining in the aqueous phase. In most cases, simple colorimetric techniques are used to measure the residual oxidant (266). For the batch experiment, 8, 20, and 50 g/L persulfate solutions were prepared using simulated groundwater (Appendix A, Table A4) as the solvent. Fifteen-ml of each persulfate solution were added to triplicate acid-washed 30-ml glass vials containing approximately 5 g (wet wt.) of original column soil (previously stored at 4°C). This corresponds to persulfate dosages of 25, 63, and 157 mg of persulfate per g of dry soil (mg/g). No-soil controls for each persulfate concentration were also included to determine the extent of persulfate auto-oxidation over time. All vials were sealed with screw-top caps (with aluminum foil-lined septa) and shaken continuously (150 rpm) at 40°C (for persulfate activation) for a period of 14 d. Each day, the vials were briefly removed from the shaker and vigorously shaken to maximize contact between the oxidant and soil particles. Over the course of the experiment, aqueous phase samples (0.2 ml) were periodically collected to monitor the disappearance of persulfate in the sample and control vials. Periodic sampling was necessary to ensure the maximum persulfate demand of the soil had been reached (indicated by the stabilization of aqueous phase persulfate concentrations between sampling time points).

Residual persulfate concentrations were quantified using a spectrophotometric method described by Huang et al. (115). Briefly, 0.1 ml of supernatant was added to a 20 ml glass culture tube containing 0.9 ml of distilled water, 10 ml of 2.5 N H_2SO_4 (Fisher Scientific), and 0.1 ml of 0.4 N ferrous ammonium sulfate ($Fe(NH_4)_2(SO_4)_2 \cdot 6H_2O$, 100.9%, Fisher Scientific). The contents were mixed and allowed to react for 40 min. After the reaction period, 0.2 ml of 0.6 N ammonium thiocyanate (NH_4SCN, 97.9%, Fisher Scientific) was added to produce a blood-red color complex of varying intensities, which are directly proportional to the residual persulfate concentration. Details on the chemistry of thiocyanate colorimetry are available in (267). The absorbance of each sample was measured using a Hitachi U3300 spectrophotometer at a wavelength of 450 nm. A calibration curve was developed using the same procedure above with persulfate standards of the following concentration: 0, 0.5, 1.3, 3.2, 8, 20, and 50 g/L ($R^2 = 0.992$).

Persulfate demand for the column soil was estimated to be 14.2 ± 0.6 mg/g and 14.9 ± 1.2 mg/g for the 25 mg/g and 63 mg/g doses, respectively. For the highest dose (157 mg/g), consumption of persulfate in the replicate samples did not deviate from the control and could not be calculated.

Batch Persulfate Efficacy

The efficacy of persulfate to oxidize PAHs was determined as part of the batch experiment discussed above. After 14 d of continuous shaking, triplicate soil incubations for each persulfate dosage (*i.e.*, 0, 25, 63, and 157 mg/g) and activation temperature (20, 30 and 40°C) were solvent-extracted and PAH concentrations quantified according to the procedures outlined earlier. Separate extractions of the original column soil were performed in triplicate to quantify PAH levels prior to persulfate exposure. PAH concentrations from the persulfate-dosed incubations were then compared to the initial PAH values to determine the percentage of each PAH oxidized at each persulfate dosage. Total PAH removal was greatest at an activation temperature of 40°C for all persulfate doses (Figure B1).

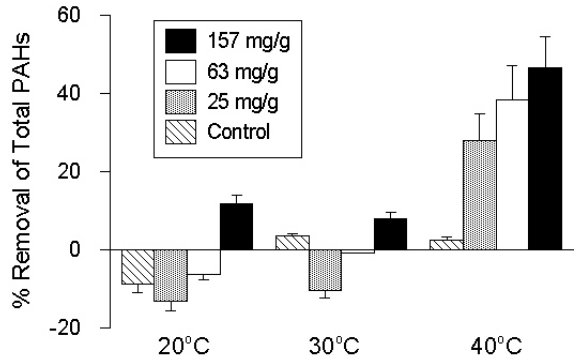

Figure B1. Percent removal of total PAHs in the column soil after persulfate oxidation at various doses for 15 d, at activation temperatures of 20°C, 30°C, and 40°C. Values represent the means and standard deviations of triplicate incubations.

qPCR Primer Sets

Table B1. qPCR primers used in this study

Target Group	Primer Name	Primer Sequence (5′→3′)	Reference
Bacteria	341F	CCT ACG GGA GGC AGC AG	(265)
	517R	ATT ACC GCG GCT GCT GG	(265)
Pyrene Group 1	Eub399F	ACT CCT ACG GGA GGC AGC	(265)
	PG1R	TAG CAG GCC GTA TTA AGA C	(184)
Pyrene Group 2	PG2F	GCA CAG GGT AGC TTG CTA TC	(184)
	PG2.1R	CGC AGG CTC ATC GTT CC	This study

Effluent Persulfate Breakthrough

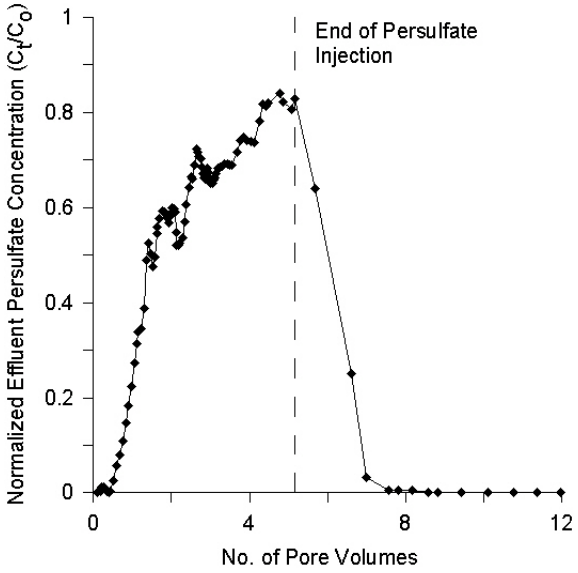

Figure B2. Breakthrough curve of effluent persulfate.

Dissolved Oxygen Profiles

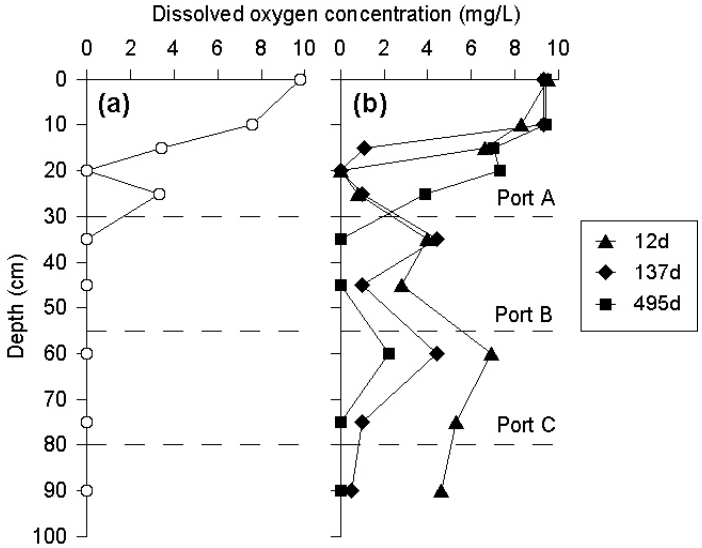

Figure B3. Dissolved oxygen profiles before persulfate injection (a) and 12, 137, and 495 d after injection (b). Oxygen concentrations at the top of the column (depth = 0) were measured in the feed reservoir for the simulated groundwater; note that the original soil bed surface was at a depth of approximately 5 cm. Data for post-oxidation time points other than those shown are omitted for clarity. The absence of oxygen at a depth of 20 cm shown in (a) and (b) was attributed to a blockage of the screened cannula due to fines accumulation.

Persulfate Batch Experiments: Effect of Temperature and Sulfate

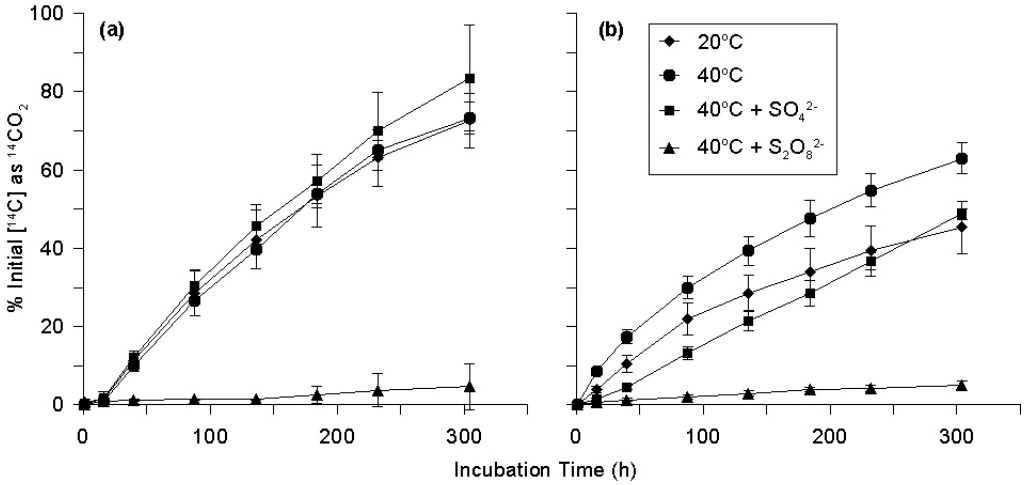

Figure B4. Mineralization of ^{14}C-acetate (a) and ^{14}C-phenanthrene (b) over 13 d under the following conditions: 20°C, 40°C, 40°C plus addition of sulfate at a dose equivalent to stoichiometric production (based on persulfate demand in column), and 40°C plus addition of persulfate at equivalent dose to column experiment. Values represent cumulative means and standard deviations of triplicate incubations.

Phylogenetic Tree of All Sequences Recovered in the Clone Libraries

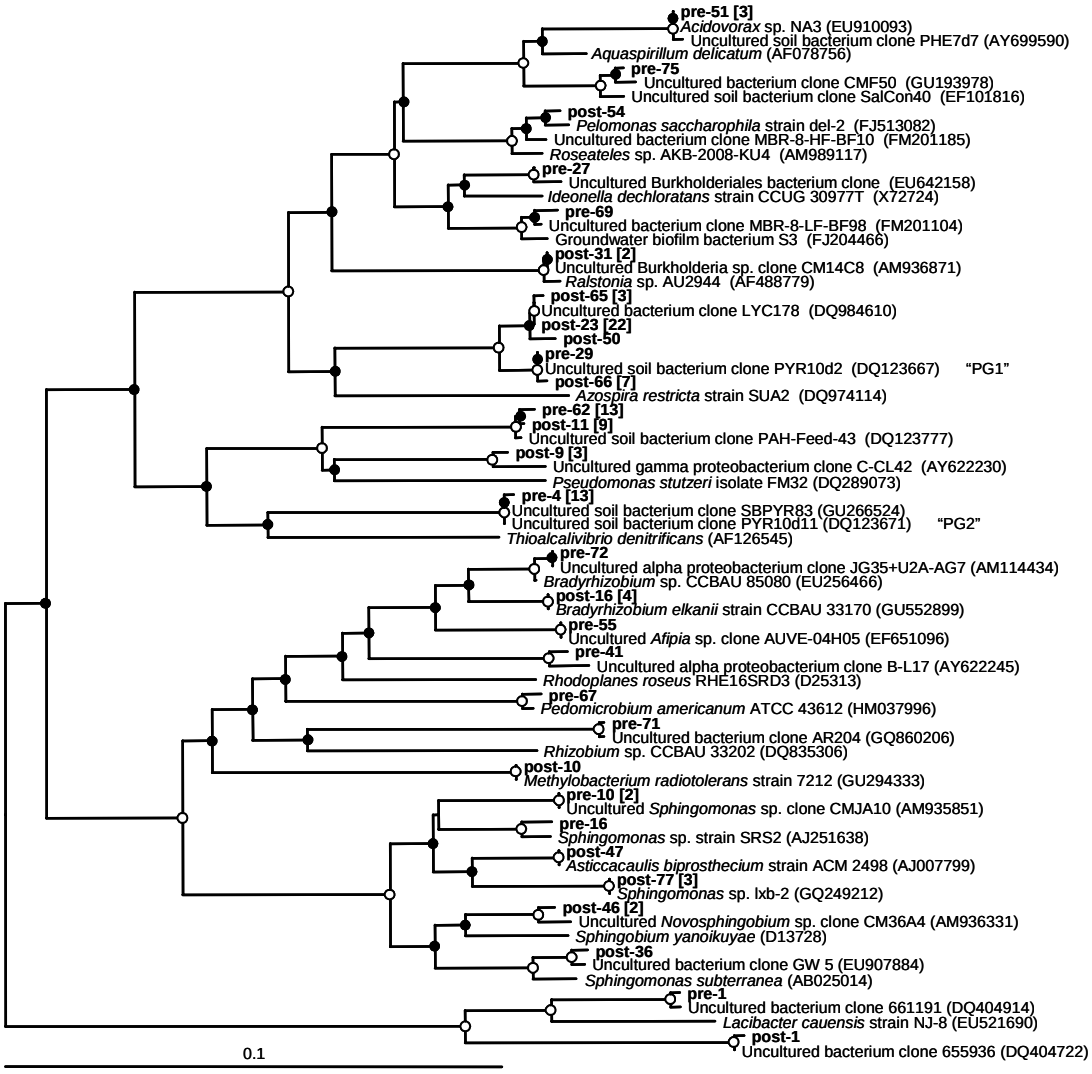

Figure B5. Neighbor-joining phylogenetic tree of 16S rRNA gene sequences recovered pre- and post-oxidation (100 d) from the column surface soil and selected close relatives. Clones from this study (in bold) follow the naming scheme of "pre" (pre-oxidation) and "post" plus an assigned number for identification purposes. Square brackets (in bold) include the number of sequences within an OTU represented by the clonal sequence shown. GenBank accession numbers are shown in parentheses for the selected reference sequences. Bootstrap values are indicated on nodes with an open (○) and closed (●) circle representing ≥95 and ≥50% bootstrap support, respectively. *Thermus aquaticus* YT-1 (L09663) was used as an outgroup (not shown).

Mass of DNA

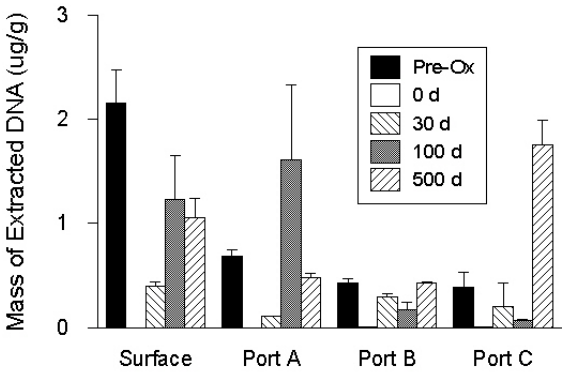

Figure B6. Mass of extracted DNA in soil samples collected before (pre-ox) and 0, 30, 100, and 500 d after persulfate injection. Values represent the means and standard deviations of triplicate DNA extractions.

Soil PAH Concentrations

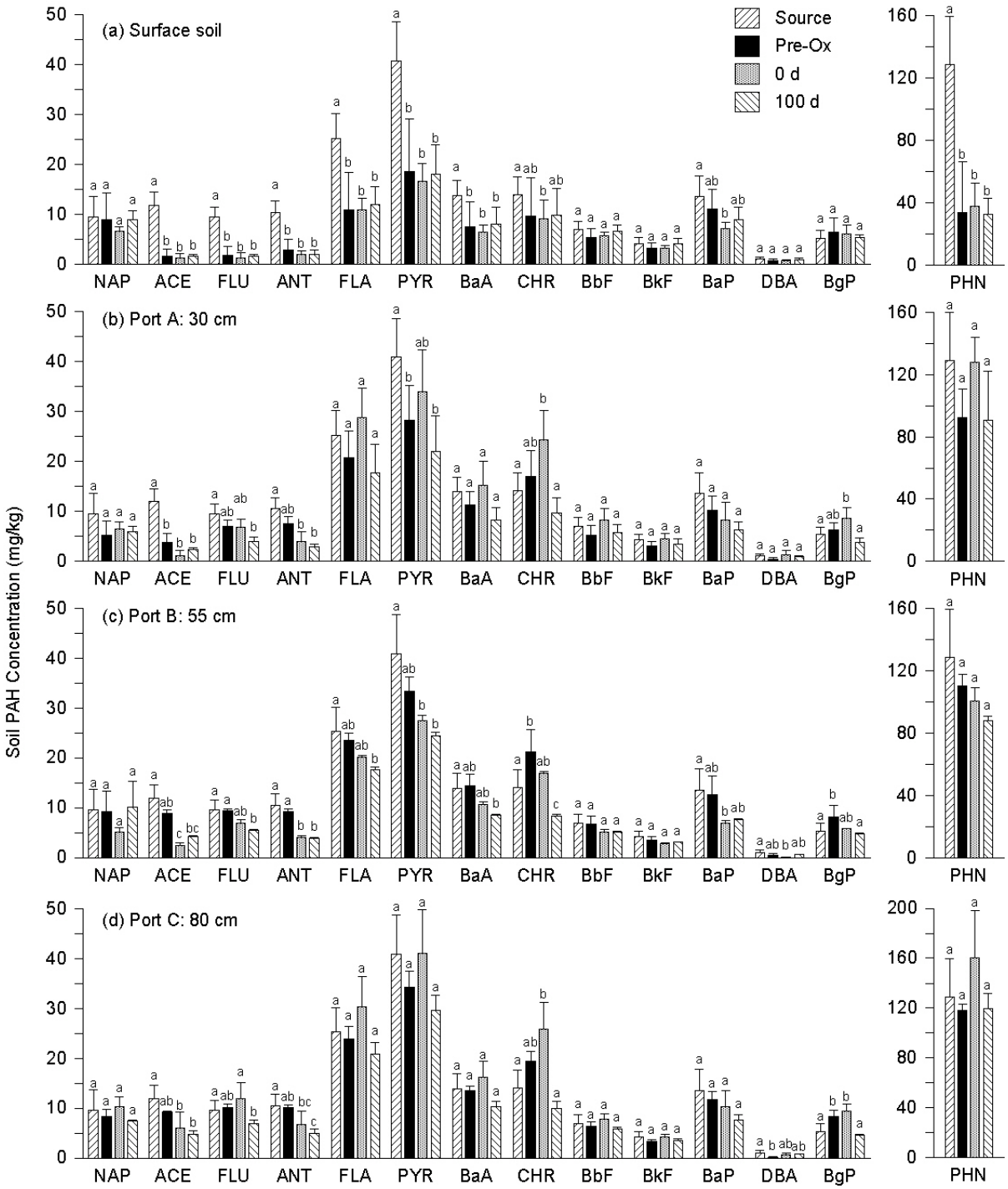

Figure B7. PAH concentrations in soil samples collected pre- and post-persulfate injection from the surface soil (a), Port A (b), Port B (c), and Port C (d). Note that phenanthrene concentrations are plotted separately in each panel. Error bars represent one standard deviation. The letters above the error bars represent the results of significance analyses using the Tukey-Kramer HSD test. For each analyte, a pair of conditions sharing a common letter is not significantly different from each other at a 95% significance level. See Table A2 for definitions of abbreviations.

Appendix C. Effects of Anaerobic Incubation on PAH Mobilization and Bioavailability in Contaminated Soil

Experimental Methods and Results

Rationale and Methods

In weathered soils, anaerobic incubation has shown promise (in batch studies) for enhancing PAH mobilization (170, 213, 215). To date, limited work has been done to assess the effects of long-term anaerobic imposition on aqueous-phase PAH concentrations under continuous-flow conditions. This study considers the hypothesis that imposed anaerobic conditions will improve PAH mobilization in the aqueous phase of the column.

Experimental methods for column soil and effluent sampling, PAH extraction and quantification, and solid-phase desorption are outlined in Appendix A.

Results

For most PAHs, no significant difference (p <0.05) in soil concentration was observed before and after anaerobic treatment (Figure C1). The significant reductions in PAH concentration observed in the surface soil were attributed to PAH dissolution and biodegradation within the oxygenated zone (during the equilibration phase). Effluent PAH concentrations for the anaerobic and control columns are presented in Figure C2. Although aqueous phase PAH concentrations in the anaerobic effluent were 2-3 times higher than the control after 534 d, the total PAH mass removed was only modestly greater (7.0 ± 1.6% vs. 6.5 ± 1.4%), indicating that PAH mobilization was not significantly enhanced by the imposed anaerobic conditions. Moreover, PAHs were below detection in all pre-filter extracts and effluent PAH concentrations remained well below (1-3 orders of magnitude) respective aqueous solubilities, suggesting that facilitated PAH transport by particle-binding (>0.7 μm) was not a significant transport mechanism. These findings are in contrast to a recent anaerobic column study (213), where apparent PAH concentrations (dissolved + DOM-bound) in the column effluent were 2.3 to 334 times greater than their respective solubilities after 235 d of highly-reducing (<-250 mV) conditions. These opposing results may reflect varying operating conditions between the studies, specifically, the operational redox state and flowrates. Highly-reducing conditions (*i.e.*, sulfate-reducing and methanogenic) have been shown to increase DOM hydrophobicity, aromaticity, and PAH sorption capacity relative to less-reducing and oxic environments (173). Perhaps, the lower reducing conditions (-112 < E_h < -56 mV) observed in the present study were less favorable for DOM alteration and subsequent PAH-DOM interactions. In addition, Kim et al. (213) reported a marked increase in aqueous phase PAH concentrations following a significant decrease 0.1 ml/min to 0.015 ml/min) in column flowrate. The authors attributed the increase in effluent PAH concentration to an increase in hydraulic retention time, providing sufficient time to maintain highly reducing conditions and stimulate organic matter modification and release into the column porewater. Flowrates in the current study were two orders of magnitude higher (1.0 – 1.5 ml/min).

Zhu et al. (215) found that anaerobic incubation of field-contaminated soil from a former wood preserving facility resulted in a modest improvement in total amount of PAH desorbed; however, little effect was observed on the bioavailable or fast-desorbing fraction of PAH mass. In the present study, no major improvement in the total PAH mass desorbed (relative to the control) was observed after 28 d for most PAHs (Figure C3).

Soil PAH Concentrations

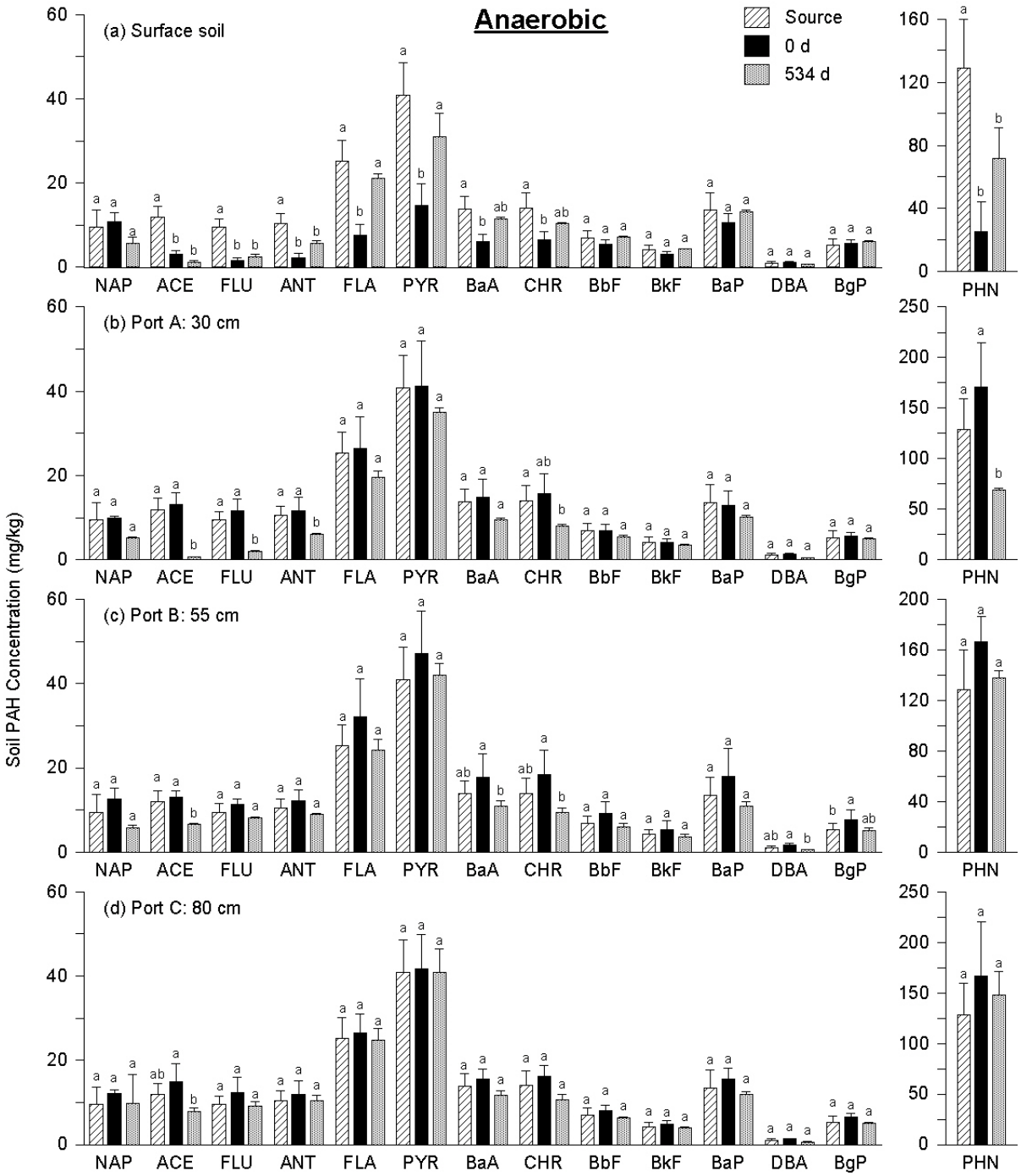

Figure C1. PAH concentrations in the column soil (source) and in soil samples collected from the surface soil (a), Port A (b), Port B (c), and Port C (d) of the anaerobic column immediately before (t = 0) and 534 d after imposition of anaerobic conditions. Note that phenanthrene concentrations are plotted separately in each panel. Error bars represent one standard deviation. The letters above the error bars represent the results of significance analyses using the Tukey-Kramer HSD test. For each analyte, a pair of conditions sharing a common letter is not significantly different from each other at a 95% significance level. See Table A2 for definitions of abbreviations.

Aqueous-Phase PAH Concentrations

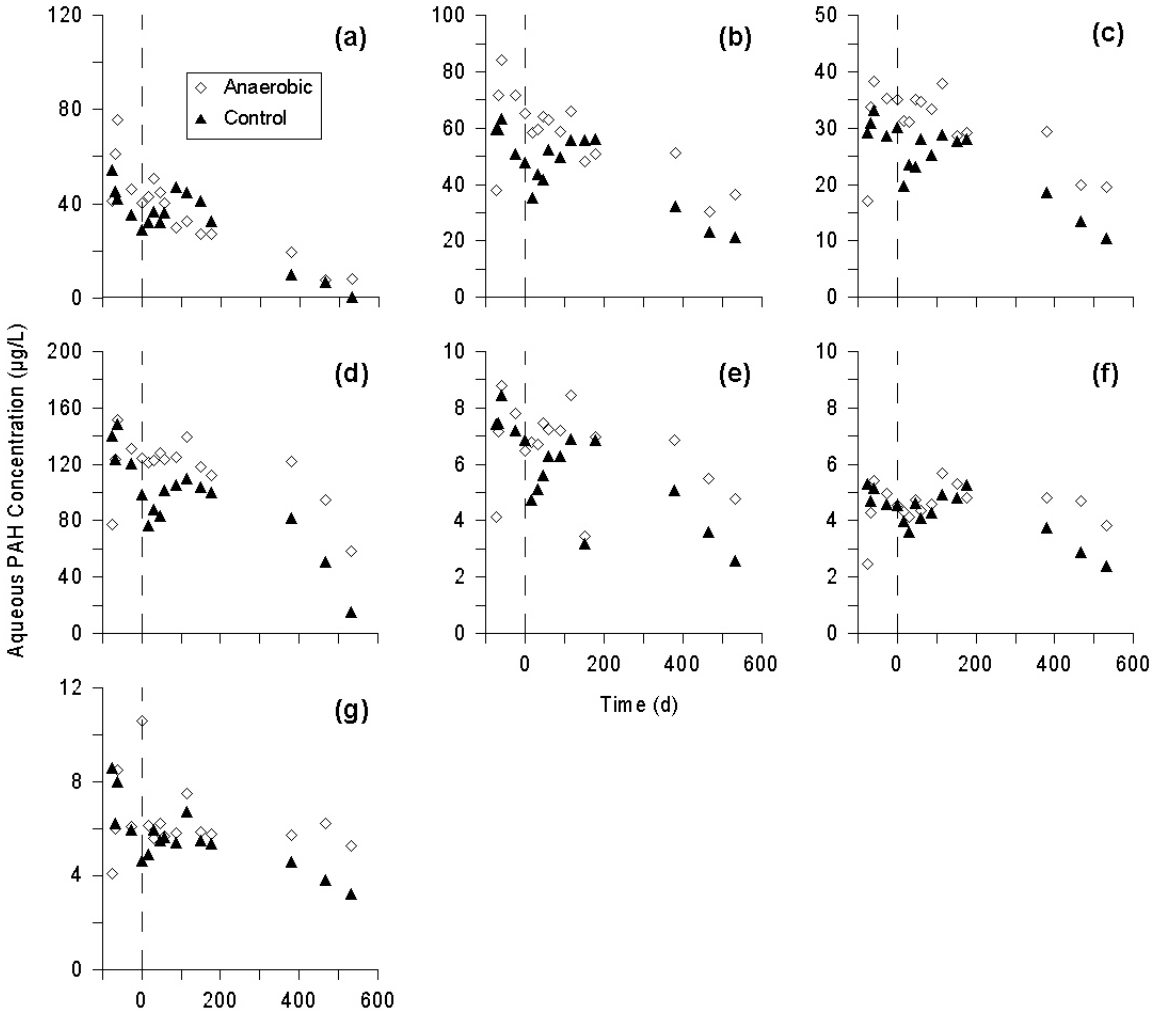

Figure C2. Aqueous-phase concentrations of naphthalene (a), acenaphthene (b), fluorene (c), phenanthrene (d), anthracene (e), fluoranthene (f), and pyrene (g) over time in the anaerobic and control columns. Time 0 (depicted with the vertical dashed line) refers to the time that anaerobic incubation commenced. Data shown in negative time were from samples collected during the equilibration phase. Concentrations of BaA, CHR, BbF, BkF, BaP, DBA, and BgP were below detection.

Desorption Curves of Whole Soil Samples

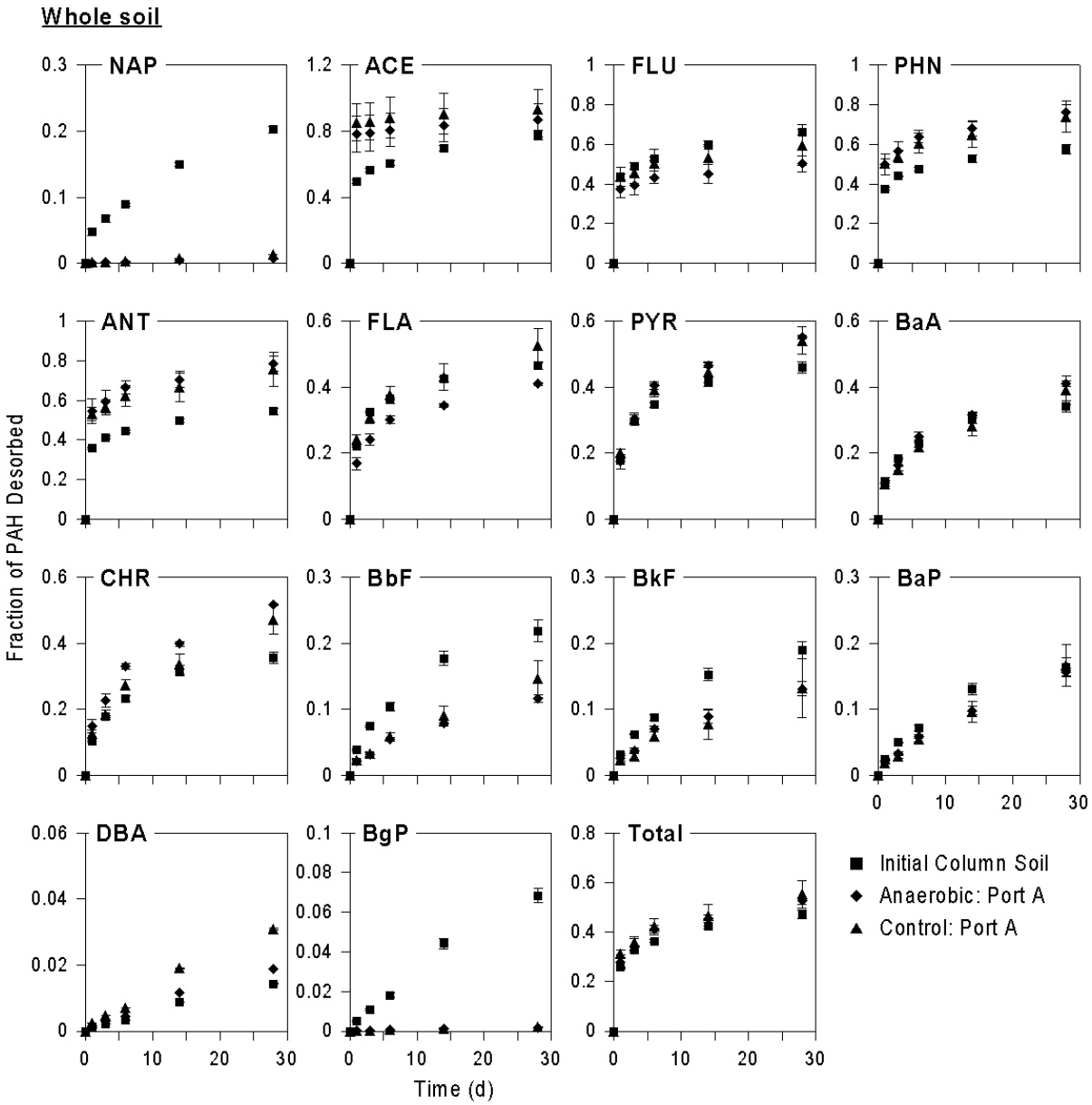

Figure C3. Desorption curves of the initial column soil and samples collected from Port A of the control and anaerobic columns after 534 d. Symbols are the mean values of duplicate analyses from triplicate vessels. Error bars represent the standard deviation and are within the size of the symbol if not visible. See Table A2 for definitions of abbreviations.

Appendix D. Long-Term Simulation of *In Situ* Biostimulation of Polycyclic Aromatic Hydrocarbon-Contaminated Soil

Oxygen Demand

Oxygen demand of the column soil was calculated using oxygen breakthrough curves at DO ports where oxygen-saturation (biostimulated column) and air-saturation (control) had been established. Specifically, the total oxygen mass advancing beyond a given port was subtracted from the oxygen mass influx and divided by the mass of dry soil above the selected port.

Sample calculation: Biostimulated column, DO Port 4

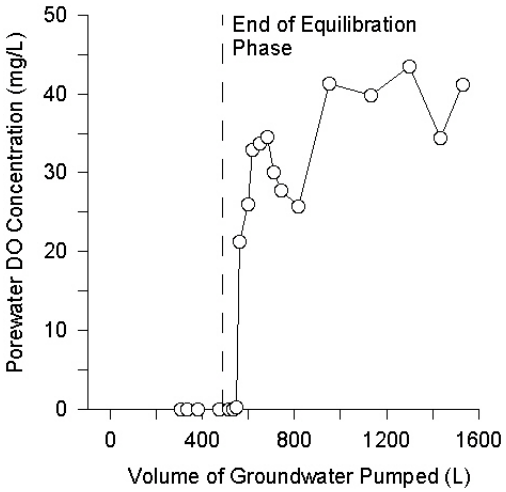

Figure D1. DO concentrations at DO Port 4, 20 cm below the top of the biostimulated column.

1. Calculate the mass of dry soil above DO Port 4

   Total mass of soil in column = 12,996 g
   Bed depth = 100 cm
   Depth of soil above Port 4 = 20 cm ∴ Mass of soil above DO Port 4 = 2,600 g

2. Calculate the mass of oxygen introduced into the column

Equilibration Phase	Biostimulation Phase
Volume pumped = 492.0 L	Volume pumped = 1,041.5 L
Oxygen concentration = 9.3 mg/L	Oxygen concentration = 44.4 mg/L
Mass of oxygen = 4,576 mg	Mass of oxygen = 46,243 mg

   ∴ Total mass of oxygen = 50,819 mg

3. Calculate mass of oxygen consumed in soil above DO Port 4

   Mass of oxygen transported beyond DO Port 4 (Area under curve) = 35,348 mg
   ∴ Mass of oxygen consumed = 50,819 – 35,348 mg = 15,471 mg

4. Calculate oxygen demand for soil above DO Port 4

   ∴ Oxygen demand = 15,471 mg / 2,600 g = <u>6.0 mg/g</u>

PAH Mass Removal in the Control Column

Table D1. Percent PAH mass removed by dissolution, sampling, and biodegradation in the control column after 534 d.

	Percent of PAH Mass Removed			
Analyte [a]	Total	Dissolution	Sampling	Biodegradation [b]
NAP	35.3 ± 47.4	25.5 ± 11.2	12.6 ± 5.6	NA
ACE	61.1 ± 26.9	34.1 ± 7.7	5.2 ± 1.2	21.8 ± 28.0
FLU	47.2 ± 23.6	22.8 ± 4.7	6.9 ± 1.5	17.5 ± 24.1
PHN	33.5 ± 26.0	6.5 ± 1.6	8.5 ± 2.1	18.6 ± 26.2
ANT	37.5 ± 23.9	5.0 ± 1.1	8.6 ± 1.9	23.9 ± 24.0
FLA	31.5 ± 20.9	1.6 ± 0.3	10.4 ± 2.1	19.6 ± 21.0
PYR	27.2 ± 20.3	1.2 ± 0.2	10.6 ± 2.1	15.4 ± 20.5
BaA	37.7 ± 23.9	[c]	11.7 ± 2.6	26.0 ± 24.0
CHR	45.3 ± 28.3	[c]	13.9 ± 3.6	31.4 ± 28.6
BbF	27.3 ± 26.5	[c]	14.5 ± 3.8	12.8 ± 26.8
BkF	27.0 ± 28.7	[c]	14.2 ± 4.0	12.8 ± 28.9
BaP	28.8 ± 32.8	[c]	14.6 ± 4.6	14.2 ± 33.1
BgP	13.0 ± 31.1	[c]	19.7 ± 6.0	NA
Total	34.1 ± 23.7	6.2 ± 1.4	10.0 ± 2.3	17.9 ± 23.9
3-ring [d]	36.5 ± 25.8	9.4 ± 2.2	8.2 ± 2.0	18.9 ± 26.0
4-ring [d]	32.6 ± 21.4	[c]	11.2 ± 2.3	21.4 ± 21.5
5-ring [d]	29.1 ± 30.5	[c]	14.3 ± 4.2	14.8 ± 30.8

[a] See Table A2 for definitions of abbreviations.
[b] Calculated by subtracting percent dissolution and percent sampled from the percent total and accounting for error propagation; NA = calculated value was negative.
[c] Value was below detection.
[d] Represents the sum of the mass removed for PAHs with the same number of rings (Table 4.1); NAP and BgP are not included in these values.

Time-Series Graphs of Soil PAH Concentrations

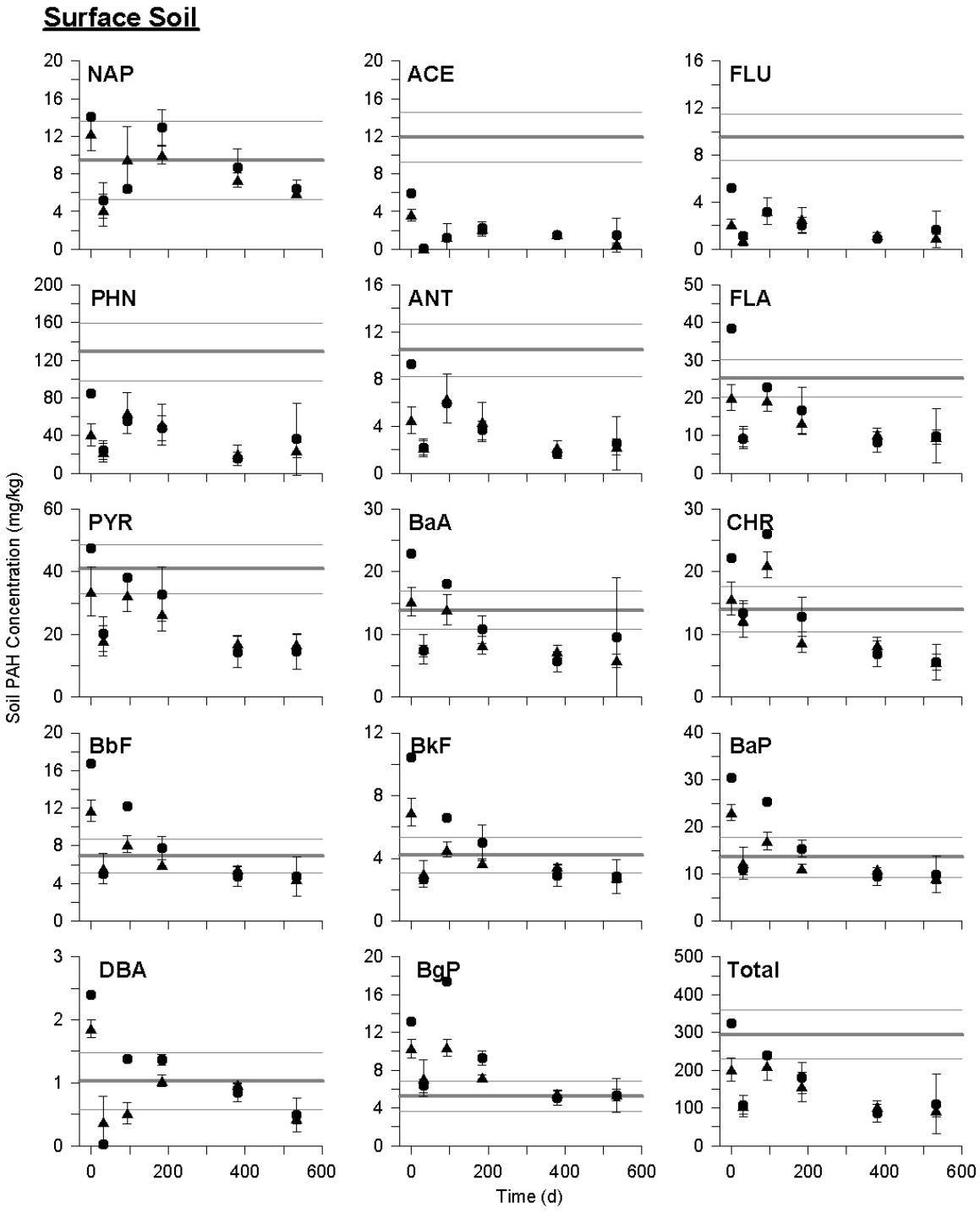

Figure D2. Time courses for PAH concentrations from soil samples collected from surface soil of the biostimulated (●) and control (▲) columns. Each point represents the mean value of duplicate or triplicate samples and the error bars are the range or standard deviation, respectively. Gray lines represent the mean and standard deviation of the PAH in the column soil (Table A2).

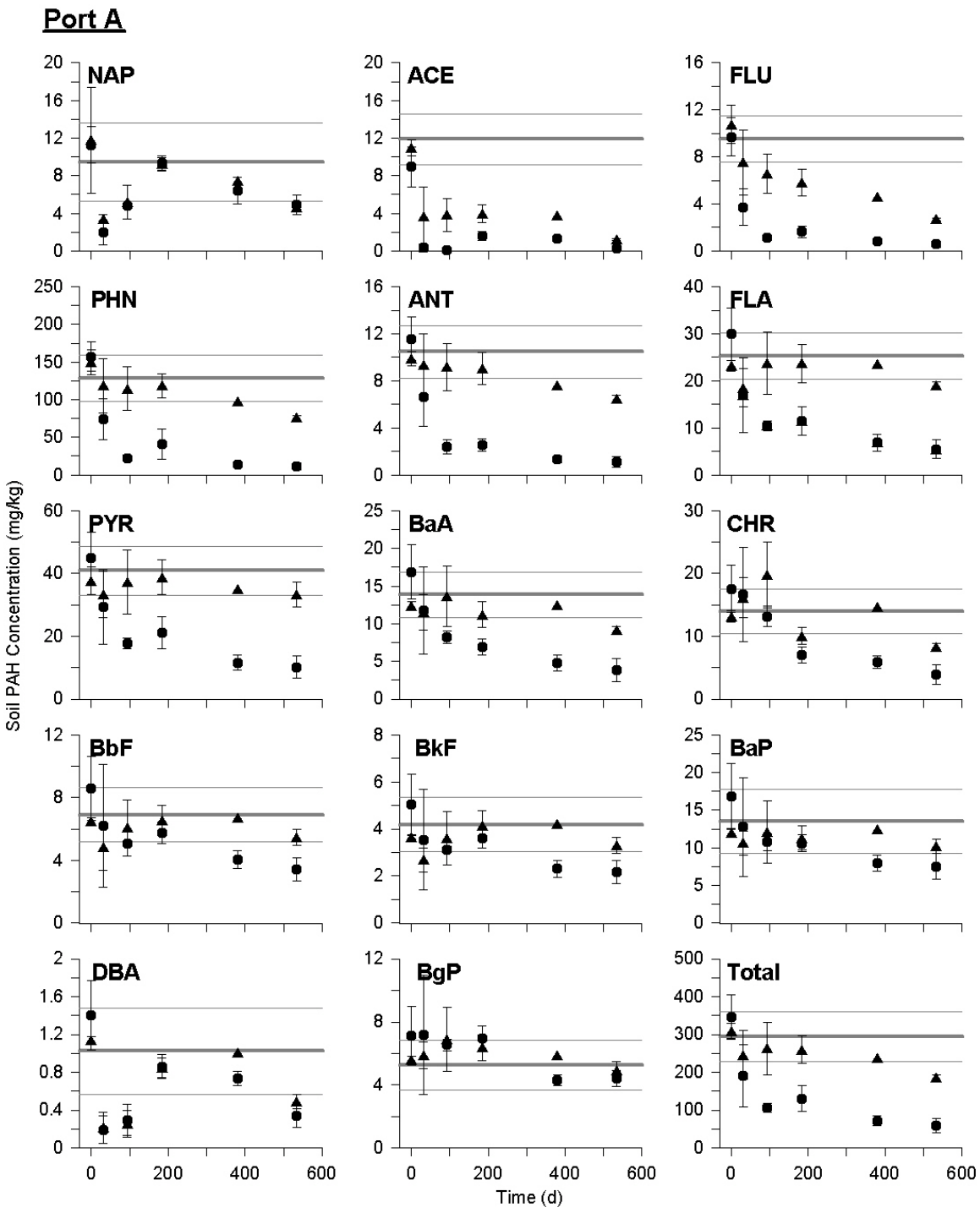

Figure D3. Time courses for PAH concentrations from soil samples collected from Port A of the biostimulated (●) and control (▲) columns. Each point represents the mean value of duplicate or triplicate samples and the error bars are the range or standard deviation, respectively. Gray lines represent the mean and standard deviation of the PAH in the column soil (Table A2).

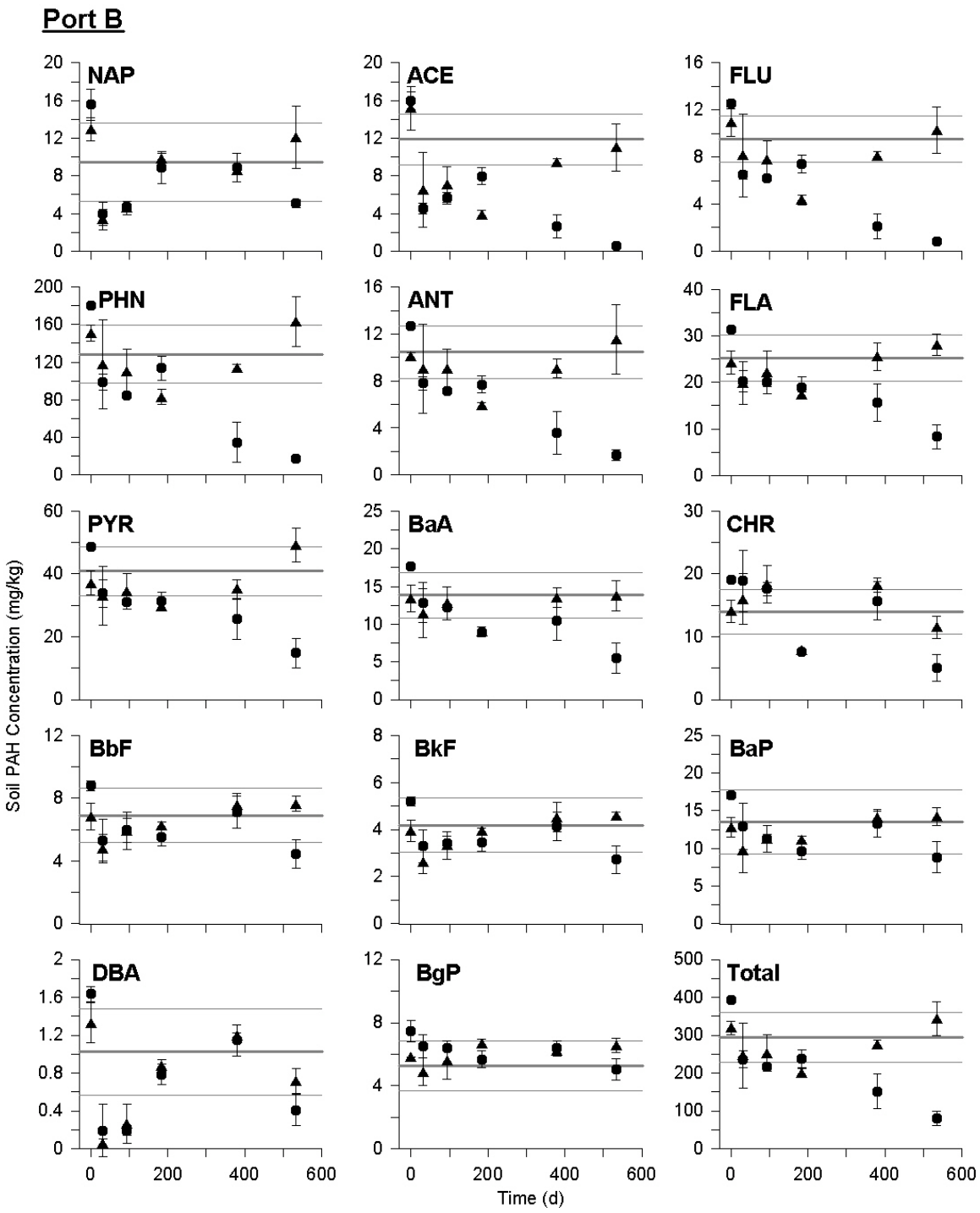

Figure D4. Time courses for PAH concentrations from soil samples collected from Port B of the biostimulated (●) and control (▲) columns. Each point represents the mean value of duplicate or triplicate samples and the error bars are the range or standard deviation, respectively. Gray lines represent the mean and standard deviation of the PAH in the column soil (Table A2).

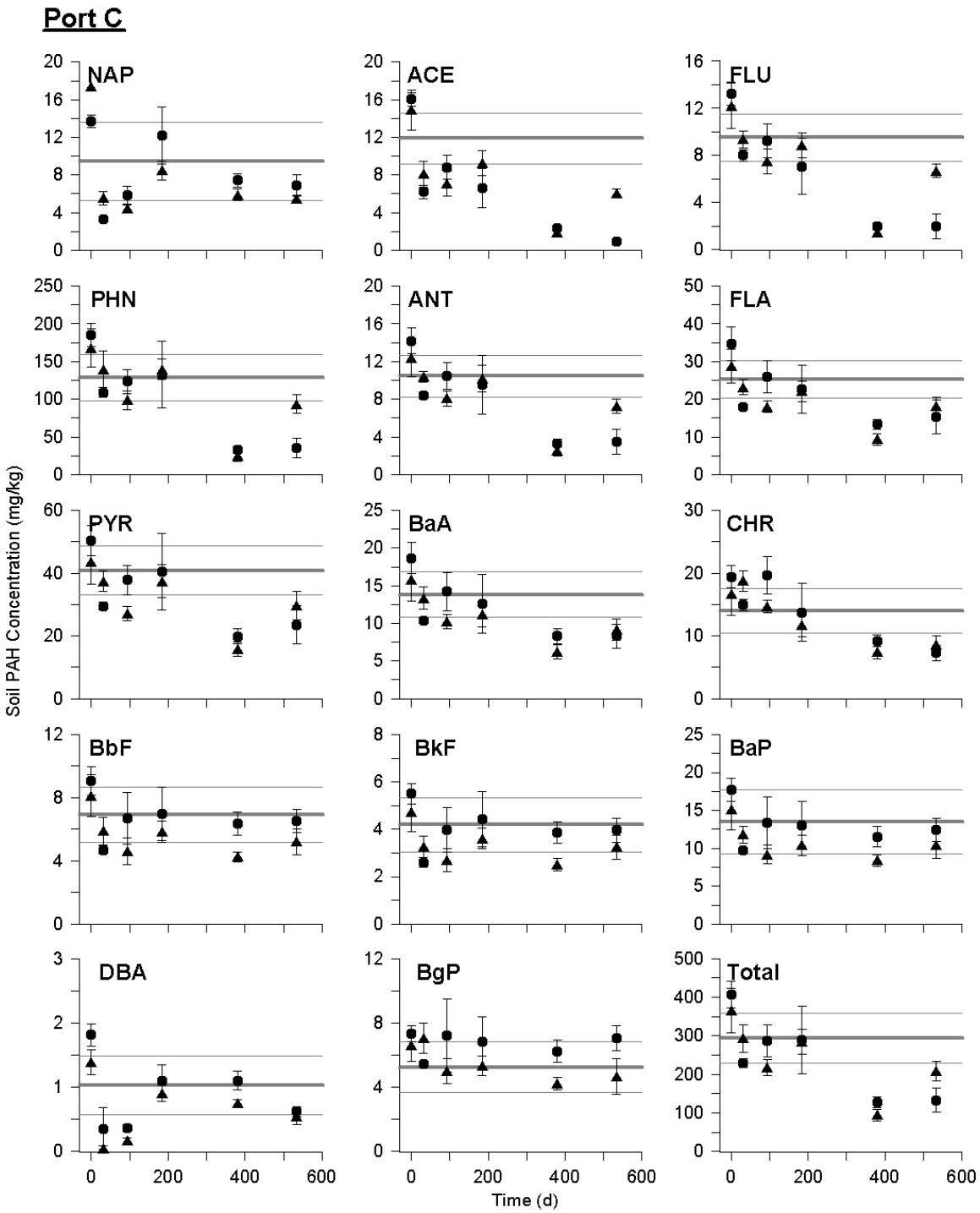

Figure D5. Time courses for PAH concentrations from soil samples collected from Port C of the biostimulated (●) and control (▲) columns. Each point represents the mean value of duplicate or triplicate samples and the error bars are the range or standard deviation, respectively. Gray lines represent the mean and standard deviation of the PAH in the column soil (Table A2).

Aqueous-Phase PAH Concentrations

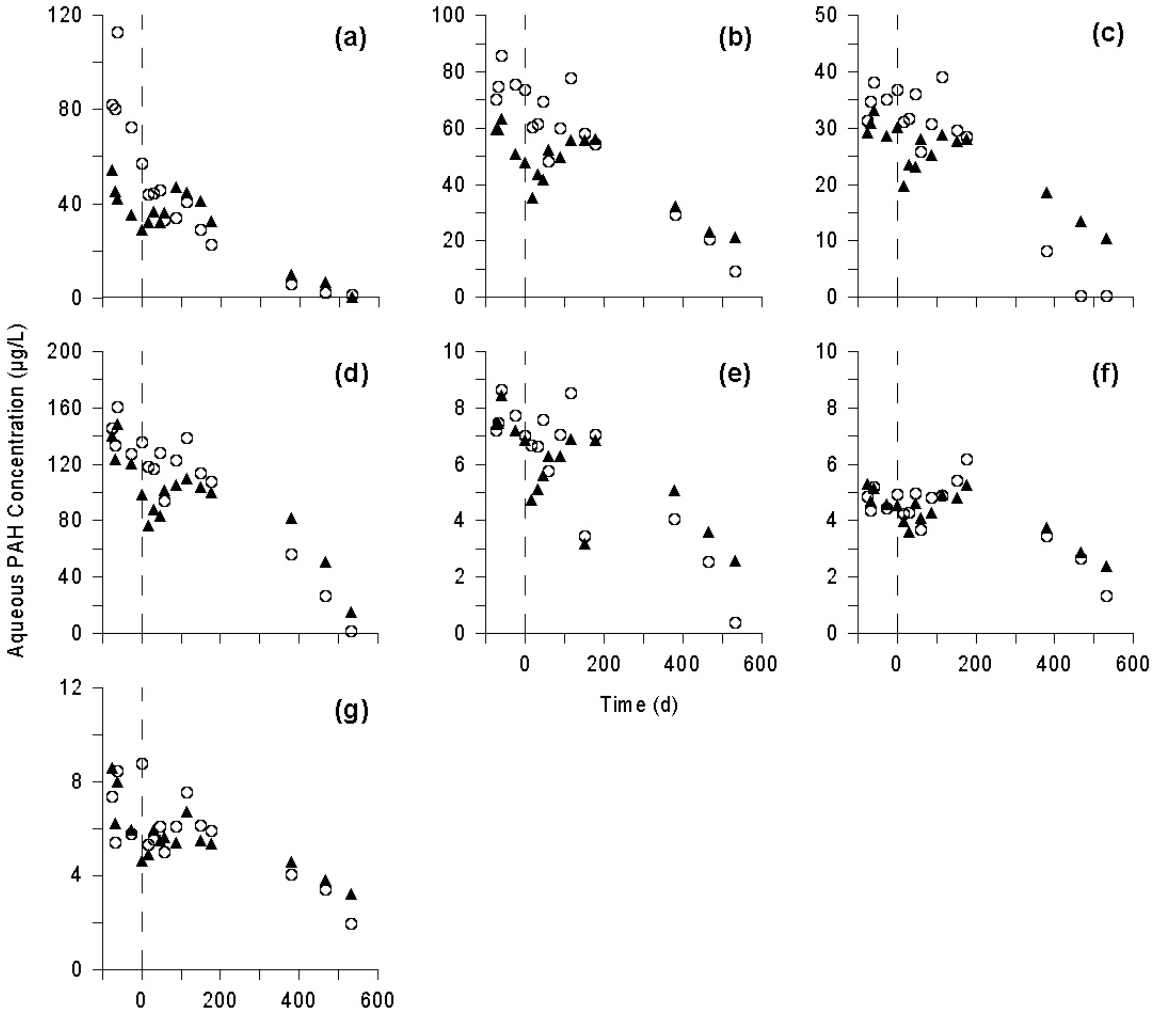

Figure D6. Aqueous-phase concentrations of naphthalene (a), acenaphthene (b), fluorene (c), phenanthrene (d), anthracene (e), fluoranthene (f), and pyrene (g) over time in the biostimulated (○) and control (▲) columns. Time 0 (depicted with the vertical dashed line) refers to the time that biostimulation commenced. Data shown before t = 0 were from samples collected during the equilibration phase. Concentrations of BaA, CHR, BbF, BkF, BaP, DBA, and BgP were below detection.

Spearman Rank Analyses

Table D2. Spearman rank coefficients (r_s) representing significant correlations between DO concentration (mg/L) and PG2 abundance (16S rRNA genes/g) in the biostimulated and control columns.

Spearman rank coefficients (r_s) [a]							
Biostimulated				Control			
Surface	Port A	Port B	Port C	Surface	Port A	Port B	Port C
0.70	0.49	**0.88**	**0.78**	-0.12	-0.20	NA	NA

[a] Only r_s values representing correlations with $p < 0.15$ are reported ($p < 0.05$ in bold and underlined; $0.05 < p < 0.1$ in bold; $0.1 < p < 0.15$ in italics).
NA = not applicable; Spearman rank correlations could not be calculated because oxygen was not detected at Ports B and C of the control column.

Table D3. Spearman rank coefficients (r_s) representing significant correlations between PAH concentrations (mg/kg) and PG2 abundance (16S rRNA genes/g) in the biostimulated and control columns.

	Spearman rank coefficients (r_s) with PG2 abundance [a]				
	Biostimulated [b]		Control [b]		
PAH [c]	Port B	Port C	Port A	Port B	Port C
ACE	**-0.77**				**-0.83**
FLU	**-0.83**	**-0.77**	*-0.71*		**-0.94**
PHN	**-0.83**				**-0.83**
ANT	**-0.94**		*-0.71*		**-0.94**
FLA	**-1.00**				**-0.83**
PYR	**-0.94**				*-0.71*
BaA	**-0.94**				**-0.94**
CHR	**-0.94**	**-0.77**			**-0.94**
BbF					**-0.83**
BkF					*-0.71*
BaP					**-0.81**
BgP	**-0.90**			*0.71*	**-0.89**

[a] Only r_s values representing correlations with $p < 0.15$ are reported ($p < 0.05$ in bold and underlined; $0.05 < p < 0.1$ in bold; $0.1 < p < 0.15$ in italics); r_s values with $p > 0.15$ are omitted for clarity.
[b] No significant correlations were identified in the surface soil and at Port A of the biostimulated column and the surface soil of the control column.
[c] Spearman rank coefficients for NAP and DBA were not significant at all sample locations and are, therefore, omitted from the table; see Table A2 for definitions of abbreviations.

Appendix E. PAH Bioavailability of Soil Fractions after Long-Term Biostimulation of Manufactured Gas Plant Soil

PAH concentrations in the high-density and low-density materials of the original column soil and the soil removed from the control and biostimulated columns are presented in Figure E1. Plots of PAH desorption vs. time for the whole soil, high-density material and low-density material are provided in Figures E2, E3 and E4, respectively. Values of the parameters fitted to either the two-site desorption model (Equation 5.1) or simple first-order model (Equation 5.2) are summarized in Tables E1, E2 and E3 for the whole soil, high-density material and low-density material, respectively.

PAH concentrations in low- and high-density material

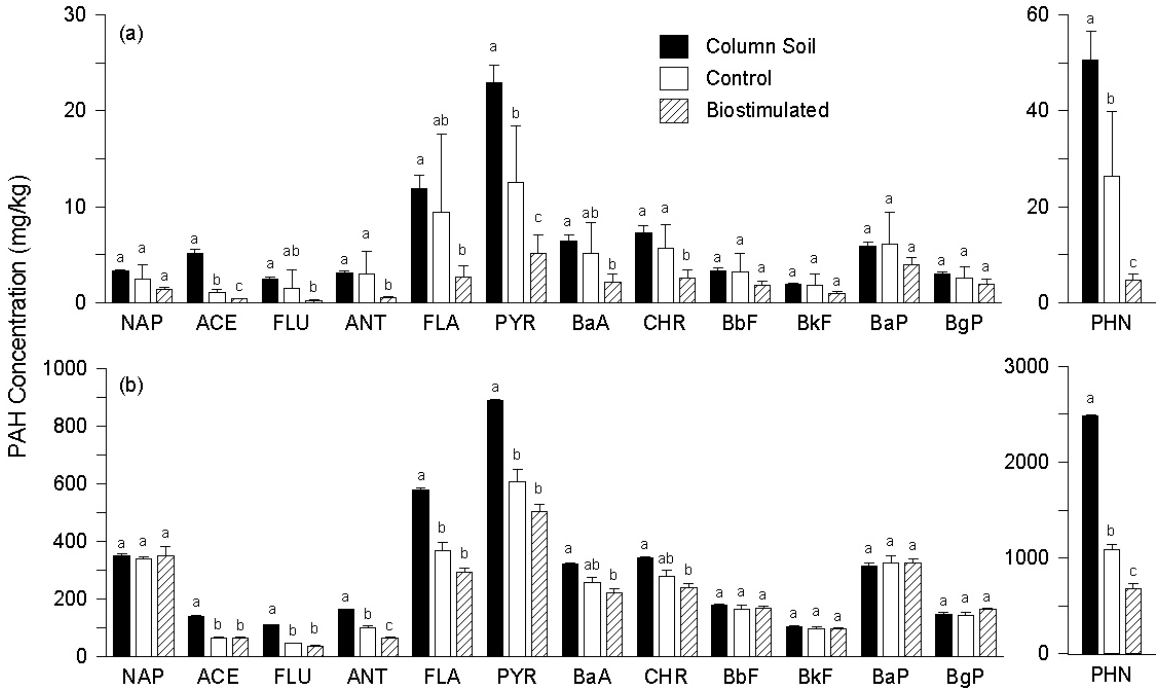

Figure E1. PAH concentrations in the high-density (a) and low-density (b) materials of the original column soil and soil from Port A of the control and biostimulated columns at day 593. Note that phenanthrene concentrations are plotted separately in each panel. Error bars represent one standard deviation in panel (a) and the range in panel (b). The letters above the error bars represent the results of significance analyses using the Tukey-Kramer HSD test. For each analyte, conditions sharing a common letter are not significantly different ($p > 0.05$). Abbreviations: NAP – naphthalene, ACE – acenaphthene, FLU – fluorene, PHN – phenanthrene, ANT – anthracene, FLA – fluoranthene, PYR – pyrene, BaA – benz[*a*]anthracene, CHR – chrysene, BbF – benzo[*b*]fluoranthene, BkF – benzo[*k*]fluoranthene, BaP – benzo[*a*]pyrene, DBA – dibenz[*a,h*]anthracene, BgP – benzo[*g,h,i*]perylene.

Desorption curves for whole soil samples and high and low-density material

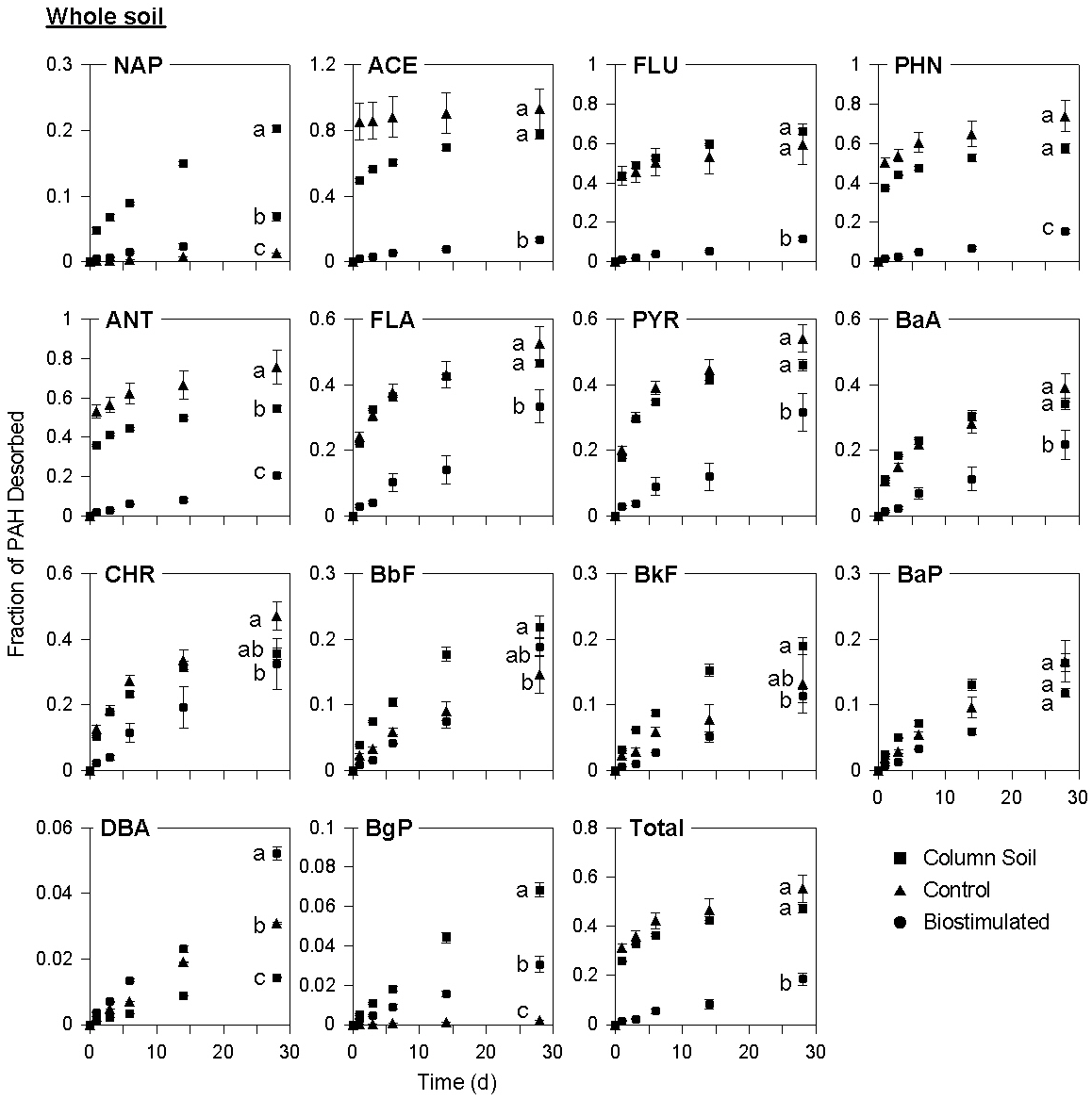

Figure E2. Desorption of PAHs vs. time for the original column soil and samples collected from Port A of the control and biostimulated columns at day 534. Symbols are the mean values of duplicate analyses from triplicate vessels. Error bars represent the standard deviation and are within the size of the symbol if not visible. The letters adjacent to the 28-d time points represent the results of significance analyses using the Tukey-Kramer HSD test. For each analyte, conditions sharing a common letter are not significantly different. Refer to Figure E1 for definitions of acronyms for the PAHs.

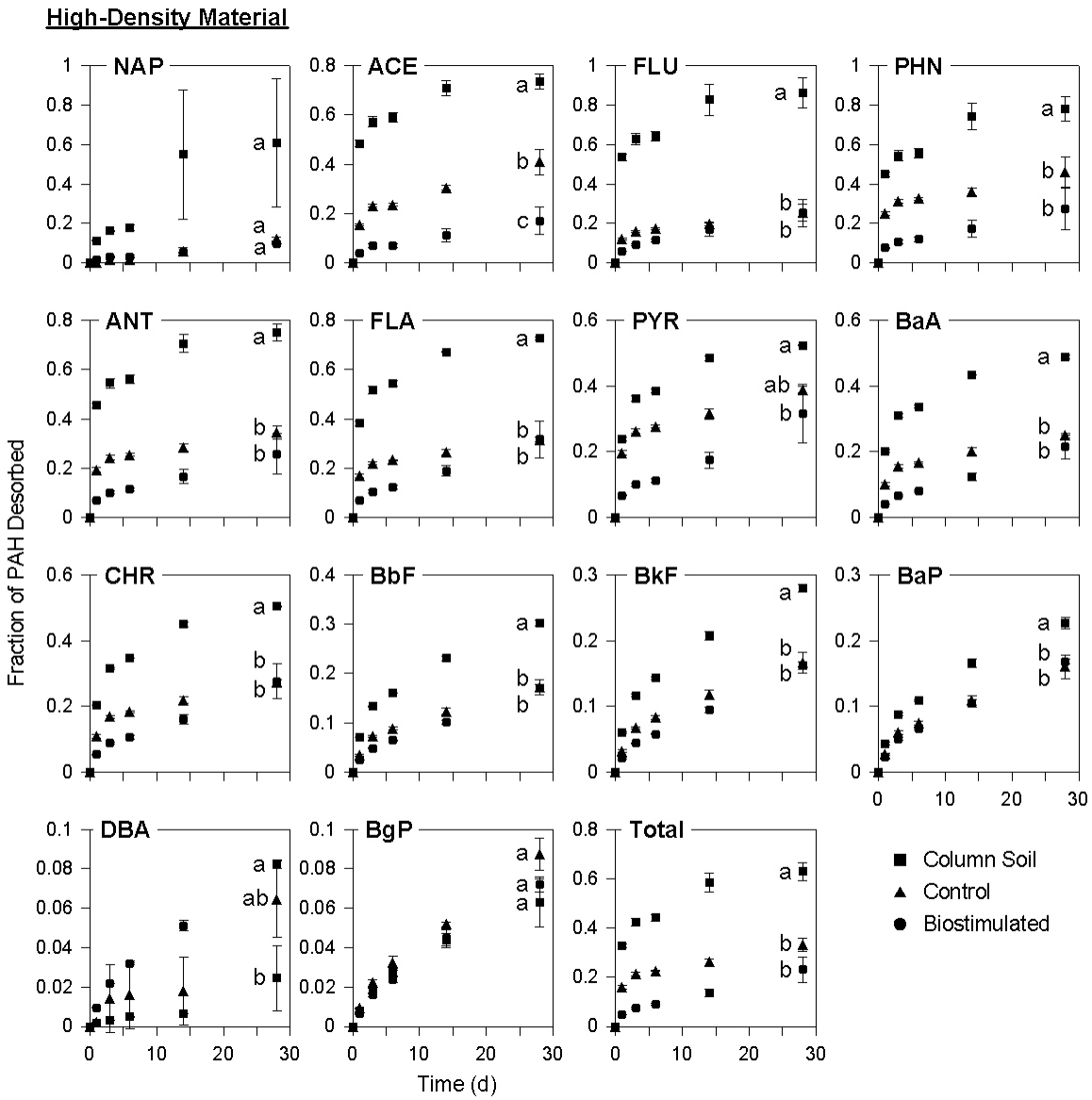

Figure E3. Desorption of PAHs vs. time for the high-density material separated from the original column soil and soil collected from Port A of the control and biostimulated columns at day 593. Notes as in Figure E2.

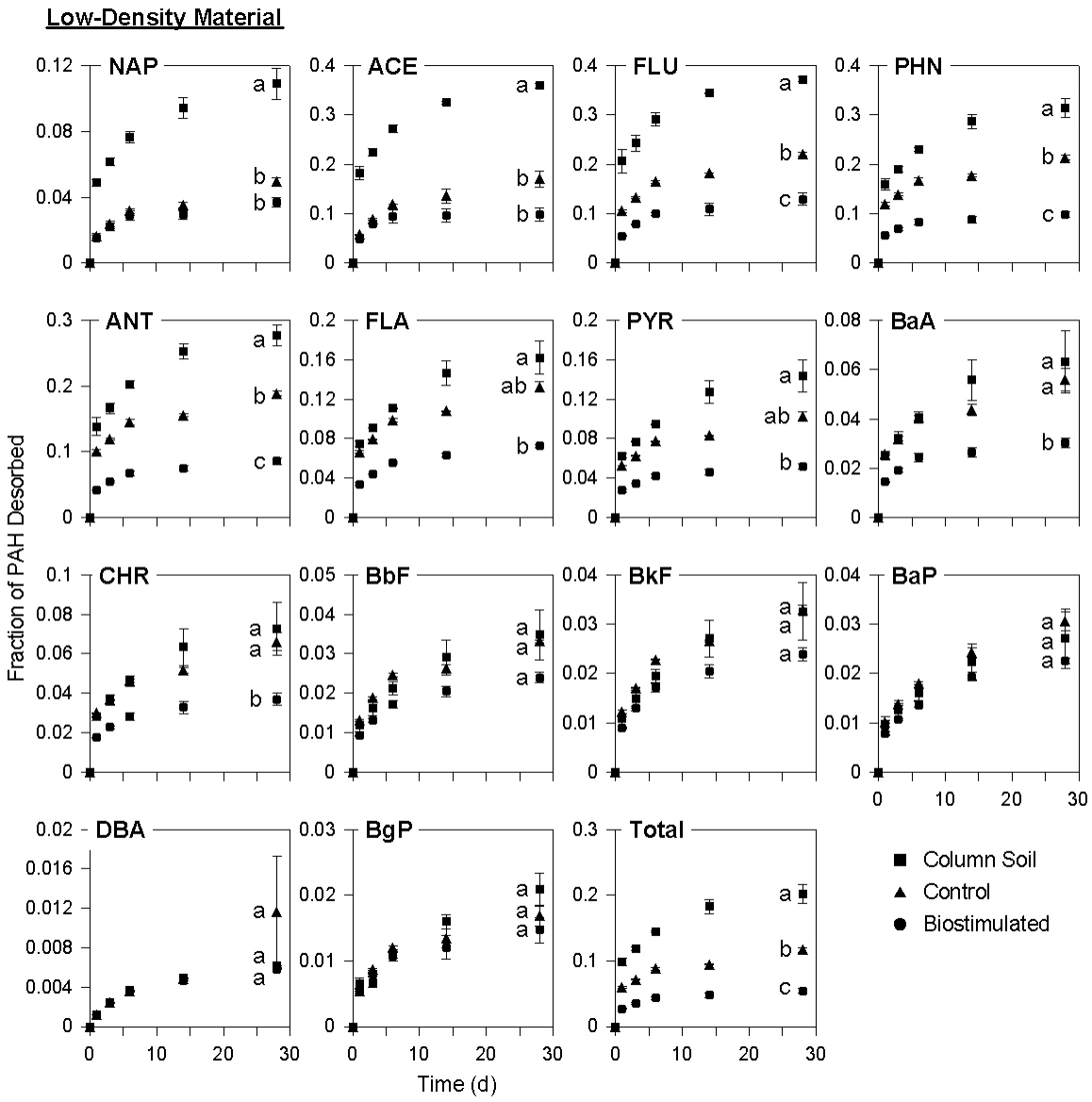

Figure E4. Desorption of PAHs vs. time for the low-density material separated from the column soil and soil collected from Port A of the control and biostimulated columns at day 593. Notes as in Figure E2.

Table E1. Fitted parameter values for the original column soil and soil collected from Port A of the biostimulated and control columns at day 534. [a]

	Fast-desorbing fraction, f			Fast-desorbing rate constant, k_1 (10^{-3}/hr)			Slow-desorbing rate constant, k_2 (10^{-3}/hr)		
Analyte[b]	Column Soil	Control	Biostim.	Column Soil	Control	Biostim.	Column Soil	Control	Biostim.
NAP	0.06 ± 0.01	0 [c]	0 [c]	48.7 ± 28.9	0 [c]	0 [c]	0.26 ± 0.03	0.02 ± 0.001[c]	0.10 ± 0.01[c]
ACE	0.53 ± 0.02	0.85 ± 0.12	0 [c]	98.1 ± 21.5	229 ± 1941	0 [c]	1.15 ± 0.16	1.20 ± 3.10	0.23 ± 0.03[c]
FLU	0.48 ± 0.02	0.45 ± 0.07	0 [c]	94.7 ± 17.7	125 ± 181	0 [c]	0.68 ± 0.09	0.47 ± 0.37	0.18 ± 0.01[c]
PHN	0.43 ± 0.02	0.53 ± 0.06	0 [c]	79.0 ± 14.6	114 ± 91.5	0 [c]	0.46 ± 0.09	0.91 ± 0.40	0.25 ± 0.27[c]
ANT	0.41 ± 0.01	0.55 ± 0.06	0 [c]	85.1 ± 14.2	122 ± 115	0 [c]	0.41 ± 0.06	0.91 ± 0.45	0.33 ± 0.03[c]
FLA	0.34 ± 0.01	0.30 ± 0.04	0 [c]	41.8 ± 5.6	59.2 ± 26.5	0 [c]	0.34 ± 0.06	0.58 ± 0.15	0.57 ± 0.07[c]
PYR	0.32 ± 0.02	0.32 ± 0.04	0 [c]	30.3 ± 5.4	34.2 ± 11.3	0 [c]	0.36 ± 0.08	0.59 ± 0.15	0.52 ± 0.07[c]
BaA	0.21 ± 0.03	0.15 ± 0.03	0 [c]	24.5 ± 8.0	40.0 ± 27.0	0 [c]	0.28 ± 0.08	0.51 ± 0.10	0.37 ± 0.04[c]
CHR	0.23 ± 0.04	0.18 ± 0.04	0 [c]	17.9 ± 5.7	33.2 ± 20.2	0 [c]	0.27 ± 0.10	0.64 ± 0.13	0.61 ± 0.09[c]
BbF	0.14 ± 0.06	0.03 ± 0.02	0 [c]	7.9 ± 4.5	23.2 ± 41.7	0 [c]	0.14 ± 0.12	0.19 ± 0.05	0.29 ± 0.02[c]
BkF	0.13 ± 0.06	0.03 ± 0.03	0 [c]	7.2 ± 4.1	25.3 ± 72.9	0 [c]	0.11 ± 0.11	0.16 ± 0.08	0.17 ± 0.01[c]
BaP	0.13 ± 0.09	0.02 ± 0.02	0 [c]	5.6 ± 4.3	64.3 ± 255	0 [c]	0.07 ± 0.15	0.25 ± 0.04	0.19 ± 0.01[c]
BgP	0 [c]	0 [c]	0 [c]	0 [c]	0 [c]	0 [c]	0.11 ± 0.007[c]	0.003 ± 0.0002[c]	0.05 ± 0.003[c]
Total	0.33 ± 0.02	0.35 ± 0.04	0 [c]	60.2 ± 11.5	82.1 ± 42.7	0 [c]	0.39 ± 0.07	0.56 ± 0.17	0.30 ± 0.03[c]
3-ring	0.44 ± 0.02	0.53 ± 0.06	0 [c]	81.2 ± 14.5	115 ± 95.5	0 [c]	0.50 ± 0.09	0.89 ± 0.40	0.25 ± 0.02[c]
4-ring	0.30 ± 0.02	0.28 ± 0.04	0 [c]	32.5 ± 6.3	41.8 ± 16.8	0 [c]	0.34 ± 0.07	0.59 ± 0.14	0.52 ± 0.06[c]
5,6-ring	0.11 ± 0.07	0.02 ± 0.02	0 [c]	6.3 ± 4.3	26.4 ± 65.7	0 [c]	0.09 ± 0.11	0.16 ± 0.04	0.16 ± 0.01[c]

[a] Values are presented as the best-fit value ± 95% confidence interval. r^2 values were greater than 0.90 for all model fits, with the exception of BkF (control) and CHR (biostimulated).

[b] Abbreviations are defined in the caption to Figure E1.

[c] Regression did not converge on unique values for f, k_1, and k_2, so regression was performed assuming a single desorption rate (*i.e.*, assuming $k_1 = 0$).

Table E2. Fitted parameter values for the high-density material in the original column soil and soil collected from Port A of the biostimulated and control columns at day 593. [a]

	Fast-desorbing fraction, f			Fast-desorbing rate constant, k_1 (10^{-3}/hr)			Slow-desorbing rate constant, k_2 (10^{-3}/hr)		
Analyte[b]	Column Soil	Control	Biostim.	Column Soil	Control	Biostim.	Column Soil	Control	Biostim.
NAP	[d]	0 [c]	0.01 ± 0.004	[d]	0 [c]	125 ± 403	[d]	0.19 ± 0.02[c]	0.13 ± 0.01
ACE	0.55 ± 0.05	0.20 ± 0.03	0.05 ± 0.03	82.8 ± 38.9	59.2 ± 29.5	53.0 ± 104	0.92 ± 0.41	0.45 ± 0.09	0.20 ± 0.07
FLU	0.56 ± 0.13	0.15 ± 0.02	0.07 ± 0.04	105 ± 132	68.1 ± 37.6	46.9 ± 76.6	2.10 ± 1.34	0.20 ± 0.06	0.32 ± 0.10
PHN	0.49 ± 0.10	0.28 ± 0.03	0.08 ± 0.05	91.5 ± 94.6	80.8 ± 47.8	88.7 ± 295	1.50 ± 0.79	0.40 ± 0.14	0.35 ± 0.14
ANT	0.51 ± 0.06	0.23 ± 0.01	0.07 ± 0.04	84.9 ± 48.1	73.1 ± 19.7	75.5 ± 174	1.15 ± 0.44	0.24 ± 0.05	0.32 ± 0.11
FLA	0.49 ± 0.04	0.21 ± 0.01	0.07 ± 0.03	58.2 ± 16.1	64.6 ± 9.7	90.7 ± 254	1.02 ± 0.26	0.21 ± 0.03	0.45 ± 0.10
PYR	0.36 ± 0.03	0.24 ± 0.01	0.07 ± 0.01	42.4 ± 12.0	63.1 ± 10.0	72.6 ± 50.1	0.48 ± 0.14	0.31 ± 0.04	0.34 ± 0.04
BaA	0.30 ± 0.03	0.15 ± 0.01	0.04 ± 0.02	42.2 ± 11.4	44.1 ± 7.5	71.7 ± 124	0.49 ± 0.10	0.19 ± 0.02	0.29 ± 0.05
CHR	0.31 ± 0.03	0.16 ± 0.01	0.06 ± 0.02	41.0 ± 11.8	43.9 ± 7.0	70.2 ± 134	0.53 ± 0.12	0.21 ± 0.02	0.39 ± 0.07
BbF	0.13 ± 0.01	0.07 ± 0.01	0.03 ± 0.01	27.9 ± 8.19	26.2 ± 11.2	35.7 ± 16.8	0.34 ± 0.04	0.18 ± 0.03	0.23 ± 0.01
BkF	0.11 ± 0.01	0.06 ± 0.01	0.03 ± 0.005	27.2 ± 8.44	25.8 ± 11.8	38.5 ± 19.5	0.32 ± 0.04	0.17 ± 0.03	0.22 ± 0.01
BaP	0.08 ± 0.02	0.05 ± 0.01	0.04 ± 0.005	24.7 ± 11.4	25.5 ± 15.5	29.9 ± 9.9	0.26 ± 0.04	0.18 ± 0.03	0.22 ± 0.01
BgP	0.02 ± 0.03	0.02 ± 0.01	0.02 ± 0.01	11.6 ± 21.2	22.6 ± 18.9	11.9 ± 9.3	0.06 ± 0.05	0.11 ± 0.01	0.09 ± 0.01
Total	0.40 ± 0.06	0.20 ± 0.01	0.05 ± 0.02	65.9 ± 39.0	65.8 ± 18.6	73.7 ± 154	0.81 ± 0.32	0.27 ± 0.05	0.31 ± 0.07
3-ring	0.50 ± 0.10	0.27 ± 0.03	0.08 ± 0.04	90.4 ± 85.5	79.1 ± 43.8	83.1 ± 249	1.44 ± 0.75	0.37 ± 0.12	0.34 ± 0.13
4-ring	0.38 ± 0.03	0.20 ± 0.01	0.06 ± 0.03	46.6 ± 12.8	58.0 ± 8.0	101 ± 360	0.59 ± 0.15	0.24 ± 0.02	0.41 ± 0.09
5,6-ring	0.08 ± 0.01	0.05 ± 0.01	0.03 ± 0.004	25.3 ± 10.8	25.9 ± 14.0	30.4 ± 10.2	0.22 ± 0.03	0.16 ± 0.02	0.19 ± 0.01

[a] Values are presented as the best-fit value ± 95% confidence interval. r^2 values were greater than 0.90 for all model fits, with the exception of ACE, PHN, and ANT (biostimulated).

[b] Abbreviations are defined in the caption to Figure E1.

[c] Regression did not converge on unique values for f, k_1, and k_2, so regression was performed assuming a single desorption rate (*i.e.*, assuming $k_1 = 0$).

[d] Values for NAP and DBA in the original column soil are not reported due to poor reproducibility between replicates at the 28-d time point.

Table E3. Fitted parameter values for the low-density material in the original column soil and soil collected from Port A of the biostimulated and control columns at day 593. [a]

	Fast-desorbing fraction, f			Fast-desorbing rate constant, k_1 (10^{-3}/hr)			Slow-desorbing rate constant, k_2 (10^{-3}/hr)		
Analyte[b]	Column Soil	Control	Biostim.	Column Soil	Control	Biostim.	Column Soil	Control	Biostim.
NAP	0.06 ± 0.01	0.02 ± 0.004	0.02 ± 0.01	50.8 ± 31.9	41.4 ± 22.5	34.2 ± 22.1	0.08 ± 0.03	0.04 ± 0.01	0.02 ± 0.01
ACE	0.23 ± 0.03	0.10 ± 0.02	0.09 ± 0.02	56.5 ± 24.2	28.3 ± 17.5	28.4 ± 18.5	0.29 ± 0.09	0.12 ± 0.06	0.01 ± 0.05
FLU	0.25 ± 0.03	0.14 ± 0.01	0.09 ± 0.02	64.6 ± 35.6	54.2 ± 16.3	36.4 ± 21.3	0.29 ± 0.12	0.16 ± 0.03	0.07 ± 0.04
PHN	0.20 ± 0.03	0.14 ± 0.01	0.07 ± 0.01	61.2 ± 37.3	71.5 ± 25.6	56.4 ± 27.6	0.26 ± 0.10	0.13 ± 0.03	0.04 ± 0.02
ANT	0.17 ± 0.03	0.12 ± 0.01	0.06 ± 0.01	59.7 ± 37.3	67.2 ± 23.4	46.9 ± 20.3	0.22 ± 0.09	0.12 ± 0.03	0.05 ± 0.02
FLA	0.09 ± 0.02	0.08 ± 0.01	0.05 ± 0.01	56.8 ± 46.8	63.8 ± 24.5	43.6 ± 15.4	0.13 ± 0.06	0.09 ± 0.02	0.04 ± 0.01
PYR	0.08 ± 0.02	0.06 ± 0.01	0.04 ± 0.005	55.6 ± 49.4	66.5 ± 26.9	51.0 ± 23.3	0.12 ± 0.05	0.06 ± 0.02	0.02 ± 0.01
BaA	0.03 ± 0.01	0.03 ± 0.005	0.02 ± 0.003	43.9 ± 56.3	57.1 ± 31.2	42.2 ± 21.6	0.05 ± 0.03	0.04 ± 0.01	0.01 ± 0.01
CHR	0.04 ± 0.01	0.04 ± 0.004	0.02 ± 0.004	43.8 ± 54.2	61.4 ± 30.4	45.2 ± 26.6	0.06 ± 0.04	0.05 ± 0.01	0.02 ± 0.01
BbF	0.02 ± 0.01	0.02 ± 0.002	0.02 ± 0.003	34.6 ± 45.2	36.4 ± 11.8	31.6 ± 15.2	0.03 ± 0.02	0.02 ± 0.01	0.01 ± 0.01
BkF	0.02 ± 0.01	0.02 ± 0.002	0.02 ± 0.003	35.4 ± 46.1	35.6 ± 12.3	29.3 ± 14.7	0.03 ± 0.02	0.02 ± 0.01	0.01 ± 0.01
BaP	0.01 ± 0.01	0.01 ± 0.003	0.01 ± 0.002	43.3 ± 69.5	41.6 ± 24.2	36.3 ± 22.8	0.02 ± 0.02	0.03 ± 0.01	0.02 ± 0.01
BgP	0.01 ± 0.00	0.01 ± 0.002	0.01 ± 0.003	79.1 ± 151	25.3 ± 15	27.6 ± 22.6	0.02 ± 0.01	0.01 ± 0.01	0.01 ± 0.01
Total	0.12 ± 0.02	0.07 ± 0.006	0.04 ± 0.01	58.4 ± 37.5	64.6 ± 23.1	46.8 ± 22.2	0.15 ± 0.06	0.07 ± 0.02	0.03 ± 0.01
3-ring	0.20 ± 0.03	0.14 ± 0.01	0.07 ± 0.01	61.0 ± 36.0	68.5 ± 24.1	51.2 ± 25.4	0.26 ± 0.10	0.13 ± 0.03	0.04 ± 0.03
4-ring	0.07 ± 0.02	0.06 ± 0.006	0.03 ± 0.004	54.0 ± 49.4	64.0 ± 26.2	46.8 ± 20.3	0.10 ± 0.05	0.06 ± 0.02	0.03 ± 0.01
5,6-ring	0.01 ± 0.01	0.01 ± 0.002	0.01 ± 0.002	40.3 ± 57.2	36.4 ± 15.2	31.5 ± 17.1	0.02 ± 0.01	0.02 ± 0.005	0.01 ± 0.01

[a] Values are presented as the best-fit value ± 95% confidence interval. r^2 values were greater than 0.90 for all model fits, with the exception of BaP (column soil).

[b] Abbreviations are defined in the caption to Figure E1.

[c] Regression did not converge on unique values for f, k_1, and k_2, so regression was performed assuming a single desorption rate (*i.e.*, assuming $k_1 = 0$).

Literature Cited

(1) U.S. Environmental Protection Agency (USEPA). Cleaning Up the Nation's Waste Sites: Markets and Technology Trends, 2004 Edition. 2004, *EPA 542-R-04-015.*

(2) U.S. Environmental Protection Agency (USEPA). A Resource for MGP Site Characterization and Remediation. 1999, *EPA 542-R-99-005,*

(3) Luthy, R.G.; Dzombak, D.A.; Peters, C.A.; Roy, S.B.; Ramaswami, A.; Nakles, D.V.; Nott, B.R. Remediating tar-contaminated soils at manufactured gas plant sites. *Environ. Sci. Technol.* **1994,** *28,* 266A-276A.

(4) Keith, L. and Telliard, W.A. Priority pollutants I-a perspective view. *Environ. Sci. Technol.* **1979,** *13,* 416-423.

(5) U.S. Environmental Protection Agency (USEPA). Provisional Guidance for Quantitative Risk Assessment of Polycyclic Aromatic Hydrocarbons. 1993, *EPA 600-R-93-089.*

(6) van Hamme, J.D.; Singh, A.; Ward, O.P. Recent advances in petroleum microbiology. *Microbiol. Mol. Biol. Rev.* **2003,** *67,* 503-549.

(7) Cerniglia, C.E. Biodegradation of polycyclic aromatic hydrocarbons. *Biodegradation* **1992,** *3,* 351-368.

(8) Kelly, W.R.; Hornberger, G.M.; Herman, J.S.; Mills, A.L. Kinetics of BTX biodegradation and mineralization in batch and column systems. *J. Contam. Hydrol.* **1996,** *23,* 113-132.

(9) Alshafie, M. and Ghoshal, S. Naphthalene biodegradation from non-aqueous-phase liquids in batch and column systems: Comparison of biokinetic rate coefficients. *Biotechnol. Prog.* **2003,** *19,* 844-852.

(10) U.S. Environmental Protection Agency (USEPA). Understanding Variation in Partition Coefficient, K_d, Values: Volume 1. 1999, *EPA 402-R-99-004,* 1-212.

(11) Brusseau, M.L.; Hu, M.Q.; Wang, J.M.; Maier, R.M. Biodegradation during contaminant transport in porous media. 2. The influence of physicochemical factors. *Environ. Sci. Technol.* **1999,** *33,* 96-103.

(12) Richardson, R.E.; James, C.A.; Bhupathiraju, V.K.; Alvarez-Cohen, L. Microbial activity in soils following steam treatment. *Biodegradation* **2002,** *13,* 285-295.

(13) Hrapovic, L.; Sleep, B.E.; Major, D.J.; Hood, E.D. Laboratory study of treatment of trichloroethene by chemical oxidation followed by bioremediation. *Environ. Sci. Technol.* **2005,** *39,* 2888-2897.

(14) Azadpour-Keeley, A.; Wood, L.A.; Lee, T.R.; Mravik, S.C. Microbial responses to *in situ* chemical oxidation, six-phase heating, and steam injection remediation technologies in groundwater. *Rem. J.* **2004,** *14,* 5-17.

(15) Stokley, K.E.; Drake, E.N.; Prince, R.C. The role of Fenton's reagent in soil bioremediation. In *In situ and On-site Bioremediation*, *Vol. 4*, Proceedings of the Fourth International Conference, New Orleans, USA, April 28-May 1, 1997, pp. 487-492.

(16) Kastner, J.R. Effect of Fenton's reagent on subsurface microbiology and biodegradation capacity. In *Engineered Approaches for In Situ Bioremediation of Chlorinated Solvent Contamination*, *Proceedings of the Fifth International Conference In Situ and On-Site Bioremediation Symposium*, San Diego, USA, April 19-22, 1999; Leeson,A.; Alleman,B.C., Eds.; Battelle Press: Columbus, OH, 1999.

(17) Allen, S.A. and Reardon, K.F. Remediation of contaminated soils by combined chemical and biological treatments. In *Physical and Thermal Technologies, Proceedings of the Second International Conference on Remediation of Chlorinated and Recalcitrant Compounds*, Monterey, USA, May 22-25, 2000; Wickramanayake, G.B.; Gavaskar, A.R., Eds.; Battelle Press: Columbus, OH, 2000.

(18) Chapelle, F.H.; Bradley, P.M.; Casey, C.C. Behavior of a chlorinated ethene plume following source-area treatment with Fenton's reagent. *Ground Water Monit. Rem.* **2005,** *25,* 131-141.

(19) Palmroth, M.; Langwaldt, J.; Aunola, T.; Goi, A.; Munster, U.; Puhakka, J.; Tuhkanen, T. Effect of modified Fenton's reaction on microbial activity and removal of PAHs in creosote oil contaminated soil. *Biodegradation* **2006,** *17,* 29-39.

(20) Rowland, M.A.; Brubaker, G.R.; Kohler, K.; Westray, M.; Morris, D. Effects of potassium permanganate oxidation on subsurface microbial activity. In *Anaerobic Degradation of Chlorinated Solvents, Proceedings of the Sixth International In Situ and On-Site Bioremediation Symposium*, San Diego, USA, June 4-7, 2001; Magar, V.S.; Fennel, D.E; Morse,J.J.; Alleman, B.C.; Leeson, A. Eds.; Battelle: Columbus, OH, 2001.

(21) Sahl, J.W.; Munakata-Marr, J.; Crimi, M.L.; Siegrist, R.L. Coupling permanganate oxidation with microbial dechlorination of tetrachloroethene. *Water Environ. Res.* **2007,** *79,* 5-12.

(22) Khalil, M.F.; Ghosh, U.; Kreitinger, J.P. Role of weathered coal tar pitch in the partitioning of polycyclic aromatic hydrocarbons in manufactured gas plant site sediments. *Environ. Sci. Technol.* **2006,** *40,* 5681-5687.

(23) Viñas, M.; Sabate, J.; Espuny, M.J.; Solanas, A.M. Bacterial community dynamics and polycyclic aromatic hydrocarbon degradation during bioremediation of heavily creosote-contaminated soil. *Appl. Environ. Microbiol.* **2005,** *71,* 7008-7018.

(24) Li, J.; Pignatello, J.J.; Smets, B.F.; Grasso, D.; Monserrate, E. Bench-scale evaluation of in situ bioremediation strategies for soil at a former manufactured gas plant site. *Environ. Toxicol. Chem.* **2005,** *24,* 741-749.

(25) Breedveld, G.D. and Karlsen, D.A. Estimating the availability of polycyclic aromatic hydrocarbons for bioremediation of creosote contaminated soils. *Appl. Microbiol. Biotechnol.* **2000,** *54,* 255-261.

(26) Eriksson, M.; Dalhammar, G.; Borg-Karlson, A.K. Biological degradation of selected hydrocarbons in an old PAH/creosote contaminated soil from a gas work site. *Appl. Microbiol. Biotechnol.* **2000,** *53,* 619-626.

(27) Amellal, N.; Portal, J.M.; Vogel, T.M.; Berthelin, J. Distribution and location of polycyclic aromatic hydrocarbons (PAHs) and PAH-degrading bacteria within polluted soil aggregates. *Biodegradation* **2001,** *12,* 49-57.

(28) Amellal, N.; Portal, J.M.; Berthelin, J. Effect of soil structure on the bioavailability of polycyclic aromatic hydrocarbons within aggregates of a contaminated soil. *Appl. Geochem.* **2001,** *16,* 1611-1619.

(29) Ehlers, L.J. and Luthy, R.G. Contaminant bioavailability in soil and sediment. *Environ. Sci. Technol.* **2003,** *37,* 295A-302A.

(30) Ghosh, U.; Gillette, J.S.; Luthy, R.G.; Zare, R.N. Microscale location, characterization, and association of polycyclic aromatic hydrocarbons on harbor sediment particles. *Environ. Sci. Technol.* **2000,** *34,* 1729-1736.

(31) Ghosh, U. The role of black carbon in influencing availability of PAHs in sediments. *Hum. Ecol. Risk Assess.* **2007,** *13,* 276-285.

(32) Hatheway, A.W. Former manufactured gas plants and other coal-tar industrial sites, In *Dangerous places: Health, safety, and archaeology,* Poirier, D.A. and Feder, K.L., Eds.; Bergin & Garvey: Westport, Conn., 2001; pp. 137-156.

(33) U.S. Environmental Protection Agency (USEPA). Survey of Town Gas and By-Product Production and Locations in the U.S. (1880-1950). 1985, *EPA 600-7-85-004,* 1-403.

(34) Hatheway, A.W. Estimated number of manufactured gas and other coal-tar sites in the United States. *Environ. Engineering GeoScience* **1997,** *3,* 141-142.

(35) Hatheway, A.W. Manufactured gas plants: Yesterday's pride, today's liability. *Civil Engineering* **1997,** *67,* 38-41.

(36) Lipson, D.S. Groundwater Remediation at Former Manufactured Gas Plants: Chapter 10, In *Handbook of Complex Environmental Remediation Problems,* Lehr, J., Hyman, M., Gass, T.E. and Seevers, W., Eds.; McGraw-Hill: New York, 2002; pp. 547-570.

(37) U.S. Environmental Protection Agency (USEPA). U.S. Production of Manufactured Gases: Assessment of Past Disposal Practices. 1988, *EPA 600-2-88-012,* 1-388.

(38) Hamper, M.J. Manufactured gas history and processes. *Environ. Forensics* **2006,** *7,* 55-64.

(39) Srivastava, V.J. Manufactured gas plant sites: Characterization of wastes and IGT's innovative remediation alternatives. **1993,** 1-21.

(40) U.S. Environmental Protection Agency (USEPA). How to Evaluate Alternative Cleanup Technologies for Underground Storage Tank Sites: A Guide for Corrective Action Plan Reviewers. 2004, *EPA 510-R-04-002.*

(41) Peters, C.A. and Luthy, R.G. Coal tar dissolution in water-miscible solvents: experimental evaluation. *Environ. Sci. Technol.* **1993,** *27,* 2831-2843.

(42) Haeseler, F.; Blanchet, D.; Druelle, V.; Werner, P.; Vandecasteele, J.P. Analytical characterization of contaminated soils from former manufactured gas plants. *Environ. Sci. Technol.* **1999,** *33,* 825-830.

(43) Harvey, R.G. *Polycyclic aromatic hydrocarbons.* Cambridge University Press: Cambridge, 1991; pp. 396.

(44) Schwarzenbach, R.P.; Gschwend, P.M.; Imboden, D.M. *Environmental Organic Chemistry: 2nd Edition.* John Wiley & Sons, Inc.: New York, 2003.

(45) Kanaly, R.A. and Harayama, S. Biodegradation of high-molecular-weight polycyclic aromatic hydrocarbons by bacteria. *J. Bacteriol.* **2000,** *182,* 2059-2067.

(46) Mackay, D.; Shia, Y.W.; Ma, K.C. *Illustrated Handbook of Physical and Environmental Fate for Organic Compounds.* Lewis Publishers, Inc.: Chelsey, MI, 1992.

(47) Agency for Toxic Substance and Disease Registry (ATSDR). 2007 Comprehensive Environmental Response, Compensation, and Liability Act (CERCLA) Priority List of Hazardous Substances. 2007, Accessed: August 12, 2010. http://www.atsdr.cdc.gov/cercla/07list.html.

(48) LaGrega, M.D.; Buckingham, P.L.; Evans, J.C. *Hazardous Waste Management: 2nd Edition.* McGraw-Hill: Boston, 2001.

(49) LaGoy, P.K. and Quirk, T.C. Establishing generic remediation goals for the polycyclic aromatic hydrocarbons: critical issues. *Environ. Health Perspect.* **1994,** *102,* 348-352.

(50) Pignatello, J.J. The Measurement and Interpretation of Sorption and Desorption Rates for Organic Compounds in Soil Media, In *Advances in Agronomy: Volume 69,* Sparks, D.L., Ed.; Academic Press: San Diego, CA, 2000; pp. 1-75.

(51) Jonker, M.T.O.; Sinke, A.J.C.; Brils, J.M.; Koelmans, A.A. Sorption of polycyclic aromatic hydrocarbons to oil contaminated sediment: Unresolved complex? *Environ. Sci. Technol.* **2003,** *37,* 5197-5203.

(52) Pignatello, J.J. and Xing, B. Mechanisms of slow sorption of organic chemicals to natural particles. *Environ. Sci. Technol.* **1996,** *30,* 1-11.

(53) Weber Jr., W.J.; McGinley, P.M.; Katz, L.E. Sorption phenomena in subsurface systems: Concepts, models, and effects on contaminant fate and transport. *Wat. Res.* **1991,** *25,* 499-528.

(54) Xing, B. and Pignatello, J.J. Dual-mode sorption of low-polarity compounds in glassy poly(vinyl chloride) and soil organic matter. *Environ. Sci. Technol.* **1997,** *31,* 792-799.

(55) Cuypers, C.; Grotenhuis, J.T.C.; Joziasse, J.; Rulkens, W.H. Rapid persulfate oxidation predicts PAH bioavailability in soils and sediments. *Environ. Sci. Technol.* **2000,** *34,* 2057-2063.

(56) Huang, W.; Peng, P.; Yu, Z.; Fu, J. Effects of organic matter heterogeneity on sorption and desorption of organic contaminants by soils and sediments. *Appl. Geochem.* **2003,** *18,* 955-972.

(57) Cornelissen, G.; Gustafsson, O.; Bucheli, T.D.; Jonker, M.T.O.; Koelmans, A.A.; vanNoort, P.C.M. Extensive sorption of organic compounds to black carbon, coal, and kerogen in sediments and soils: Mechanisms and consequences for distribution, bioaccumulation, and biodegradation. *Environ. Sci. Technol.* **2005,** *39,* 6881-6895.

(58) Alexander, M. How toxic are toxic chemicals in soil? *Environ. Sci. Technol.* **1995,** *29,* 2713-2717.

(59) Huang, W.; Young, T.M.; Schlautman, M.A.; Yu, H.; Weber, W.J. A distributed reactivity model for sorption by soils and sediments. 9. General isotherm nonlinearity and applicability of the dual reactive domain model. *Environ. Sci. Technol.* **1997,** *31,* 1703-1710.

(60) LeBoeuf, E.J. and Weber, W.J. A distributed reactivity model for sorption by soils and sediments. 8. Sorbent organic domains: Discovery of a humic acid glass transition and an argument for a polymer-based model. *Environ. Sci. Technol.* **1997,** *31,* 1697-1702.

(61) Song, J.; Peng, P.; Huang, W. Black carbon and kerogen in soils and sediments. 1. Quantification and characterization. *Environ. Sci. Technol.* **2002,** *36,* 3960-3967.

(62) Brusseau, M.L.; Jessup, R.E.; Rao, P.S.C. Nonequilibrium sorption of organic chemicals: Elucidation of rate-limiting processes. *Environ. Sci. Technol.* **1991,** *25,* 134-142.

(63) Alexander, M. Aging, bioavailability, and overestimation of risk from environmental pollutants. *Environ. Sci. Technol.* **2000,** *34,* 4259-4265.

(64) Northcott, G.L. and Jones, K.C. Partitioning, extractability, and formation of nonextractable PAH residues in soil. 1. Compound differences in aging and sequestration. *Environ. Sci. Technol.* **2001,** *35,* 1103-1110.

(65) Lee, L.S.; Rao, P.S.C.; Okuda, I. Equilibrium partitioning of polycyclic aromatic hydrocarbons from coal tar into water. *Environ. Sci. Technol.* **1992,** *26,* 2110-2115.

(66) Brown, D.G.; Gupta, L.; Kim, T.H.; Moo-Young, H.K.; Coleman, A.J. Comparative assessment of coal tars obtained from 10 former manufactured gas plant sites in the Eastern United States. *Chemosphere* **2006,** *65,* 1562-1569.

(67) Hawthorne, S.B.; Grabanski, C.B.; Miller, D.J. Measured partitioning coefficients for parent and alkyl polycyclic aromatic hydrocarbons in 114 historically contaminated sediments: Part 1. K_{oc} values. *Environ. Toxicol. Chem.* **2006,** *25,* 2901-2911.

(68) Eberhardt, C. and Grathwohl, P. Time scales of organic contaminant dissolution from complex source zones: coal tar pools vs. blobs. *J. Contam. Hydrol.* **2002,** *59,* 45-66.

(69) Lane, W.F. and Loehr, R.C. Estimating the equilibrium aqueous concentrations of polynuclear aromatic hydrocarbons in complex mixtures. *Environ. Sci. Technol.* **1992,** *26,* 983-990.

(70) Cline, P.V.; Delfino, J.J.; Rao, P.S.C. Partitioning of aromatic constituents into water from gasoline and other complex solvent mixtures. *Environ. Sci. Technol.* **1991,** *25,* 914-920.

(71) Lee, L.S.; Hagwall, M.; Delfino, J.J.; Rao, P.S.C. Partitioning of polycyclic aromatic hydrocarbons from diesel fuel into water. *Environ. Sci. Technol.* **1992,** *26,* 2104-2110.

(72) Banerjee, S. Solubility of organic mixtures in water. *Environ. Sci. Technol.* **1984,** *18,* 587-591.

(73) Peters, C.A.; Mukherji, S.; Weber, W.J. UNIFAC modeling of multicomponent nonaqueous phase liquids containing polycyclic aromatic hydrocarbons. *Environ. Toxicol. Chem.* **1999,** *18,* 426-429.

(74) Birak, P.S. and Miller, C.T. Dense non-aqueous phase liquids at former manufactured gas plants: Challenges to modeling and remediation. *J. Contam. Hydrol.* **2009,** *105,* 81-98.

(75) Dudal, Y.; Samson, R.; Deschênes, L. Rate of contaminant bioavailability in artificial soil-water column experiments. *Soil Sediment Contam.* **2003,** *12,* 835-850.

(76) National Research Council (NRC) *Bioavailability of contaminants in soils and sediments: Processes, tools, and applications.* National Academies Press: Washington D.C., 2003; pp. 432.

(77) Semple, K.T.; Doick, K.J.; Jones, K.C.; Burauel, P.; Craven, A.; Harms, H. Defining bioavailability and bioaccessibility of contaminated soil and sediment is complicated. *Environ. Sci. Technol.* **2004,** *38,* 228A-231A.

(78) Braida, W.J.; White, J.C.; Pignatello, J.J. Indices for bioavailability and biotransformation potential of contaminants in soils. *Environ. Toxicol. Chem.* **2004,** *23,* 1585-1591.

(79) Cornelissen, G.; Rigterink, H.; Ferdinandy, M.M.A.; van Noort, P.C.M. Rapidly desorbing fractions of PAHs in contaminated sediments as a predictor of the extent of bioremediation. *Environ. Sci. Technol.* **1998,** *32,* 966-970.

(80) Cuypers, C.; Pancras, T.; Grotenhuis, J.T.C.; Rulkens, W.H. The estimation of PAH bioavailability in contaminated sediments using hydroxypropyl-[beta]-cyclodextrin and Triton X-100 extraction techniques. *Chemosphere* **2002,** *46,* 1235-1245.

(81) Lei, L.; Suidan, M.T.; Khodadoust, A.P.; Tabak, H.H. Assessing the bioavailability of PAHs in field-contaminated sediment using XAD-2 assisted desorption. *Environ. Sci. Technol.* **2004,** *38,* 1786-1793.

(82) Hawthorne, S.B.; Poppendieck, D.G.; Grabanski, C.B.; Loehr, R.C. PAH release during water desorption, supercritical carbon dioxide extraction, and field bioremediation. *Environ. Sci. Technol.* **2001,** *35,* 4577-4583.

(83) Volkering, F.; Breure, A.M.; Rulkens, W.H. Microbiological aspects of surfactant use for biological soil remediation. *Biodegradation* **1997,** *8,* 401-417.

(84) Hatzinger, P.B. and Alexander, M. Effect of aging of chemicals in soil on their biodegradability and extractability. *Environ. Sci. Technol.* **1995,** *29,* 537-545.

(85) Kelsey, J.W.; Kottler, B.D.; Alexander, M. Selective chemical extractants to predict bioavailability of soil-aged organic chemicals. *Environ. Sci. Technol.* **1997,** *31,* 214-217.

(86) Reid, B.J.; Stokes, J.D.; Jones, K.C.; Semple, K.T. Nonexhaustive cyclodextrin-based extraction technique for the evaluation of PAH bioavailability. *Environ. Sci. Technol.* **2000,** *34,* 3174-3179.

(87) Liste, H.H. and Alexander, M. Butanol extraction to predict bioavailability of PAHs in soil. *Chemosphere* **2002,** *46,* 1011-1017.

(88) Stroo, H.F.; Jensen, R.; Loehr, R.C.; Nakles, D.V.; Fairbrother, A.; Liban, C.B. Environmentally acceptable endpoints for PAHs at a manufactured gas plant site. *Environ. Sci. Technol.* **2000,** *34,* 3831-3836.

(89) Pignatello, J.J. Slowly reversible sorption of aliphatic halocarbons in soils. I. Formation of residual fractions. *Environ. Toxicol. Chem.* **1990,** *9,* 1107-1115.

(90) Pignatello, J.J. Slowly reversible sorption of aliphatic halocarbons in soils. II. Mechanistic aspects. *Environ. Toxicol. Chem.* **1990,** *9,* 1117-1126.

(91) Guerin, W.F. and Boyd, S.A. Differential bioavailability of soil-sorbed naphthalene to two bacterial species. *Appl. Environ. Microbiol.* **1992,** *58,* 1142-1152.

(92) Swindell, A.L. and Reid, B.J. Comparison of selected non-exhaustive extraction techniques to assess PAH availability in dissimilar soils. *Chemosphere* **2006,** *62,* 1126-1134.

(93) Carmichael, L.M.; Christman, R.F.; Pfaender, F.K. Desorption and mineralization kinetics of phenanthrene and chrysene in contaminated soils. *Environ. Sci. Technol.* **1997,** *31,* 126-132.

(94) Prichard, H.; Jones-Meehan, J.; Nestler, C.; Hansen, L.D.; Straube, W.; Jones, W.; Hind, J.; Talley, J.W. Polycyclic aromatic hydrocarbons (PAHs): Improved land treatment with bioaugmentation, In *Bioremediation of Recalcitrant Compounds,* Talley, J.W., Ed.; Taylor & Francis Group: Boca Raton, 2006; pp. 215-300.

(95) Yavuz Corapcioglu, M. and Haridas, A. Transport and fate of microorganisms in porous media: A theoretical investigation. *J. Hydrol.* **1984,** *72,* 149-169.

(96) Pignatello, J.J. Fundamental issues in sorption related to physical and biological remediation of soils, In *Viable Methods of Soil and Water Pollution Monitoring, Protection and Remediation: NATO-OTAN Advanced Research Workshop, Krakow, Poland,* Twardowska, I., Allen, H.E. and Haggblom, M.H.H., Eds.; Springer: Netherlands, 2006; Vol.69 pp. 41-68.

(97) Cassidy, D.P. Biological surfactant production in a biological slurry reactor treating diesel fuel contaminated soil. *Water Environ. Res.* **2001,** *73,* 87-94.

(98) Ron, E.Z. and Rosenberg, E. Biosurfactants and oil bioremediation. *Curr. Opin. Biotechnol.* **2002,** *13,* 249-252.

(99) Johnsen, A.R.; Wick, L.Y.; Harms, H. Principles of microbial PAH-degradation in soil. *Environ. Pollut.* **2005,** *133,* 71-84.

(100) Huesemann, M.H.; Hausmann, T.S.; Fortman, T.J. Microbial factors rather than bioavailability limit the rate and extent of PAH biodegradation in aged crude oil contaminated model soils. *Bioremed. J.* **2002,** *6,* 321-337.

(101) Huesemann, M.H.; Hausmann, T.S.; Fortman, T.J. Assessment of bioavailability limitations during slurry biodegradation of petroleum hydrocarbons in aged soil. *Environ. Toxicol. Chem.* **2003,** *22,* 2853-2860.

(102) Arnot, J.A. and Mackay, D. Policies for chemical hazard and risk priority setting: Can persistence, bioaccumulation, toxicity, and quantity information be combined? *Environ. Sci. Technol.* **2008,** *42,* 4648-4654.

(103) Kelsey, J.W. and Alexander, M. Declining bioavailability and inappropriate estimation of risk of persistent compounds. *Environ. Toxicol. Chem.* **1997,** *16,* 582-585.

(104) Barraclough, D.; Kearney, T.; Croxford, A. Bound residues: Environmental solution or future problem? *Environ. Pollut.* **2005,** *133,* 85-90.

(105) Huling, S.G. and Pivetz, B.E. *In-Situ Chemical Oxidation*, Engineering Issue Paper, EPA 600-R-06-072; U.S. Environmental Protection Agency: Cincinnati OH, 2006.

(106) Watts, R.J. and Teel, A.L. Treatment of contaminated soils and groundwater using ISCO. *Pract. Periodical of Haz. Toxic and Radioactive Waste Mgmt* **2006,** *10,* 2-9.

(107) Huang, K.C.; Zhao, Z.; Hoag, G.E.; Dahmani, A.; Block, P.A. Degradation of volatile organic compounds with thermally activated persulfate oxidation. *Chemosphere* **2005,** *61,* 551-560.

(108) Dahmani, M.; Huang, K.; Hoag, G.E. Sodium persulfate oxidation for the remediation of chlorinated solvents (USEPA superfund innovative technology evaluation program). *Wat. Air Soil Pollut. Focus* **2006,** *6,* 127-141.

(109) Liang, C.; Bruell, C.J.; Marley, M.C.; Sperry, K.L. Thermally activated persulfate oxidation of trichloroethylene (TCE) and 1,1,1-trichloroethane (TCA) in aqueous systems and soil slurries. *Soil Sed. Contam.* **2003,** *12,* 207-228.

(110) Liang, C.; Wang, Z.; Bruell, C.J. Influence of pH on persulfate oxidation of TCE at ambient temperatures. *Chemosphere* **2007,** *66,* 106-113.

(111) Liang, C.; Lee, I.L.; Hsu, I.Y.; Liang, C.P.; Lin, Y.L. Persulfate oxidation of trichloroethylene with and without iron activation in porous media. *Chemosphere* **2008,** *70,* 426-435.

(112) Liang, C.; Wang, Z.; Mohanty, N. Influences of carbonate and chloride ions on persulfate oxidation of trichloroethylene at 20°C. *Sci. Total Environ.* **2006,** *370,* 271-277.

(113) Crimi, M.L. and Taylor, J. Experimental evaluation of catalyzed hydrogen peroxide and sodium persulfate for destruction of BTEX contaminants. *Soil Sed. Contam.* **2007,** *16,* 29-45.

(114) Barbash, A.; Hoag, G.E.; Nadim, F. Oxidation and removal of 1,2,4-trichlorobenzene using sodium persulfate in a sorption-desorption experiment. *Wat. Air Soil Pollut.* **2006,** *172,* 67-80.

(115) Huang, K.C.; Couttenye, R.A.; Hoag, G.E. Kinetics of heat-assisted persulfate oxidation of methyl tert-butyl ether (MTBE). *Chemosphere* **2002,** *49,* 413-420.

(116) Cao, J.; Zhang, W.X.; Brown, D.G.; Sethi, D. Oxidation of lindane with Fe(II)-activated sodium persulfate. *Environ. Eng. Sci.* **2008,** *25,* 221-228.

(117) Peyton, G.R.; LeFaivre, M.H.; Smith, M.A. Treatability of contaminated ground water and aquifer solids at town gas sites, using photolytic ozonation and chemical in-situ reclamation. Hazardous Water Research and Information Center, Illinois State Water Survey Division, Savoy, IL, 1990, *HWRIC-RR-048*.

(118) Nadim, F.; Huang, K.C.; Dahmani, A. Remediation of soil and ground water contaminated with PAH using heat and Fe(II)-EDTA catalyzed persulfate oxidation. *Wat. Air Soil Pollut. Focus* **2006,** *6,* 227-232.

(119) Osgerby, I. ISCO Technology Overview: Do You Really Understand the Chemistry? In *Contaminated Soils, Sediments, and Water: Volume 10,* Calabrese, E.J., Kostecki, P.T. and Dragun, J., Eds.; Springer: New York, 2006; pp. 287-308.

(120) Kolthoff, I.M. and Miller, I.K. The chemistry of persulfate. I. The kinetics and mechanism of the decomposition of the persulfate ion in aqueous medium. *J. Am. Chem. Soc.* **1951,** *73,* 3055-3059.

(121) Waldemer, R.H.; Tratnyek, P.G.; Johnson, R.L.; Nurmi, J.T. Oxidation of chlorinated ethenes by heat-activated persulfate: Kinetics and products. *Environ. Sci. Technol.* **2007,** *41,* 1010-1015.

(122) Fordham, J.W.L. and Williams, H.L. The persulfate-iron(II) initiator system for free radical polymerizations. *J. Am. Chem. Soc.* **1951,** *73,* 4855-4859.

(123) Johnson, R.L.; Tratnyek, P.G.; Johnson, R.O. Persulfate persistence under thermal activation conditions. *Environ. Sci. Technol.* **2008,** *42,* 9350-9356.

(124) U.S. Environmental Protection Agency (USEPA) and Centers for Disease Control and Prevention (CDC). Health Effects from Exposure to High Levels of Sulfate in Drinking Water Study. 1999, *EPA 815-R-99-001.*

(125) House, D.A. Kinetics and mechanism of oxidations by peroxydisulfate. *Chem. Rev.* **1962,** *62,* 185-203.

(126) Madsen, E.L. The use of stable isotope probing techniques in bioreactor and field studies on bioremediation. *Curr. Opin. Biotechnol.* **2006,** *17,* 92-97.

(127) Sutherland, J.B.; Rafii, F.; Khan, A.A.; Cerniglia, C.E. Mechanisms of polycyclic aromatic hydrocarbon degradation, In *Microbial transformation and degradation of toxic organic chemicals,* Young, L.Y. and Cerniglia, C.E., Eds.; Wiley-Liss, Inc.: Boston, 1995; pp. 269-306.

(128) Tang, Y.J.; Qi, L.; Krieger-Brockett, B. Evaluating factors that influence microbial phenanthrene biodegradation rates by regression with categorical variables. *Chemosphere* **2005,** *59,* 729-741.

(129) Bouwer, E.J.; Zhang, W.; Wilson, L.P.; Durant, N.D. Biotreatment of PAH-contaminated soils/sediments. *Ann. N. Y. Acad. Sci.* **1997,** *829,* 103-117.

(130) Shuttleworth, K.L. and Cerniglia, C.E. Environmental aspects of PAH degradation. *Appl. Biochem. Biotech.* **1995,** *54,* 291-302.

(131) Aitken, M.D. and Long, T.C. Biotransformation, biodegradation, and bioremediation of polycyclic aromatic hydrocarbons, In *Soil Biology, 2: Biodegradation and Bioremediation,* Singh, A. and Ward, O.P., Eds.; Springer-Verlag: Heidelberg, Germany, 2004; pp. 83-124.

(132) Gibson, D. and Subramanian, V. Microbial Degradation of Aromatic Hyrocarbons, In *Microbial Degradation of Organic Compounds,* Gibson, D., Ed.; Marcel Dekker, Inc.: New York, 1984; pp. 181-252.

(133) Kanaly, R.A.; Bartha, R.; Watanabe, K.; Harayama, S. Rapid mineralization of benzo[*a*]pyrene by a microbial consortium growing on diesel fuel. *Appl. Environ. Microbiol.* **2000,** *66,* 4205-4211.

(134) Dyer, M.; van Heiningen, E.; Gerritse, J. *In situ* bioremediation of 1,2-dichloroethane under anaerobic conditions. *Geotech. Geol. Eng.* **2000,** *18,* 313-334.

(135) Lovley, D.R. Bioremediation: Anaerobes to the rescue. *Science* **2001,** *293,* 1444-1446.

(136) Lovley, D.R. Cleaning up with genomics: Applying molecular biology to bioremediation. *Nat. Rev. Micro* **2003,** *1,* 35-44.

(137) Bamforth, S.M. and Singleton, I. Bioremediation of polycyclic aromatic hydrocarbons: current knowledge and future directions. *J. Chem. Technol. Biotechnol.* **2005,** *80,* 723-736.

(138) Mueller, J.G.; Chapman, P.J.; Pritchard, P.H. Creosote-contaminated sites: Their potential for bioremediation. *Environ. Sci. Technol.* **1989,** *23,* 1197-1201.

(139) Miller, R.R. Technology Overview Report: Air Sparging. 1996, *TO-96-04.*

(140) van Cauwenberghe, L. and Roote, D.S. Technology Overview Report: *In Situ* Bioremediation. 1998, *TO-98-01.*

(141) U.S. Environmental Protection Agency (USEPA). Use of Bioremediation at Superfund Sites. 2001, *EPA 542-R-01-019,* 1-60.

(142) U.S. Environmental Protection Agency (USEPA). Application, Performance, and Costs of Biotreatment Technologies for Contaminated Soils. 2002, *EPA 600-R-03-037,* 1-114.

(143) Morgan, P. and Watkinson, R.J. Factors limiting the supply and efficiency of nutrient and oxygen supplements for the in situ biotreatment of contaminated soil and groundwater. *Water Res.* **1992,** *26,* 73-78.

(144) Johnson, C.R. and Scow, K.M. Effect of nitrogen and phosphorus addition on phenanthrene biodegradation in four soils. *Biodegradation* **1999,** *10,* 43-50.

(145) Breedveld, G.D. and Sparrevik, M. Nutrient-limited biodegradation of PAH in various soil strata at a creosote contaminated site. *Biodegradation* **2000,** *11,* 391-399.

(146) Carmichael, L.M. and Pfaender, F.K. The effect of inorganic and organic supplements on the microbial degradation of phenanthrene and pyrene in soils. *Biodegradation* **1997,** *8,* 1-13.

(147) MacNaughton, S.J.; Stephen, J.R.; Venosa, A.D.; Davis, G.A.; Chang, Y.J.; White, D.C. Microbial population changes during bioremediation of an experimental oil spill. *Appl. Environ. Microbiol.* **1999,** *65,* 3566-3574.

(148) Ogino, A.; Koshikawa, H.; Nakahara, T.; Uchiyama, H. Succession of microbial communities during a biostimulation process as evaluated by DGGE and clone library analyses. *J. Appl. Microbiol.* **2001,** *91,* 625-635.

(149) Evans, F.F.; Rosado, A.S.; Sebastián, G.V.; Casella, R.; Machado, P.; Holmström, C.; Kjelleberg, S.; Elsas, J.D.; Seldin, L. Impact of oil contamination and biostimulation on the diversity of indigenous bacterial communities in soil microcosms. *FEMS Microbiol. Ecol.* **2004,** *49,* 295-305.

(150) Iwamoto, T.; Tani, K.; Nakamura, K.; Suzuki, Y.; Kitagawa, M.; Eguchi, M.; Nasu, M. Monitoring impact of in situ biostimulation treatment on groundwater bacterial community by DGGE. *FEMS Microbiol. Ecol.* **2000,** *32,* 129-141.

(151) Kao, C.M.; Chen, C.Y.; Chen, S.C.; Chien, H.Y.; Chen, Y.L. Application of in situ biosparging to remediate a petroleum-hydrocarbon spill site: Field and microbial evaluation. *Chemosphere* **2008,** *70,* 1492-1499.

(152) Ringelberg, D.B.; Talley, J.W.; Perkins, E.J.; Tucker, S.G.; Luthy, R.G.; Bouwer, E.J.; Fredrickson, H.L. Succession of phenotypic, genotypic, and metabolic community characteristics during in vitro bioslurry treatment of polycyclic aromatic hydrocarbon-contaminated sediments. *Appl. Environ. Microbiol.* **2001,** *67,* 1542-1550.

(153) Mihelcic, J.R. and Luthy, R.G. Degradation of polycyclic aromatic hydrocarbon compounds under various redox conditions in soil-water systems. *Appl. Environ. Microbiol.* **1988,** *54,* 1182-1187.

(154) McNally, D.L.; Mihelcic, J.R.; Lueking, D.R. Biodegradation of three- and four-ring polycyclic aromatic hydrocarbons under aerobic and denitrifying conditions. *Environ. Sci. Technol.* **1998,** *32,* 2633-2639.

(155) Rockne, K.J. and Strand, S.E. Biodegradation of bicyclic and polycyclic aromatic hydrocarbons in anaerobic enrichments. *Environ. Sci. Technol.* **1998,** *32,* 3962-3967.

(156) McNally, D.L.; Mihelcic, J.R.; Lueking, D.R. Biodegradation of mixtures of polycyclic aromatic hydrocarbons under aerobic and nitrate-reducing conditions. *Chemosphere* **1999,** *38,* 1313-1321.

(157) Mihelcic, J.R. and Luthy, R.G. Microbial degradation of acenaphthene and naphthalene under denitrification conditions in soil-water systems. *Appl. Environ. Microbiol.* **1988,** *54,* 1188-1198.

(158) Al-Bashir, B.; Cseh, T.; Leduc, R.; Samson, R. Effect of soil/contaminant interactions on the biodegradation of naphthalene in flooded soil under denitrifying conditions. *Appl. Microbiol. Biotechnol.* **1990,** *34,* 414-419.

(159) Leduc, R.; Samson, R.; Al-Bashir, B.; Al-Hawari, J.; Cseh, T. Biotic and abiotic disappearance of four PAH compounds from flooded soil under various redox conditions. *Water Sci. Technol.* **1992,** *26,* 51-60.

(160) Rockne, K.J.; Chee-Sanford, J.C.; Sanford, R.A.; Hedlund, B.P.; Staley, J.T.; Strand, S.E. Anaerobic naphthalene degradation by microbial pure cultures under nitrate-reducing conditions. *Appl. Environ. Microbiol.* **2000,** *66,* 1595-1601.

(161) Anderson, R.T. and Lovley, D.R. Naphthalene and benzene degradation under Fe(III)-reducing conditions in petroleum-contaminated aquifers. *Bioremediation J.* **1999,** *3,* 121-135.

(162) Coates, J.D.; Anderson, R.T.; Woodward, J.C.; Phillips, E.J.P.; Lovley, D.R. Anaerobic hydrocarbon degradation in petroleum-contaminated harbor sediments under sulfate-reducing and artificially imposed iron-reducing conditions. *Environ. Sci. Technol.* **1996,** *30,* 2784-2789.

(163) Coates, J.D.; Anderson, R.T.; Lovley, D.R. Oxidation of polycyclic aromatic hydrocarbons under sulfate-reducing conditions. *Appl. Environ. Microbiol.* **1996,** *62,* 1099-1101.

(164) Zhang, X. and Young, L.Y. Carboxylation as an initial reaction in the anaerobic metabolism of naphthalene and phenanthrene by sulfidogenic consortia *Appl. Environ. Microbiol.* **1997,** *63,* 4759-4764.

(165) Coates, J.D.; Woodward, J.C.; Allen, J.Y.; Philp, P.; Lovley, D.R. Anaerobic degradation of polycyclic aromatic hydrocarbons and alkanes in petroleum-contaminated marine harbor sediments. *Appl. Environ. Microbiol.* **1997,** *63,* 3589-3593.

(166) Bedessem, M.E.; Swoboda-Colberg, N.G.; Colberg, P.J.S. Naphthalene mineralization coupled to sulfate reduction in aquifer-derived enrichments. *FEMS Microbiol. Lett.* **1997,** *152,* 213-218.

(167) Hayes, L.A.; Nevin, K.P.; Lovley, D.R. Role of prior exposure on anaerobic degradation of naphthalene and phenanthrene in marine harbor sediments. *Org. Geochem.* **1999,** *30,* 937-945.

(168) Rothermich, M.M.; Hayes, L.A.; Lovley, D.R. Anaerobic, sulfate-dependent degradation of polycyclic aromatic hydrocarbons in petroleum-contaminated harbor sediment. *Environ. Sci. Technol.* **2002,** *36,* 4811-4817.

(169) Chang, B.V.; Shiung, L.C.; Yuan, S.Y. Anaerobic biodegradation of polycyclic aromatic hydrocarbon in soil. *Chemosphere* **2002,** *48,* 717-724.

(170) Pravecek, T.L.; Christman, R.F.; Pfaender, F.K. Impact of imposed anaerobic conditions and microbial activity on aqueous-phase solubility of polycyclic aromatic hydrocarbons from soil. *Environ. Toxicol. Chem.* **2005,** *24,* 286-293.

(171) McCarthy, J.F. and Zachara, J.M. Subsurface transport of contaminants. *Environ. Sci. Technol.* **1989,** *23,* 496-502.

(172) D'Angelo, E. and Reddy, K.R. Effect of aerobic and anaerobic conditions on chlorophenol sorption in wetland soils. *Soil Sci. Soc. Am. J.* **2003,** *67,* 787-794.

(173) Kim, H.S. and Pfaender, F.K. Effects of microbially mediated redox conditions on PAH-soil interactions. *Environ. Sci. Technol.* **2005,** *39,* 9189-9196.

(174) Sahl, J. and Munakata-Marr, J. The effects of *in situ* chemical oxidation on microbiological processes: A review. *Rem. J.* **2006,** *16,* 57-70.

(175) Siegrist, R.L.; Urynowicz, M.A.; West, O.R.; Crimi, M.L.; Lowe, K.S. *Principles and Practices of In Situ Chemical Oxidation Using Permanganate.* Battelle Press: Columbus, 2001; pp. 348.

(176) Imlay, J.A. and Linn, S. DNA damage and oxygen radical toxicity. *Science* **1988,** *240,* 1302-1309.

(177) Büyüksönmez, F.; Hess, T.F.; Crawford, R.L.; Watts, R.J. Toxic effects of modified Fenton reactions on Xanthobacter flavus FB71. *Appl. Environ. Microbiol.* **1998,** *64,* 3759-3764.

(178) Klens, J.; Pohlmann, D.; Scarborough, S.; Graves, D. The effects of permanganate oxidation on subsurface microbial populations. **2001,** 253-259.

(179) National Research Council (NRC). *In Situ Bioremediation: When Does It Work?* National Academy Press: Washington, D.C., 1993; pp. 207.

(180) Stehmeier, L.G.; Francis, M.M.; Jack, T.R.; Diegor, E.; Winsor, L.; Abrajano, T.A. Field and in vitro evidence for in-situ bioremediation using compound-specific $^{13}C/^{12}C$ ratio monitoring. *Org. Geochem.* **1999,** *30,* 821-833.

(181) Madsen, E.L. Identifying microorganisms responsible for ecologically significant biogeochemical processes. *Nat. Rev. Micro.* **2005,** *3,* 439-446.

(182) Jeon, C.O.; Park, W.; Padmanabhan, P.; DeRito, C.; Snape, J.R.; Madsen, E.L. Discovery of a bacterium, with distinctive dioxygenase, that is responsible for in situ biodegradation in contaminated sediment. *PNAS* **2003,** *100,* 13591-13596.

(183) Singleton, D.R.; Powell, S.N.; Sangaiah, R.; Gold, A.; Ball, L.M.; Aitken, M.D. Stable-isotope probing of bacteria capable of degrading salicylate, naphthalene, or phenanthrene in a bioreactor treating contaminated soil. *Appl. Environ. Microbiol.* **2005,** *71,* 1202-1209.

(184) Singleton, D.R.; Sangaiah, R.; Gold, A.; Ball, L.M.; Aitken, M.D. Identification and quantification of uncultivated Proteobacteria associated with pyrene degradation in a bioreactor treating PAH-contaminated soil. *Environ. Microbiol.* **2006,** *8,* 1736-1745.

(185) Jones, M.; Singleton, D.; Carstensen, D.; Powell, S.; Swanson, J.; Pfaender, F.; Aitken, M. Effect of incubation conditions on the enrichment of pyrene-degrading bacteria identified by stable-isotope probing in an aged, PAH-contaminated soil. *Microb. Ecol.* **2008,** *56,* 341-349.

(186) Siegrist, R.L.; Crimi, M.L.; Munakata-Marr, J.; Illangasekare, T.; Dugan, P.; Heiderscheidt, J.; Petri, B.; Sahl, J. Chemical oxidation for clean up of contaminated ground water, In *Methods and Techniques for Cleaning-up Contaminated Sites,* Annable, M.D., Teodorescu, M., Hlavinek, P. and Diels, L., Eds.; Springer: Netherlands, 2008; pp. 45-58.

(187) Kastner, J.R.; Domingo, J.S.; Denham, M.; Molina, M.; Brigmon, R.L. Effect of chemical oxidation on subsurface microbiology and trichloroethene (TCE) biodegradation. *Bioremediation J.* **2000,** *4,* 219-236.

(188) Bartlett, P.D. and Cotman, J.D. The kinetics of the decomposition of potassium persulfate in aqueous solutions of methanol. *J. Am. Chem. Soc.* **1949,** *71,* 1419-1422.

(189) Tsitonaki, A.; Smets, B.F.; Bjerg, P.L. Effects of heat-activated persulfate oxidation on soil microorganisms. *Water Res.* **2008,** *42,* 1013-1022.

(190) Lukasewycz, M.T. and Burkhard, L.P. Complete elimination of carbonates: A critical step in the accurate measurement of organic and black carbon in sediments. *Environ. Toxicol. Chem.* **2005,** *24,* 2218-2221.

(191) Groves, M.R. Preliminary Report on Groundwater Resources in Rowan County, North Carolina. North Carolina Department of Natural and Economic Resources, 1976.

(192) Singleton, D.; Richardson, S.; Aitken, M. Effects of enrichment with phthalate on polycyclic aromatic hydrocarbon biodegradation in contaminated soil. *Biodegradation* **2008,** *19,* 577-587.

(193) Singleton, D.R.; Hunt, M.; Powell, S.N.; Frontera-Suau, R.; Aitken, M.D. Stable-isotope probing with multiple growth substrates to determine substrate specificity of uncultivated bacteria. *J. Microbiol. Methods* **2007,** *69,* 180-187.

(194) Cohen Jr., A.C. Simplified estimators for the normal distribution when samples are singly censored or truncated. *Technometrics* **1959,** *1,* 217-237.

(195) Jung, H.; Ahn, Y.; Choi, H.; Kim, I.S. Effects of in-situ ozonation on indigenous microorganisms in diesel contaminated soil: Survival and regrowth. *Chemosphere* **2005,** *61,* 923-932.

(196) Tsitonaki, A.; Petri, B.; Crimi, M.; Mosbaek, H.; Siegrist, R.L.; Bjerg, P.L. *In situ* chemical oxidation of contaminated soil and groundwater using persulfate: A review. *Crit. Rev. Environ. Sci. Technol.* **2010,** *40,* 55.

(197) Wilson, S.C. and Jones, K.C. Bioremediation of soil contaminated with polynuclear aromatic hydrocarbons (PAHs): A review. *Environ. Pollut.* **1993,** *81,* 229-249.

(198) Hughes, J.B.; Beckles, D.M.; Chandra, S.D.; Ward, C.H. Utilization of bioremediation processes for the treatment of PAH-contaminated sediments. *J. Ind. Microbiol. Biotechnol.* **1997,** *18,* 152-160.

(199) Madsen, E.L.; Mann, C.L.; Bilotta, S.E. Oxygen limitations and aging as explanations for the field persistence of naphthalene in coal tar-contaminated surface sediments. *Environ. Toxicol. Chem.* **1996,** *15,* 1876-1882.

(200) Luthy, R.G.; Aiken, G.R.; Brusseau, M.L.; Cunningham, S.D.; Gschwend, P.M.; Pignatello, J.J.; Reinhard, M.; Traina, S.J.; Weber, W.J.; Westall, J.C. Sequestration of hydrophobic organic contaminants by geosorbents. *Environ. Sci. Technol.* **1997,** *31,* 3341-3347.

(201) Murarka, I.; Neuhauser, E.; Sherman, M.; Taylor, B.B.; Mauro, D.M.; Ripp, J.; Taylor, T. Organic substances in the subsurface: Delineation, migration, and remediation. *J. Hazard. Mater.* **1992,** *32,* 245-261.

(202) Borchert, S.; Mueller, J.; Alesi, E.; Leins, C.; Haninger, V. *In-situ* bioremediation application strategies for soil and groundwater impacted by PAHs. *Land Contam. Reclam.* **1995,** *3,* 6-1-6-4.

(203) Mohan, S.V.; Kisa, T.; Ohkuma, T.; Kanaly, R.A.; Shimizu, Y. Bioremediation technologies for treatment of PAH-contaminated soil and strategies to enhance process efficiency. *Rev. Environ. Sci. Biotechnol.* **2006,** *5,* 347-374.

(204) Liebeg, E.W. and Cutright, T.J. The investigation of enhanced bioremediation through the addition of macro and micro nutrients in a PAH contaminated soil. *Int. Biodeterior. Biodegrad.* **1999,** *44,* 55-64.

(205) Talley, J.W.; Ghosh, U.; Tucker, S.G.; Furey, J.S.; Luthy, R.G. Particle-scale understanding of the bioavailability of PAHs in sediment. *Environ. Sci. Technol.* **2002,** *36,* 477-483.

(206) Lundstedt, S.; Haglund, P.; Oberg, L. Degradation and formation of polycyclic aromatic compounds during bioslurry treatment of an aged gasworks soil. *Environ. Toxicol. Chem.* **2003,** *22,* 1413-1420.

(207) Tiehm, A.; Stieber, M.; Werner, P.; Frimmel, F.H. Surfactant-enhanced mobilization and biodegradation of polycyclic aromatic hydrocarbons in manufactured gas plant soil. *Environ. Sci. Technol.* **1997,** *31,* 2570-2576.

(208) Millette, D.; Butler, B.J.; Frind, E.O.; Comeau, Y.; Samon, R. Substrate interaction during aerobic biodegradation of creosote-related compounds in columns of sandy aquifer material. *J. Contam. Hydrol.* **1998,** *29,* 165-183.

(209) Lahlou, M.; Harms, H.; Springael, D.; Ortega-Calvo, J.J. Influence of soil components on the transport of polycyclic aromatic hydrocarbon-degrading bacteria through saturated porous media. *Environ. Sci. Technol.* **2000,** *34,* 3649-3656.

(210) Bodour, A.A.; Wang, J.-.; Brusseau, M.L.; Maier, R.M. Temporal change in culturable phenanthrene degraders in response to long-term exposure to phenanthrene in a soil column system. *Environ. Microbiol.* **2003,** *5,* 888-895.

(211) Chi, F.H. and Amy, G.L. Transport of anthracene and benz(*a*)anthracene through iron-quartz and three aquifer materials in laboratory columns. *Chemosphere* **2004,** *55,* 515-524.

(212) Wehrer, M. and Totsche, K.U. Determination of effective release rates of polycyclic aromatic hydrocarbons and dissolved organic carbon by column outflow experiments. *Eur. J. Soil Sci.* **2005,** *56,* 803-813.

(213) Kim, H.; Lindsay, K.; Pfaender, F. Enhanced mobilization of field contaminated soil-bound PAHs to the aqueous phase under anaerobic conditions. *Wat. Air Soil Pollut.* **2008,** *189,* 135-147.

(214) Zhang, Y.; Zhu, S.; Xiao, R.; Wang, J.; Li, F. Vertical transport of polycyclic aromatic hydrocarbons in different particle-size fractions of sandy soils. *Environ. Geol.* **2008,** *53,* 1165-1172.

(215) Zhu, H.; Roper, J.C.; Pfaender, F.; Aitken, M.D. Effects of anaerobic incubation on the desorption of polycyclic aromatic hydrocarbons from contaminated soils. *Environ. Toxicol. Chem.* **2008,** *27,* 837-844.

(216) U.S. Environmental Protection Agency (USEPA). Method 3535: Solid Phase Extraction *in* Test Methods for Evaluating Solid Waste Physical/Chemical Methods, 1996.

(217) Reemtsma, T. and Mehrtens, J. Determination of polycyclic aromatic hydrocarbon (PAH) leaching from contaminated soil by a column test with on-line solid phase extraction. *Chemosphere* **1997,** *35,* 2491-2501.

(218) Gustavson, K.E. and Harkin, J.M. Comparison of sampling techniques and evaluation of semipermeable membrane devices (SPMDs) for monitoring polynuclear aromatic hydrocarbons (PAHs) in groundwater. *Environ. Sci. Technol.* **2000,** *34,* 4445-4451.

(219) Zamfirescu, D. and Grathwohl, P. Occurrence and attenuation of specific organic compounds in the groundwater plume at a former gasworks site. *J. Contam. Hydrol.* **2001,** *53,* 407-427.

(220) North Carolina Department of Environment and Natural Resources (NCDENR). North Carolina Administrative Code: Title 15A, Classifications and Water Quality Standards Applicable to the Groundwaters of North Carolina. N.C. Division of Water Quality. January 1, 2010.

(221) Adams, J.A. and Reddy, K.R. Extent of benzene biodegradation in saturated soil column during air sparging. *Ground Water Monit. Rem.* **2003,** *23,* 85-94.

(222) Talley, J.W.; Zhang, X.; Waisner, S.; Ringelberg, D.; Hansen, L. Study of the potential for bioremediation of petroleum hydrocarbons within smear zone soils. *J. Environ. Eng.* **2004,** *130,* 1401-1407.

(223) Volkering, F.; Breure, A.M.; Sterkenburg, A.; Andel, J.G. Microbial degradation of polycyclic aromatic hydrocarbons: Effect of substrate availability on bacterial growth kinetics. *Appl. Microbiol. Biotechnol.* **1992,** *36,* 548-552.

(224) Bouchez, M.; Blanchet, D.; Vandecasteele, J. Substrate availability in phenanthrene biodegradation: Transfer mechanism and influence on metabolism. *Appl. Microbiol. Biotechnol.* **1995,** *43,* 952-960.

(225) Aitken, C.M.; van Duin, A.C.T.; Collins, M.J. Understanding bioavailability of polycyclic aromatic hydrocarbons: Mechanisms and prediction, In *Bioremediation: A critical review,* Head, I.M., Singleton, I. and Milner, M.G., Eds.; Horizon Scientific Press: Norfolk, England, 2003; pp. 185-204.

(226) Hong, L.; Ghosh, U.; Mahajan, T.; Zare, R.N.; Luthy, R.G. PAH sorption mechanism and partitioning behavior in lampblack-impacted soils from former oil-gas plant sites. *Environ. Sci. Technol.* **2003,** *37,* 3625-3634.

(227) Ghosh, U.; Zimmerman, J.R.; Luthy, R.G. PCB and PAH speciation among particle types in contaminated harbor sediments and effects on PAH bioavailability. *Environ. Sci. Technol.* **2003,** *37,* 2209-2217.

(228) Ahn, S.; Werner, D.; Luthy, R.G. Physicochemical characterization of coke-plant soil for the assessment of polycyclic aromatic hydrocarbon availability and the feasibility of phytoremediation. *Environ. Toxicol. Chem.* **2005,** *24,* 2185-2195.

(229) Bosma, T.N.P.; Middeldorp, P.J.M.; Schraa, G.; Zehnder, A.J.B. Mass transfer limitation of biotransformation: Quantifying bioavailability. *Environ. Sci. Technol.* **1997,** *31,* 248-252.

(230) Harms, H. and Bosma, T.N.P. Mass transfer limitation of microbial growth and pollutant degradation. *J. Ind. Microbiol. Biotechnol.* **1997,** *18,* 97-105.

(231) Kan, A.T.; Fu, G.; Hunter, M.; Chen, W.; Ward, C.H.; Tomson, M.B. Irreversible sorption of neutral hydrocarbons to sediments: Experimental observations and model predictions. *Environ. Sci. Technol.* **1998,** *32,* 892-902.

(232) Birdwell, J.E. and Thibodeaux, L.J. PAH repartitioning in field-contaminated sediment following removal of the labile chemical fraction. *Environ. Sci. Technol.* **2009,** *43,* 8092-8097.

(233) Birdwell, J.; Cook, R.L.; Thibodeaux, L.J. Desorption kinetics of hydrophobic organic chemicals from sediment to water: A review of data and models. *Environ. Toxicol. Chem.* **2007,** *26,* 424-434.

(234) Connaughton, D.F.; Stedinger, J.R.; Lion, L.W.; Shuler, M.L. Description of time-varying desorption kinetics: Release of naphthalene from contaminated soils. *Environ. Sci. Technol.* **1993,** *27,* 2397-2403.

(235) Shor, L.M.; Rockne, K.J.; Taghon, G.L.; Young, L.Y.; Kosson, D.S. Desorption kinetics for field-aged polycyclic aromatic hydrocarbons from sediments. *Environ. Sci. Technol.* **2003,** *37,* 1535-1544.

(236) Jonker, M.T.O.; Hawthorne, S.B.; Koelmans, A.A. Extremely slowly desorbing polycyclic aromatic hydrocarbons from soot and soot-like materials: Evidence by supercritical fluid extraction. *Environ. Sci. Technol.* **2005,** *39,* 7889-7895.

(237) Rutherford, P.M.; Gray, M.R.; Dudas, M.J. Desorption of [^{14}C]naphthalene from bioremediated and nonbioremediated soils contaminated with creosote compounds. *Environ. Sci. Technol.* **1997,** *31,* 2515-2519.

(238) Hawthorne, S.B. and Grabanski, C.B. Correlating selective supercritical fluid extraction with bioremediation behavior of PAHs in a field treatment plot. *Environ. Sci. Technol.* **2000,** *34,* 4103-4110.

(239) Kim, H.S. and Weber, W.J. Optimizing contaminant desorption and bioavailability in dense slurry systems. 2. PAH bioavailability and rates of degradation. *Environ. Sci. Technol.* **2005,** *39,* 2274-2279.

(240) Cajthaml, T. and Sasek, V. Application of supercritical fluid extraction (SFE) to predict bioremediation efficacy of long-term composting of PAH-contaminated soil. *Environ. Sci. Technol.* **2005,** *39,* 8448-8452.

(241) Sabate, J.; Viñas, M.; Solanas, A.M. Bioavailability assessment and environmental fate of polycyclic aromatic hydrocarbons in biostimulated creosote-contaminated soil. *Chemosphere* **2006,** *63,* 1648-1659.

(242) Loehr, R.C.; Lamar, M.R.; Poppendieck, D.G. A protocol to estimate the release of anthropogenic hydrocarbons from contaminated soils. *Environ. Toxicol. Chem.* **2003,** *22,* 2202-2208.

(243) Cornelissen, G.; van Noort, P.C.M.; Govers, H.A.J. Mechanism of slow desorption of organic compounds from sediments: A study using model sorbents. *Environ. Sci. Technol.* **1998,** *32,* 3124-3131.

(244) Abu, A. and Smith, S. Mechanistic characterization of adsorption and slow desorption of phenanthrene aged in soils. *Environ. Sci. Technol.* **2006,** *40,* 5409-5414.

(245) Hawthorne, S.B.; Poppendieck, D.G.; Grabanski, C.B.; Loehr, R.C. Comparing PAH availability from manufactured gas plant soils and sediments with chemical and biological tests. 1. PAH release during water desorption and supercritical carbon dioxide extraction. *Environ. Sci. Technol.* **2002,** *36,* 4795-4803.

(246) Rockne, K.J.; Shor, L.M.; Young, L.Y.; Taghon, G.L.; Kosson, D.S. Distributed sequestration and release of PAHs in weathered sediment: The role of sediment structure and organic carbon properties. *Environ. Sci. Technol.* **2002,** *36,* 2636-2644.

(247) U.S. Environmental Protection Agency (USEPA). National Secondary Drinking Water Regulations: Final Rule. 1979, *Federal Register 44, no. 140: 42195*

(248) Cassidy, D.; Hampton, D. Hydrogen sulfide production from persulfate oxidation: Implications for remediation., *Proceedings of the Tenth International In Situ and On-Site Bioremediation Symposium*, Baltimore, USA, May 5-8, 2009. Battelle Press: Columbus, OH, 2009.

(249) Geyer, R.; Peacock, A.D.; Miltner, A.; Richnow, H.H.; White, D.C.; Sublette, K.L.; Kastner, M. In situ assessment of biodegradation potential using biotraps amended with ^{13}C-labeled benzene or toluene. *Environ. Sci. Technol.* **2005,** *39,* 4983-4989.

(250) Wilkinson, K. "Salisbury City Council Receives Duke Energy Report on Manufactured Gas Plant Site Remediation". City of Salisbury. Press release: July 9, 2006. Accessed: August 2, 2010. http://www.ci.salisbury.nc.us/press/2006-2005.html.

(251) Schroth, M.H.; Istok, J.D.; Ahearn, S.J.; Selker, J.S. Characterization of miller-similar silica sands for laboratory hydrologic studies. *Soil Sci. Soc. Am. J.* **1996,** *60,* 1331-1339.

(252) American Society for Testing and Materials (ASTM). Standard Test Method for Particle-Size Analysis of Soil, ASTM D422-63, In *Annual Book of ASTM Standards,* American Society for Testing and Materials: Philadelphia, PA, 1999; Vol.04.08, pp. 10-17.

(253) American Society for Testing and Materials (ASTM). Standard Test Method for Laboratory Determination of Water (Moisture) Content of Soil and Rock by Mass, ASTM D2216-98, In *Annual Book of ASTM Standards,* American Society for Testing and Materials: Philadelphia, PA, 1999; Vol.04.08, pp. 190-194.

(254) American Society for Testing and Materials (ASTM). Standard Test Method for pH of Soil, ASTM D4972-01, In *Annual Book of ASTM Standards,* American Society for Testing and Materials: Philadelphia, PA, 2001; Vol.04.08.

(255) American Society for Testing and Materials (ASTM). Standard Test Method for Specific Gravity of Soil Solids by Water Pycnometer, ASTM D854-92, In *Annual Book of ASTM Standards,* American Society for Testing and Materials: Philadelphia, PA, 1999; Vol.04.08.

(256) Ocean Optics, Inc. OOISensors Fiber Optic Sensors System Installation and Operation Manual. **2007,** *FOXY-AL300-000-02-0207,* 1-127.

(257) Shaw, A.D.; Li, Z.; Thomas, Z.; Stevens, C.W. Assessment of tissue oxygen tension: comparison of dynamic fluorescence quenching and polarographic electrode technique. *Crit. Care* **2002,** *6,* 76-80.

(258) Bohn, H.L. Redox Potentials. *Soil Sci.* **1971,** *112,* 39-45.

(259) Rao, S.M. *Practical Isotope Hydrology.* New India Publishing: 2006; pp. 213.

(260) Edwards, U.; Rogall, T.; Blöcker, H.; Emde, M.; Böttger, E.C. Isolation and direct complete nucleotide determination of entire genes. Characterization of a gene coding for 16S ribosomal RNA. *Nucleic Acids Res* **1989,** *17,* 7843-7853.

(261) Lane, D.J. 16S/23S rRNA sequencing, In *Nucleic acid sequencing techniques in bacterial systematics.* Stackebrandt, E. and Goodfellow, M., Eds.; Wiley: New York, 1991; pp. 115-175.

(262) Altschul, S.F.; Gish, W.; Miller, W.; Myers, E.W.; Lipman, D.J. Basic local alignment search tool. *J. Mol. Biol.* **1990,** *215,* 403-410.

(263) Thompson, J.D.; Higgins, D.G.; Gibson, T.J. CLUSTAL W: improving the sensitivity of progressive multiple sequence alignment through sequence weighting, position-specific gap penalties and weight matrix choice. *Nucleic Acid Res* **1994,** *22,* 4673-4680.

(264) Huber, T.; Faulkner, G.; Hugenholtz, P. Bellerophon: a program to detect chimeric sequences in multiple sequence alignments. *Bioinformatics* **2004,** *20,* 2317-2319.

(265) Muyzer, G.; De Waal, E.C.; Uitierlinde, A.G. Profiling of complex microbial populations by denaturing gradient gel electrophoresis analysis of polymerase chain reaction-amplified genes coding for 16S rRNA. *Appl. Environ. Microbiol.* **1993,** *59,* 695-700.

(266) Haselow, J.S.; Siegrist, R.L.; Crimi, M.; Jarosch, T. Estimating the total oxidant demand for in situ chemical oxidation design. *Rem. J.* **2003,** *13,* 5-16.

(267) Stugart, R. Determination of iron in milk and other biological materials. *Ind. Eng. Chem.* **1931,** *3,* 390-393.